International Journal of Analytical Chemistry

Characterization of Fossil and Renewable Fuels

Lead Guest Editor: Xing Fan
Guest Editors: Bo Chen, Xun Hu, Nilusha Sudasinghe, and Ya-He Zhang

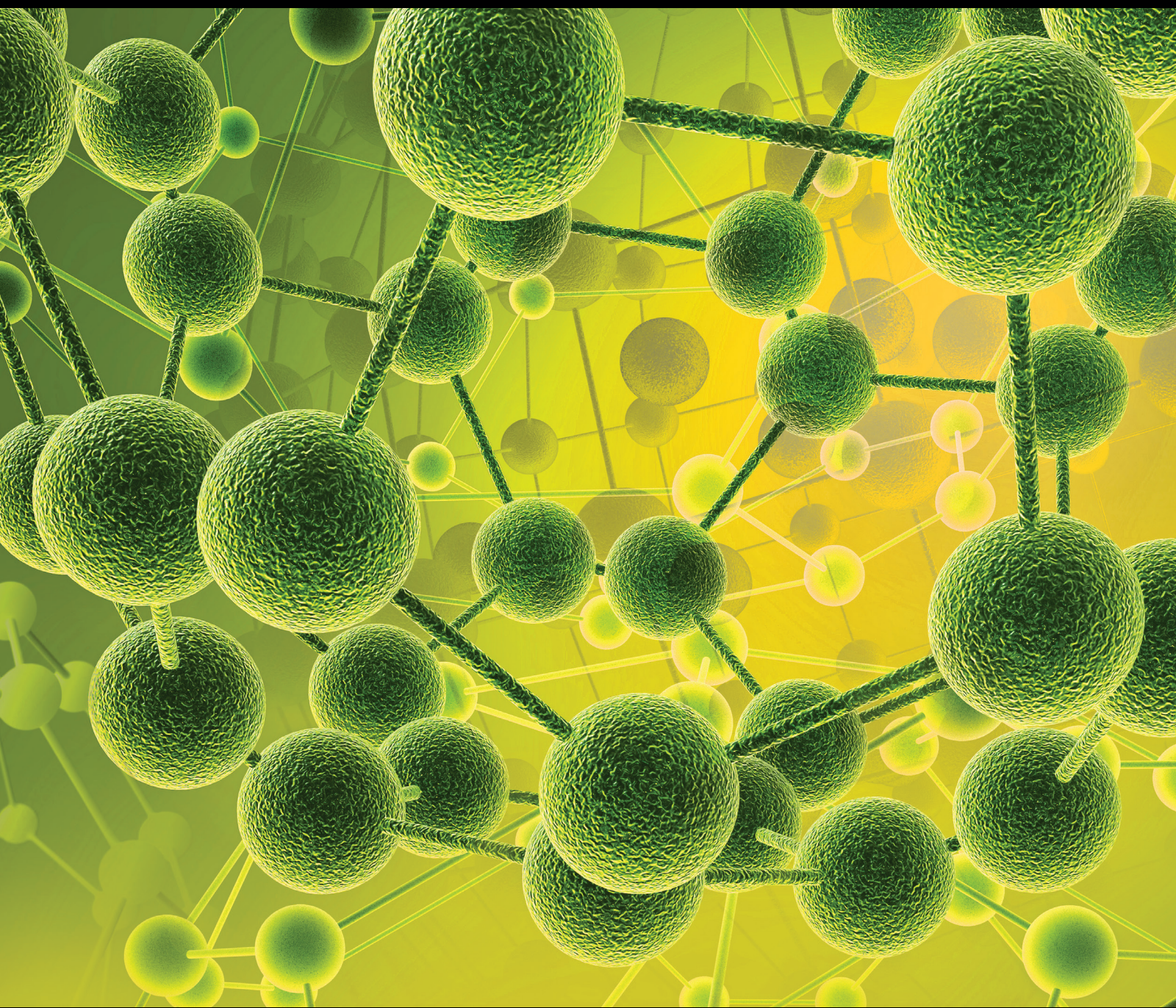

Characterization of Fossil and Renewable Fuels

International Journal of Analytical Chemistry

Characterization of Fossil and Renewable Fuels

Lead Guest Editor: Xing Fan
Guest Editors: Bo Chen, Xun Hu, Nilusha Sudasinghe, and Ya-He Zhang

Editorial Board

Contents

Hindawi
International Journal of Analytical Chemistry
Volume 2018, Article ID 5264942, 1 page
https://doi.org/10.1155/2018/5264942

Editorial

Characterization of Fossil and Renewable Fuels

Xing Fan,[1] **Bo Chen**,[2] **Xun Hu**,[3] **Nilusha Sudasinghe**,[4] **and Ya-He Zhang**[5]

[1]*Department of Applied Chemistry, China University of Mining and Technology, Xuzhou 221116, China*
[2]*Department of Chemical & Petroleum Engineering, University of Wyoming, Laramie, WY 82071, USA*
[3]*Fuels and Energy Technology Institute, Curtin University, Bentley, WA 6102, Australia*
[4]*Bioscience Division, Los Alamos National Laboratory, Los Alamos, NM 87545, USA*
[5]*State Key Laboratory of Heavy Oil Processing, China University of Petroleum, Beijing 102249, China*

Correspondence should be addressed to Xing Fan; fanxing@cumt.edu.cn

Received 16 October 2017; Accepted 18 October 2017; Published 1 January 2018

The special issue aims to provide contributions from a variety of topics relating to the characterization of properties, structures or molecular compositions of fossil fuels, and biomass, as well as the corresponding derivatives or products through thermal, chemical, and biochemical methods.

The special issue presents six papers relating to biomass, crude oil, and coal. We feel that the published articles represent a certain wide range of researches in the scope of special issue. A series of analytical techniques in chromatography, microscopy, and spectroscopy were included in the researches. This special issue is dedicated to the readers in the research fields of analytical chemistry, biochemical engineering, chemical engineering, geology, and mineral processing engineering.

In X. Yue et al.'s paper, liquefaction residue of a bituminous coal was subject to hydroconversion reactions and the products were analyzed using Fourier transform infrared spectroscopy and gas chromatography/mass spectrometry. More than 200 organic compounds were detected in the products and divided into alkanes, aromatic hydrocarbons, phenols, ketones, ethers, and other species.

Scanning electron microscopy was applied in Z. Lu et al.'s research to characterize particle morphology, including size and shape, which is an important factor significantly influencing the physical and chemical properties of biomass material. An image segmentation algorithm based on particle geometrical information was proposed to recognize the finer clustered powders.

Biomarkers derived from early living organisms play an important role in oil and gas geochemistry and exploration since they can record the diagenetic evolution of the parent materials of crude oil and reflect the organic geochemical characteristics of crude oil and source rocks. Therefore, gas chromatography/mass spectrometry was applied by X. Zhang et al. to study the biomarker compounds of crude oil in Southwestern Yishan Slope of Ordos Basin.

S. Wang et al. used X-ray fluorescence spectrometer, X-ray diffractometer, X-ray photoelectron spectrometer, and field emission electron probe microanalyzer to study the composition of heavy products in fine coal powders separated by ultrasonic vibration gas-solid fluidized bed. The particle separation process based on density was strengthened by the introduction of ultrasonic vibration.

The paper by Y.-C. Lu et al. reported componential characterization of extractable species in wheat straw. Analytical methods like Fourier transformed infrared spectroscopy, gas chromatography/mass spectrometry, X-ray photoelectron spectroscopy, transmission electron microscopy, energy dispersive spectrometry, and electron probe microanalysis were used, and detailed molecular information was provided.

Analytical strategies involved in the componential characterization of bio-oil produced from lignocellulosic biomass were reviewed by Y. Lu et al. The use of chromatographic and spectrometric methods such as gas chromatography/mass spectrometry and high performance liquid chromatography/mass spectrometry was highlighted. Fourier transform infrared spectroscopy and nuclear magnetic resonance were also mentioned.

Xing Fan
Bo Chen
Xun Hu
Nilusha Sudasinghe
Ya-He Zhang

Hindawi
International Journal of Analytical Chemistry
Volume 2017, Article ID 9298523, 19 pages
https://doi.org/10.1155/2017/9298523

Review Article

Analytical Strategies Involved in the Detailed Componential Characterization of Biooil Produced from Lignocellulosic Biomass

Yao Lu,[1,2,3] Guo-Sheng Li,[1,3] Yong-Chao Lu,[4] Xing Fan,[1,3] and Xian-Yong Wei[1,3]

[1]*Key Laboratory of Coal Processing and Efficient Utilization, Ministry of Education, China University of Mining & Technology, Xuzhou 221116, China*
[2]*Advanced Analysis & Computation Center, China University of Mining & Technology, Xuzhou 221116, China*
[3]*School of Chemical and Engineering Technology, China University of Mining & Technology, Xuzhou 221116, China*
[4]*School of Basic Education Sciences, Xuzhou Medical University, Xuzhou 221004, China*

Correspondence should be addressed to Yong-Chao Lu; 28386958@qq.com and Xing Fan; fanxing@cumt.edu.cn

Received 17 March 2017; Accepted 16 August 2017; Published 13 December 2017

Academic Editor: Valentina Venuti

Elucidation of chemical composition of biooil is essentially important to evaluate the process of lignocellulosic biomass (LCBM) conversion and its upgrading and suggest proper value-added utilization like producing fuel and feedstock for fine chemicals. Although the main components of LCBM are cellulose, hemicelluloses, and lignin, the chemicals derived from LCBM differ significantly due to the various feedstock and methods used for the decomposition. Biooil, produced from pyrolysis of LCBM, contains hundreds of organic chemicals with various classes. This review covers the methodologies used for the componential analysis of biooil, including pretreatments and instrumental analysis techniques. The use of chromatographic and spectrometric methods was highlighted, covering the conventional techniques such as gas chromatography, high performance liquid chromatography, Fourier transform infrared spectroscopy, nuclear magnetic resonance, and mass spectrometry. The combination of preseparation methods and instrumental technologies is a robust pathway for the detailed componential characterization of biooil. The organic species in biooils can be classified into alkanes, alkenes, alkynes, benzene-ring containing hydrocarbons, ethers, alcohols, phenols, aldehydes, ketones, esters, carboxylic acids, and other heteroatomic organic compounds. The recent development of high resolution mass spectrometry and multidimensional hyphenated chromatographic and spectrometric techniques has considerably elucidated the composition of biooils.

1. Introduction

Fossil resources, namely, coal, petroleum, and natural gas, are still the main raw materials to meet the global requirements for energy and fine chemicals. The fast depletion and increasing demands increase price of fossil resources, leading to serious economic and social crises, which strongly motivates the search for alternative and renewable resources [1]. Lignocellulosic biomass (LCBM), which is considered as the most abundant renewable and low-cost organic resource with global production of 15 M tons per year, is the most promising choice [2]. LCBM can be degraded via thermochemical and biological techniques to produce solid, liquid, and gaseous fuels [3–5], which provides about 15% of the world's primary energy consumption and is treated as an additional CO_2 neutral process. On the other hand, from the chemical point of view, the main parts of LCBM are cellulose, hemicellulose, and lignin [3, 6]. Cellulose is a linear polysaccharide of β-(1→4)-D-glucopyranose with degree of polymerization around 5000–10000. Hemicellulose is a heterogeneous polysaccharide mixture of various polymerized monosaccharides (i.e., glucose, mannose, galactose, xylose, arabinose, etc.) with a degree of polymerization around tens to hundreds. Lignin is an amorphous, three-dimensional, highly branched polyphenolic substance consisting of an irregular array of hydroxy-/methoxy-substituted

phenylpropane units supported by β-O-4, α-O-4, 5-5, β-5, and β-β linkages [3, 7, 8].

Currently, no process can be accepted exclusively and considered as the superior option for the thermochemical conversion of LCBM into liquid fuels and organic chemicals. Pyrolysis is a promising conversion method and attracts increasing attention in the last three decades because it is more suitable for the direct production of a second-generation liquid fuel [3, 9–13]. Pyrolysis of dry LCBM is a thermal degradation process in the absence of O_2, at high temperature (i.e., >350°C), with short residence times (several seconds) and under specific pressure (especially N_2, >1 MPa), which produces major content of biooil and biochar, as well as small amount of gas. Biooil can be used as fuel and feedstock of value-added chemicals directly or with simple pretreatments [3]. To maximize the biooil yield from various LCBMs, the optimization of pyrolysis parameters such as the residence time, heating rate, temperature, and pressure is applied [3, 10, 14, 15]. In order to use biooil in value-added ways, more detailed information regarding the composition of biooil should be carried out [16–19]. The compositions of the degradation products from different LCBMs are extremely complex [3, 20, 21] and depend on the kind, part, or growth stage of LCBM [20]. A significant factor affecting the composition of biooils is the pyrolytic conditions such as pretreatment method, reactor style, heating rate, quenching rate, residence time, and temperature [3, 10, 11, 14, 15, 22]. Different from biodiesel and bioethanol, biooils are produced from pyrolysis of LCBM, resulting in dark brown oily liquid with extremely complex compositions, including water and hundreds of organic species which can be classified into hydrocarbons (alkanes, alkenes, alkynes, and aromatics), oxygen-containing species (ethers, alcohols, phenols, aldehydes, ketones, furans, esters, and carboxylic acids), and other heteroatomic organic compounds [21]. Classes of organic components contained in biooils are listed in Table 1.

Table 1: Contents of classes of organic components contained in typical biooils.

Classes of organic components	Contents (%, wt)
Hydrocarbons	1–10
Alcohols	2–5
Furans	1–5
Aldehydes	15–25
Ketones	1–5
Carboxylic acids	5–20
Esters	1–4
Benzene-ring containing species	15–30
Sugars	15–30
Hetroatom-containing species	1–3
Others	1–5

The compositional analysis of biooil covers a wide range of its characteristics, including macroscopical and integral features such as solid-liquid phases distribution, acidity, stability, heating value, elemental contents, and molecular weight distribution and microscopical and specific features such as chemical composition, distribution of moieties of species, distributions of functional groups and chemical bonds, and connection styles of organic matters. Most of these analyses require qualitative analysis and quantitative analysis. The physicochemical fuel properties of biooil, such as water content, elemental contents, heating value, acidity, and density, as well as phase distribution, are determined by corresponding techniques which are similar with the conventional methods used in the evaluation of petroleum-based fuels [16, 23, 24]. Typical values for the physicochemical fuel properties of biooil are shown in Table 2. The water content of biooil is often determined by Karl Fischer titration method. The solid content is determined from the residue after filtering the biooil through a polyethersulfone syringe filter. The contents of C, H, O, N, and P in biooil are often analyzed through complete oxidation with an elementary analyzer. Gel permeation chromatography (GPC) is often used to measure the size and molecular weight of macromolecules. The methods used in the physicochemical fuel properties determination of biooil are not included in this review.

Some of the undesirable properties [33] for the utilization as fuel may include high water content, high viscosity, high corrosiveness (high acidity), high oxygen content, low heating value, and multiphase instability (polymerization reaction attributed to the presence of aldehydes and phenols). Thus, the biooil upgrading with economical sustainable techniques aiming at improving the physicochemical properties as fuel is necessary. From the viewpoint of production of value-added chemicals, upgrading processes leading to economic profit are also needed to be carried out [34–37]. In situ heterogeneous catalysis during pyrolysis and separated catalytic hydrotreatment (hydrodeoxygenation) are promising methods used in the upgrading of biooil production [38–41]. After these processes, yield of conversion, ratio of light weight moieties, and stability can be increased, and acidity and oxygen content can be decreased. The upgrading methods are not included in this review, because there is no obvious difference on componential characterization methods between the biooil and upgraded biooil [18, 42, 43].

Insight into the detailed compositional characterization of LCBM derived biooil is crucial for the development of efficient conversion processes and better upgrading strategies, for the evaluation of value-added utilization of biooil, for the understanding of the composition of LCBM, and for the probing of the degradation mechanisms in pyrolytic process. The final goal of compositional characterization is to produce fuels and chemicals to meet the demand for energy and chemical feedstock. The elucidation of composition of biooil or upgraded biooil brings great analytical challenge. Due to the complexity and diversity of the components, it is impossible to completely characterize a biooil by a single analytical method [44]. Typically, biooils contain more than 300 organic compounds which could be detected by gas chromatography-mass spectrometry (GC-MS) [3, 21]. This number of organic species only accounts for a small part of the full components due to the determination limit of GC-MS, which only works for species with lower boiling point

Table 2: Typical values for the bulk physicochemical fuel properties of biooil.

Physicochemical fuel properties	Values
Water content	15–30%, wt
Acidity	pH 2–3.5
Density	1.0–1.5 g/mL
Viscosity	10^{-3}–10^{4} Pa·s
Heating value	15–25 MJ/kg
Ash content	0.01–0.15%, wt
MW distribution of organic components	30–10000 Da
Mineral contents	10–50 ppm
Solid content	0.2–3.5%, wt
Surface tension	15–30 mM/m (25°C)
Flash point	40–120°C
Elemental contents	C (50–65%), H (5–8%), O (30–40%), N (0.1–0.8%), S (0.01–0.2%), wt

(<350°C) and low to medium polarity [45, 46]. A report stated that more than 8000 peaks were characterized in a biooil with a high resolution mass spectrometer (HRMS) [47].

The chemical compositions of biooils are extremely complex; hence, specific, comprehensive, and robust analytical methodologies should be used. Several review works have been carried out for the detailed compositional characterization of biooil [17, 18, 48, 49]. To determine the functional groups and chemical bonds distribution, and individual species in biooil, distinct separation and detection methodologies were applied. After preseparation of moieties in biooil [21, 33, 49], such as liquid-liquid extraction (LLE), distillation, and column chromatography, both spectroscopic and chromatographic methods are applied to the qualitative analysis and quantitative analysis of the species in biooil [17, 44, 50–53]. For spectroscopic methods, Fourier transform infrared (FTIR) spectroscopy [29, 54–56] and nuclear magnetic resonance (NMR) spectroscopy [56–59] are mostly used, which can provide information on the functional groups of species in biooil. However, such information is integral information, and not for a specific compound. Thus, the separation and isolation of individual components are needed. Based on physicochemical properties of the components that need to be analyzed, that is, solubility, volatility, molecular weight, and ionization potential, chromatographic techniques can provide effective componential separation and give the qualitative and quantitative estimation for individual species. Some of the majority of components in biooils have very low concentrations (*i.e.*, <0.2 wt%), and a detailed compositional analysis requires the combination of separation techniques. HPLC [60–65] and GC [21, 33, 66–69] allow primary qualitative and quantitative classification of the detectable components and are the most commonly available techniques used for effective separation of species for complex samples. GC usually concentrates on the volatile organic species with lower polarity and lower boiling point (<350°C) with molecular weight range 50–500 Da typically, and HPLC is usually used for the separation of species with lower vapor pressures, lower thermal stability, and higher polarity. However, only a portion of the sample is identified. The other components with higher molecular weight (MW) can be determined, that is, by GPC for species with MW up to 1000–2000 Da without any further information regarding their structure [25, 60], unless coupled with other techniques [70]. Comprehensive two-dimensional gas chromatography (GC × GC) is a powerful technique for the determination of volatile fractions in different types of biooils providing detailed information on the molecular composition. It provides complementary qualitative and quantitative analyses of a wide variety of compounds [25, 71–76]. Both the chromatographic methods are linked to various detectors, such as atomic emission detector (AED) [77], flame ionization detector (FID) [73, 78], and various mass spectrometers [25, 71–74, 79, 80]. A single technique cannot provide complete analysis. Different detectors have different sensitivities and resolutions to specific species and elements, also with inherent limitations. For example, AED is less sensitive to oxygen than other heteroatoms [77, 81], and MS is more sensitive to species easy to be ionized [19, 69, 72–74, 82]. GC×GC with higher resolution over GC has been successfully used for the separation of components in various biooils produced from different LCBMs. However, the identification of individual species is a difficult task since comprehensive databases and retention time libraries are not widely available. Improved analytical methods were emerged to take advantage on the characterization of species in biooil. HRMSs were extensively used to identify individual component according to the monoisotopic mass in complex mixtures [17, 44, 47, 74, 76, 83, 84].

Sometimes, the chromatographic and spectrometric methods are not sufficient to identify all the species with similar retention behavior and spectra since their limited resolution. To overcome this problem and for better qualitative and quantitative analyses of species, internal standard and external standard methods are often applied by using reference compounds [21, 78, 85, 86]. However, not all the compounds are synthetically or commercially available due to the complexity, namely, hundreds of species contained in the pyrolytic biooils. Therefore, more powerful techniques aiming at exact identification of organic species in complex samples with outstanding resolution are needed. HRMSs, such as Orbitrap MS, Q-TOFMS, and Fourier transform-ion

cyclotron resonance mass spectrometry (FT-ICR MS), were reported to have advantage on the identification of complex mixtures due to the superior mass resolution [17, 27, 28, 30, 31, 44, 47, 70, 74, 76, 83, 87, 88].

In the current review, analytical strategies involved in the detailed componential characterization of biooil produced from LCBM in recent years were reviewed. Pretreatments of biooil before further compositional analyses were summarized, and the instrumental analyses for detailed characterization of biooil samples with chromatographic and spectrometric methods especially the hyphenated chromatographic techniques, comprehensive NMR spectroscopy, and HRMS techniques were highlighted. These compositional assessments were compared and discussed, and the future work on the componential characterization of biooil was also prospected and suggested.

2. Production of Pyrolytic Biooils

Pyrolysis is a process of thermal decomposition of dry LCBM in absence of O_2, leading to the cleavage of chemical bonds for the production of biooil, biochar, and gas, with controlled conditions, *that is*, programmed temperature, residence time, and pressure and with/without a catalyst [3]. The distribution of these products changing with pyrolysis parameters, and the maximum liquid fraction yield can be obtained under optimized conditions. Slow, fast, and flash pyrolysis are the three main methods used in the degradation of LCBM according to the pyrolytic conditions. The main product of slow pyrolysis is biochar with typical pyrolytic conditions, *that is*, temperature 350–500°C, heating rate about 10°C/s, and residence time 5–30 min. Typical conditions for fast pyrolysis are as follows, *that is*, temperature 500–650°C, heating rate about 100°C/s, and residence time 0.5–5 s. The formation of biooil, biochar, and gas with different yields varies with starting material and conditions used in the pyrolysis. Under the vigorous pyrolytic conditions, *that is*, temperature 700–1000°C, heating rate up to 10000°C/,s and residence time < 0.1 s, flash pyrolysis takes place with the main product of gas. Among the three pyrolysis methods, fast pyrolysis is a promising technique for the conversion of biomass to fuels because of relatively mild conditions, effective degradable ability, and appropriate distribution of products. One of the disadvantages of fast pyrolysis is that considerable amount of lignin in LCBM could not be decomposed effectively, which is left in the biochar as residue [3].

Some pyrolysis processes with modification or optimization are similar with in situ upgrading of biooil aiming at improving the fuel properties and/or utilization as feedstock of chemicals [12, 22]. The type of pyrolysis reaction system such as microwave-assisted pyrolysis and stepwise pyrolysis system also influences the yield and composition of biooil [89–92]. Catalytic pyrolysis of LCBM with various catalysts, including activated carbon [93–95], and alkaline catalysts [96, 97], for the production of biooil, has been carried out [98].

Typically, biooils contain 15–30 wt% of water, 55–65 wt% of organic components that can be quantified with conventional chromatographic and spectrometric techniques [3], and 5–30 wt% components with condensed structure and high MW cannot be detected by conventional methods [17, 44].

3. Fractionation Techniques

For the complexity of biooils, sample pretreatments focused on fractionation were often employed to achieve more detailed information or to impart selectivity and specificity in componential analysis. Pretreatments are typically applied to biooils to obtain fractions according to the difference in properties of components before the subsequent chromatographic analysis. Among the methods used in pretreatment, extraction, distillation, filtration, centrifugation, and adsorption chromatography have been widely explored for various applications [17, 44, 49, 98, 99]. Table 3 lists the regular techniques used in the pretreatment before componential analysis of biooil.

3.1. Solvent Extraction. Solvent extraction, also known as LLE, is a process in which solvent is used for recovery of components from biooil. In a typical process, the addition of a relatively immiscible organic solvent to the sample results in two phases, namely, extract phase and raffinate phase, also known as solvent-rich phase and water-rich phase, respectively. Based on the difference of solubility or affinity between the two phases, redistribution of the components takes place according to their distribution or partition coefficient. Commonly used solvents for the extraction include water, methanol, ethanol, ethyl acetate, acetonitrile, *n*-hexane, benzene and toluene, ketones, dichloromethane, and carbon tetrachloride [21, 28, 29, 33, 99, 100]. By using hexane, petroleum ether, or chloroform as the extraction solution in LLE, phenols, and guaiacol were enriched into the solvent phase with high concentrations (85%), while sugar, acid, and alcohol were concentrated into the water phase [100]. For complex mixtures with multiple moieties of components to be extracted, such as biooil, selected solvents extraction can be performed for multiple stages [101]. Hence, in typical solvent extraction procedure, in order to conduct the extraction of moieties of components effectively, large volumes of solvents and tedious extraction program are required, making it a time consuming process [17].

Supercritical fluid extraction (SFE) offers several advantages compared to conventional solvent extraction and has received much attention applied for the componential separation of biooil [102–105]. CO_2, the solvent in SFE, is inexpensive, nontoxic, nonflammable, noncorrosive, and readily available in large quantities with high purity. The SFE process with CO_2 is generally carried out at relatively low temperature and low pressure, because the low critical pressure (*i.e.*, 73.8 atm) and critical temperature (*i.e.*, 31.1°C) of CO_2 prevent undesirable reactions among biooil components. Continuous modulation of the conditions in the process of SFE is flexible for selective extraction of the supercritical fluid; furthermore, it is easy to remove CO_2 from the extracts after SFE, preventing undesirable pollution during the extraction. The organic fraction of a biooil produced from mixed biomass of wheat and wood sawdust was isolated by supercritical CO_2 (SC-CO_2), and the first fraction of SC-CO_2 extraction collected

Table 3: Selected techniques used in the pretreatment based on properties of components.

Property	Techniques
Solubility	Extraction, precipitation, crystallization, centrifugation
Polarity	Extraction, chromatography
Volatility	Distillation
Density	Sedimentation, centrifugation, flotation
Size and shape	Chromatography, centrifugation, filtration
Electrostatic charge	Chromatography, electrophoresis, flotation

at 25 MPa was enriched with furanoids (9.9%), pyranoids (9.0%), and benzenoids (44.8%) [102]. Cheng et al. [106] carried out a three-step SC-CO_2 extraction for the selective fractionation of fast pyrolysis biooil. Different classes of oxygen-containing compounds in biooil were enriched in different fractions, facilitating the following detailed analysis.

3.2. Distillation. Distillation usually follows LLE for further treatment of extracts, such as purification of products and recovery of solvents [21, 28, 29, 33]. In distillation of biooil, separation is based on the volatilities of components such as the vapor pressures and boiling points of the species. According to the characteristics of components and the purpose of distillation, atmospheric pressure, vacuum, steam, and molecular distillation can be applied flexibly to the separation. Under atmospheric pressure, due to the composition of biooil, with temperature lower than 100°C as the starting point, the distillation of biooil would be stopped at 280°C and left 35–50 wt% of the original material as a residue [107]. Distilled fractions with high purity can be obtained by using vacuum distillation (VD). VD can be conducted at much lower temperatures, and the vapor pressures of components decrease significantly according to the vacuum degree used in the process. By introducing steam into the distilling column to heat biooil and decrease its viscosity, the steam distillation allows thermally sensitive components to be separated avoiding conversion. Molecular distillation (MD) has some advantages compared to conventional distillations, such as lower operating temperatures, shorter heating time, and higher separation efficiency [108–110]. The principle of MD is based on the specific mean free paths of molecules, rather than difference in their boiling points. Different fractions of biooil could be enriched with various chemical families by MD. Small molecules formed a water-rich light fraction and monophenols accumulated in the middle fraction, while sugars and phenolic oligomers remained in the heavy fraction because of their high MWs [108–110].

Hydrotreated biooils with different oxygen contents can be distilled to produce lights (<71°C), naphtha (71–182°C), jet (182–260°C), diesel (260–338°C), and gas oil (338–566°C) boiling range fractions to enhance the detailed characterization of oxygen-containing species with advanced analytical instruments [63]. Carboxylic acids and carbonyl compounds were detected in fractions with boiling point under 260°C, *that is*, in the lights, naphtha, and jet fractions. A new approach to the fractionation of biooil by temperature-swing extraction was reported by Kumar et al. [111], in which hot extraction (around 70°C) of the light fraction with a suitable extraction solvent followed by cold (around 25°C) demixing of the light fraction and the extraction solvent allows solvent regeneration by spontaneous liquid/liquid phase split upon cooling. They illustrated a broader potential of utilization in the fractionation of crude oil [111].

3.3. Column Chromatography. Column chromatography is a conventional method to fractionate biooils according to the different adsorption capabilities of biooil components onto the stationary phase, prior to chromatographic or spectrometric analysis. Silica gel and aluminum oxide are often used as stationary phase. Organic solvents, such as pentane, benzene, carbon disulfide, toluene, dichloromethane, ethyl acetate, and methanol, are often used as elutes to isolate species in biooils into aliphatic, aromatic, and polar fractions and so forth [14, 69, 112–115]. However, the main disadvantages of column chromatography are low throughput making it only suitable for high value-added compounds [116], and the consuming of large amount of solvent as elute.

3.4. Other Chromatographic Techniques. The principles of chromatographic techniques are based on difference of components in the interaction with stationary phase in the chromatography column, inducing the difference of retention time. GPC was frequently used in the fractionation of species and the MW distribution analysis of biooil [15, 25, 117, 118]. A detailed GPC analysis of MW distribution in biooil was carried out for different fractions [25], as shown in Figure 1. Other chromatographic techniques, such as adsorption chromatography (AC) [60, 119], ion-exchange chromatography (IEC) [120, 121], and size exclusion chromatography (SEC) [122, 123], are potentially used in the preseparation or fractionation of components in biooil. AC, like thin layer chromatography [60, 119] with providing retention behavior of species, based on the weak interactions between molecules and stationary phase, such as van der Waals forces and steric attraction. Solvents, such as *n*-pentane, toluene, and methanol, were often used to isolate aliphatic, aromatic, and polar fractions, readily for further characterization. IEC is based on the adsorption of charged molecules or ions on the surface of ion-exchange resins due to the attraction induced by electrostatic forces. High polar species, such as hydrolysable sugars in water or acidic solutions, can be qualified with IEC [120, 121]. In SEC, packing material with a certain size of pores is used as stationary phase, and

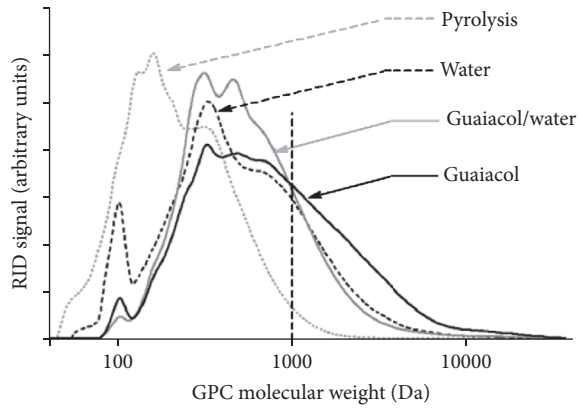

Figure 1: GPC results of the isolated biooils with guaiacol, guaiacol/water, and water, respectively [25].

the separation of components is based on the difference in penetration of molecules according to their size and shape [122, 123].

4. Advanced Instrumental Strategies

The most commonly used technique to identify biooil components is GC-MS. However, GC-MS is limited to qualifying short-chain and/or nonpolar compounds, depending on the chromatographic column used in GC, and derivatization is usually required to analyze polar species [33]. Thermostable components with low MW can be analyzed by GC-MS owing to the low injector temperature in GC. HPLC is often used to identify polar and high MW species providing complementary information with GC for the more detailed elucidation of components in biooil [58, 60, 61]. Detectors coupled with GC and HPLC cover a wide range, *that is*, variable wavelength detector (VWD), diode array detector (DAD), FID, electron capture detection (ECD), nitrogen phosphorus detector (NPD), fluorescence detector (FLD), flame photometric detector (FPD), MS, and so forth. Among them, MS has exhibited flexible application in the organic compounds detection by varying ionization sources and mass analyzers. HRMSs are treated as ideal techniques for componential analysis of complex mixtures due to considerable resolving power [17, 27, 28, 30, 31, 44, 47, 74, 76, 87]. Comprehensive chromatographic techniques such as GC × GC [75–77, 124] and LC × LC [65] with high throughput for identification of components in complex mixtures attract more and more attention recently. Spectrometric techniques, such as FTIR and NMR [58, 74, 125] with various types (*i.e.*, ^{1}H, ^{13}C, and ^{31}P), providing both qualitative and quantitative results were applied in the characterization of functional groups in biooils. Moreover, two-dimensional NMR (2D NMR) [59] is another promising technique used in the detailed characterization of components in biooil.

4.1. FTIR. FTIR is the most conventional technique used in the qualitative and quantitative analyses of organic substance for the determination of functional groups in almost all areas of contemporary chemical and biological researches [21, 29, 33, 54, 55, 69, 115]. In practice, mid-infrared region is extensively utilized to reveal the presence of various structures in molecules because of significant characteristic absorptions of functional groups. FTIR analysis is simple, straightforward, and useful for fast componential evaluation of biooil. Biooil contains enormous species, from hydrocarbons and alcohols to aromatics and carboxylic acids, so the spectra of biooil may include most of the characteristic peaks [126, 127]. Generally, peaks around 3050 cm^{-1} with strong absorbance are attributed to C-H stretching vibration indicating the presence of aliphatic hydrocarbons. Peaks around 3300–3400 cm^{-1} correspond to O-H stretching vibrations indicating the presence of carboxylic acids and/or alcohols. Peaks between 1450 and 1600 cm^{-1} indicate a C=C stretching vibration caused by aliphatic or aromatic structure. A significant peak between 1600 and 1800 cm^{-1} attributes to the presence of C=O containing species, such as aldehydes, ketones, carboxylic acids, and/or esters. Peak between 1000 and 1100 cm^{-1} is assigned to C-O stretching indicating the presence of ethers, alcohols, carboxylic acids, and/or esters. Since the table containing characteristic stretching wavelengths corresponding to functional groups can be easily found in textbooks, handbooks, and other publications [17], it is not concluded in this review.

Thermogravimetric analysis (TGA) coupled to FTIR, known as TGA-FTIR, was often used in the analysis of pyrolytic biooil [128–131]. TGA-FTIR shows the accurate weight loss of feedstock with time and provides the information on functional groups of the volatile species produced during the pyrolysis [132]. The three-dimensional TGA-FTIR spectra including infrared absorbance, wave number, and temperature showed that many volatile compounds are released in the pyrolysis of dried rice husk. Spectral intensity as a function of time can be obtained when the wave number is fixed. This information can be used to analyze the generation of specific components [129]. Stankovikj and Garcia-Perez [131] proposed a new method to identify the position and shape of the peaks of chemical families in the derivative thermogravimetry (DTG) curves and further to estimate the changes in the content of water, light volatile compounds, and water-soluble/insoluble fractions.

Due to the advantages of FTIR analysis, it can be used in biooil analysis for understanding molecular characteristics, evaluation of upgrading process, judging the further utilization, distinguishing biooils from different LCBMs, and so forth.

4.2. GC and Comprehensive Gas Chromatography (GC × GC). GC-FID quantification of hydrocarbons can be performed with a high degree of accuracy using the effective carbon number (ECN) approach [60, 133–135], even when no authentic standard is available. Relative response factors (RRFs) could be calculated by correlation with the chemical formula and were used to qualify compounds in biooil with GC-FID [53, 136]. When considering MW, molecular formula, chemical composition, functional group, and chromatographic retention time, better results could be obtained [60].

Although GC-MS is extensively employed for the componential analysis of biooils, one of the challenges encountered in GC-MS analysis is assay of the mass spectrum of species. The resulting chromatograms are complicated due to the overlapping of peaks and the identification of components relied heavily on the basis of the NIST database. Furthermore, similarities among spectra of substituted species increase the difficulty of identification. Nevertheless, only part of the species could be characterized in the sample. In order to enhance the separation, pretreatments were carried out to concentrate or enrich moieties of species of interest by extraction, distillation, column chromatography, and so forth.

To obtain high peak capacity and resolution, and to gain accurate quantification of the individual components, GC × GC is often used in the compositional analysis of complex samples. GC × GC techniques have the advantage of increased chromatographic resolving power, allowing the detection and characterization of many classes of compounds [71–77, 85–87, 124, 137–139]. The separation is carried out on two columns with different polarities, and a device called modulator located between the two columns transfers the effluent periodically. For a GC × GC system, orthogonal system consists of a nonpolar column and a polar one, while a nonorthogonal system has the opposite combination, called reversed phase system. After simple pretreatments, such as dilution, extraction, and adsorption, biooils can be conducted in a GC × GC system with various detectors including ECD, FID, and MSs. Based on the analysis of GC × GC, retention behavior of species to be determined is plotted along the *x*-/*y*-axis with respect to the two columns concluded in the dispersion graphics (DGs), and the varying color or contour lines of spots represent the intensity of the peaks. Identification and classification of species are performed via statistic and chemometric methods. The qualitative and quantitative approaches of grouped classes of species are demonstrated by the peak density and intensity in different areas on the DGs.

The quantification of species in biooil is based on internal [140] or external standard calibration method [86] with chosen reference compounds, depending on the detector used and the targeted compounds. External calibration can provide accurate quantitative analysis for selected species. However, the analysis is limited to only a few species in the samples because only a small part of species in biooil are commercially available and the concentrations of interested species vary in a wide range. Internal calibration method is a much more versatile quantification method in which an internal standard is chosen as a reference compound with similar structure, retention behavior, and ionization efficiency, compared to the analyte. Based on the RRF of each compound and the internal standard, internal standard quantification can be applied to a wide range of classes of species for quantitative analysis, whatever the variation of sample preparation and analytical instrument [60].

The use of GC × GC, frequently coupled with TOFMS [74] or Q-MS [124], is a promising combination used in the qualitative analysis of biooils for the detailed characterization of compounds. Relatively, GC × GC/TOFMS provides a higher number of identified species compared to GC/Q-MS [141]. Typical 3D plot for componential analysis of biooils using GC × GC/TOFMS is presented in Figure 2. This is most likely attributed to the coelution of species resulting in the overlapping of peaks in GC-MS. Using GC × GC/TOFMS, semiquantitative analysis [26, 142] of samples can be performed using a relative area of detected compounds with a signal-to-noise ratio higher than 1000 and the total of identified compounds in each sample was higher than 80%. With similar method, biooils from catalytic pyrolysis of pine wood and sugarcane bagasse were analyzed, and the results showed that acids, ketones/cyclic ketones, phenols, and O-heterocyclic and aromatic hydrocarbons were the main components [74]. Zhang et al. [124] carried out chemical characterization of crude and ethanol-stabilized biooils before and after accelerated aging treatment using a GC × GC/TOFMS to discuss stabilization mechanism of the addition of ethanol into biooil. Twenty-six standards (C_7–C_{32} *n*-alkanes) in the calibration mixture were used to test instrument capability and evaluate selected quality control parameters. There were 2728, 2212, 2674, and 2781 peaks identified in the crude biooil before/after aging and the ethanol-stabilized biooil before/after aging, respectively, and the major component groups were ketones, phenols, furanones, and acids. The addition of ethanol and accelerated aging treatment could both slightly change the chemical composition of biooils. By using GC × GC/TOFMS, more detailed information could be obtained for comprehensive understanding of internal mechanism of ethanol addition and aging treatment on the storage stability of pyrolysis biooil. Purcaro et al. [73] constructed a GC × GC system coupled with simultaneous dual detectors, FID and MS, for quantitative and qualitative analyses of minor compounds in vegetable oils. Such technique proved to be effective not only in a qualitative viewpoint but also for quantitative purposes, especially for investigation of minor compounds in a single run.

The identification of species was significantly improved by coupling several sensitive detectors or using advanced data handling methods. Meanwhile, the combined analytical system with higher resolution needs to be set up, and the quantitative analysis methods also need to be established.

4.3. HPLC and Two-Dimensional Liquid Chromatography (LC × LC). Compared to GC, HPLC is good at characterizing nonvolatile, unstable, and high MW compounds in the fractions of biooil products. However, the resolution may be poorer than GC due to the length limitation of column and other separation conditions used. Coupled with MS, HPLC is also the extensively used combination for analysis of components in biooil with high sensitivity for species easy to be ionized.

Various HPLC detectors have been used for analyte characterization. Carbonyl compounds, such as aldehydes and ketones, can be qualified by HPLC-UV after derivation with 2,4-dinitrophenylhydrazine (DNPH) [63, 143]. By HPLC, coupled with evaporative light scattering detector (ELSD) [144], triglyceride molecular species of the extracted oil were identified by their ECN and the elution order was

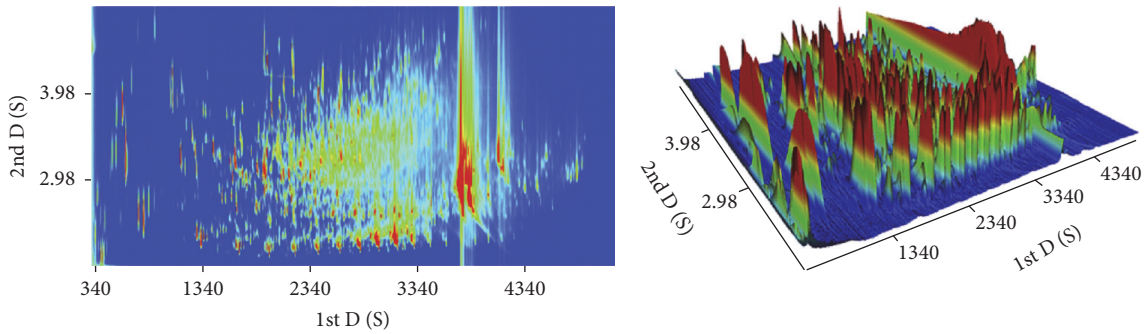

Figure 2: Typical GC × GC/TOFMS analysis of crude pyrolysis oil. (a) Topographic map and (b) tridimensional view [26].

tentatively predicted according to fatty acid composition [145]. As mentioned above, MS detectors including HRMS (e.g., TOFMS, Orbitrap, and FT-ICR) were extensively used in the characterization of components in biooil. More than 400 compounds with MWs mainly distributed between 100 and 400 Da were identified in a biooil by HPLC-Orbitrap MS [60].

The LC × LC separates samples comprehensively via elution in two columns connected in series [65, 146–148]. The establishment of two dimensions is based on either stationary phase in the two columns with different separation mechanisms or elute. Similar with GC × GC system, a modulator or switch (also called interface) was mounted between the two columns. The modulator transfers elute from the primary column to the secondary column quickly with high pressure inside the separation system. The fraction injected into the secondary column should be completely analyzed before the successive transfer occurs, while the second dimension analysis time should be at least equal to or less than the duration of a modulation period. However, because of the retention space being delimited by the retention times of the least and the most retained compounds in both dimensions [146–148], the separation of biooil extracts by LC × LC with a percentage of retention space covers around 50%. Detectors used in the conventional LC system, such as UVD, PDA, ELSD, and MS, can be applied in LC × LC system by direct on-line coupling. Tomasini et al. [148] demonstrated the efficiency of LC×LC equipped with PDA for the componential analysis of a dihydroxygenated biooil with a non-silica-based column and a sub-2 μm silica-based column for the primary and the second dimension, respectively. They prospected number of detectable species up to 2000.

4.4. Mass Spectrometry. MS are often used as detector coupled with chromatographic techniques for the assignment of components in biooils [31, 47, 149–151]. Ionization methods of MS include electrospray ionization (ESI), atmospheric pressure photoionization (APPI), atmospheric pressure chemical ionization (APCI), electron ionization (EI), chemical ionization (CI), fast atom bombardment (FAB), laser desorption ionization (LDI), and matrix assisted laser desorption ionization (MALDI). The former three methods were commonly used due to their mild conditions at either positive or negative mode, also called "soft" ionization methods. ESI is more effective for the detection of polar compounds with lower MWs, while APCI and APPI are more applicable to identify nonpolar molecules [152–154]. Among the ionization methods reported, ESI with negative mode has been used mostly to detect a relative wider range of compounds in biooils. Recent study showed that the combination of ionization methods was more suitable for the characterization of species in biooils [59, 155]. With ESI/APPI FT-ICR MS, furfural derivatives, phenolics, aliphatics, and oligomers were well detected in hydrothermal liquefaction production of glucose and cellulose as model compounds [59]. After comparison of two ionization methods, namely, ESI and APCI, a combination of ESI and APCI at their negative modes were found to be well suited for the characterization of biooils. In the studied biooils, mostly compounds with 1–8 oxygen atoms per molecule were detected and their degree of unsaturation (double-bond equivalence, DBE) was about 1–10 (ESI) and 1–17 (APCI), respectively [155].

In recent years, in order to enhance the sensitivity and selectivity, direct-infusion mass spectrometry (DIMS) analysis has been widely used to detect and identify many chemical compounds in different matrices [156–158], such as liquids produced of pyrolysis and hydrothermal liquefaction. Some advantages of this technique are minimal sample preparation steps, faster analysis, and a wider range of compounds detected at the same injection.

HRMS analysis is based on the accurate mass measurement with sufficiently high mass resolving power for the compounds with different elemental composition. The mass resolving power of HRMS refers to the ability of increasing the mass accuracy with low m/z measurement error allowing separating two narrow mass spectral peaks with similar MW. Generally, the required mass resolving power and accuracy of the mass measurement depend on the complexity of the analyzed sample and the purpose of analysis.

FT-ICR MS provides nonspecific identification of molecular species within a wide range of MW (200–1000 Da) with considerable high mass resolution (better than 0.003 Da) and elucidates the detailed composition of complex samples, such as crude oils, biooils, and liquefied products of coals [28, 50, 74, 76, 159, 160]. The species to be determined should be ionized to fragments first by an ionization source without

structural changes that could potentially lead to misinterpretation of the acquired data. The produced ions are introduced into a cyclotron (called ICR cell) via a high vacuum pump and then undergo cyclotron motion in a homogeneous magnetic field. After sufficient time, the frequency of the ion with expected high accuracy and precision can be acquired. By using the measured frequency, the *m*/*z* of specific ion can be calculated. Mass spectrum can be obtained by resolving the frequencies of ions with Fourier transformation. Due to the high mass resolution power of FT-ICR MS, each spectrum may contain thousands of peaks, and the data interpretation for assessment of corresponding species is crucial issue for the elucidation of the componential of complex mixtures. Kendrick mass defect representation (KMD) [27] (see Figure 3), van Krevelen analytical methods [28] (see Figure 4), and DBE versus carbon number plots [29] (see Figure 5) are frequently used to describe the componential features of classes of species contained in samples detected with FT-ICR MS. More than 800 components composed of heteroatom classes from O_2 to O_{14} with a carbon number of C_6–C_{27} and a DBE of 1–14 were identified in biooil by using ESI(−)-FT-ICR MS [31]. But only 40 of them were detected with conventional GC-MS. An advantage of the FT-ICR MS analysis is that only dilution or addition of ionization assists reagents for sample pretreatment, which is much simpler compared to conventional chromatographic analysis. Elucidation of components with high MWs is a crucial and difficult challenge for the full understanding of the composition of biooil. Another outstanding advantage of FT-ICR MS is that high MW species and heteroatom-containing compounds can be identified and quantified effectively [47, 150, 161, 162]. FT-ICR MS reveals that this part is mainly composed of polyoxygenated highly condensed structures, which is important for direction further treatment and evaluation the utilization [52, 163]. However, FT-ICR MS is not competent for the detection of components with low MWs, indicating that conventional chromatographic techniques are necessary for the complete elucidation of biooils [76, 164]. Another factor limiting its application is the high cost of the instrument setup, which impels researchers to search for alternative HRMS techniques.

In Orbitrap MS, the produced ions from the ionization source are passing throw a series of quadrupoles and deflection lenses before being introduced to analyzer by switching the voltage applied to the deflector lens located on the Orbitrap. In the Orbitrap, ions rotate around the central electrode and oscillate with frequencies of 50–150 kHz for corresponding *m*/*z* of 200–2000 [30, 165]. Alsbou and Helleur [156] carried out a successful componential analysis of species in biooil derived from lignin, cellulose, and forest residue, and levoglucosan, carbohydrates, and lignin derivatives were identified. By using Orbitrap Velos and Orbitrap Elite (in the negative-ion mode of ESI and APCI), significant resolving power was obtained, *that is*, 100000 and 480000 at *m*/*z* 400, and 1900 components were identified in the wood derived biooil [30] (see Figure 6).

TOFMS analysis is fast and sensitive to mass assessment of ions, and the operating principle is very simple. In TOFMS, the produced ions from the ionization source are introduced into the flight tube with the same velocity, and then they are accelerated simultaneously by a pulsed direct-current electric field to a kinetic energy of specific electron volts. The ions fly freely in the high vacuum flight tube to a detector located certain distance away. The *m*/*z* of ions can be calculated based on the proportional relationship to the time required. Masses of ions are measured simultaneously in the process. Compared to FT-ICR MS, Q-TOFMS does not have enough resolution to separate compounds with the same accurate nominal mass. However, Q-TOFMS is a good choice for the effective detection of major components in biooils since it is cheaper and simpler [27, 166, 167].

Orbitrap and Q-TOFMS show better discrimination of smaller ions, while FT-ICR MS is more efficient in distinguishing charged fragments with higher *m*/*z*, *that is*, >300 [74, 83]. FT-ICR MS has been proven to be an ideal technique for the deep componential characterization of biooils, since its significant high resolving power for identification thousands of peaks at the level of molecular formula assignment. The choice of MS depending on the requirement of the analysis of complex mixtures, for most of the cases, Orbitrap and Q-TOFMS, can provide satisfactory results, such as the determination of the MW range, the rough assignment of the high MW components, comparison compositional characters between different biooils, and optimization of pyrolytic conditions. FT-ICR MS is a final choice among the HRMS techniques when the detailed and comprehensive analyses of a biooil are required. Orbitrap or TOFMS can be used for the detection of volatile compounds with fewer carbon and oxygen atoms, *that is*, classes from O_0 to O_8 with a carbon number of C_3–C_{14}, while with ESI-FT-ICR MS allows the identification of a much broader range of polar, volatile and nonvolatile classes, *that is*, O_2–O_{14} with carbon numbers of C_6–C_{27} [74, 76]. More than 8000 and 16000 peaks were identified with ESI(−)-FT-ICR MS in the pine pellet oil and peanut hull biooil, respectively [47]. Typical spectra of HRMS were shown in Figure 7 based on negative ions produced by ESI [31]. Consider the mass resolution and accuracy, the HRMSs follow the order FT-ICR MS > Orbitrap > Q-TOFMS [31, 44, 83].

4.5. NMR and Comprehensive NMR (2D NMR). NMR is a powerful technique for componential characterization of complex mixtures. NMR allows qualitative and quantitative analyses of chemical functionalities and structures in the whole biooil sample without fractionation and assists interpretation of the results of other analytical techniques. Carbon and hydrogen are the main atoms in biooil, so ^1H and ^{13}C NMR were usually used for the determination of their distributions in different structures, such as aliphatic, olefinic, aromatic, methoxy/hydroxy, and carbonyl [168, 169]. ^1H NMR is the most convenient and extensively spectrometric technique used for the quantification analysis of the major components in biooil [15]. The major components identified in biooil with their typical shifts are as follows: alkanes (0.5–1.6 ppm), aromatics (6.4–7.6 ppm), aldehydes (9.5–10.5 ppm), formic acid (8.10 ppm), acetaldehyde (9.58 and 2.08 ppm), levoglucosan (3.27, 3.84–3.85, 4.31–4.33, and 5.13 ppm), glycolaldehyde (9.55 ppm), hydroxyacetone (4.01 ppm), and acetic acid

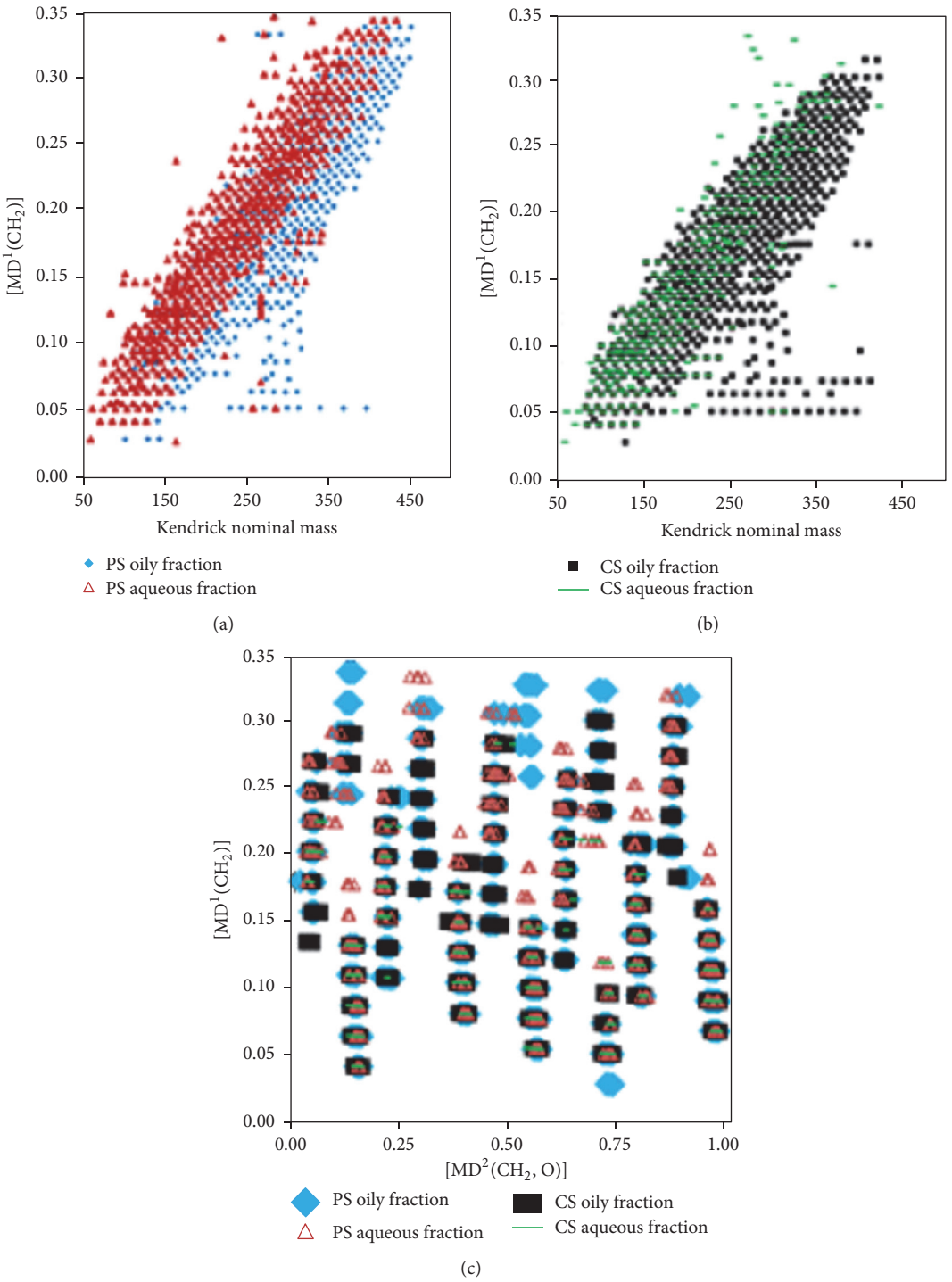

Figure 3: Kendrick mass defect (KMD) analyses for biooil fractions (plotted as a Kendrick mass of CH_2) [27].

(1.88 ppm). ^{13}C NMR can provide quantitative results of carbon in the various functional groups with complementary information for full characterization of species in fractions of biooil [63]. The $^{13}C\{^1H\}$UDEFT (uniform driven equilibrium Fourier transform) sequence allowing for recording the spectra devoid of heteronuclear NOE (nuclear Overhauser effect) was carried out by Díaz-Urrutia et al. [170] for the characterization of lignin with shorter acquisition times. Different types of carbon atoms in various structures were qualified. After derivatization with 2-chloro-4,4,5,5-tetramethyl-1,3,2-dioxaphospholane, hydroxyl and carboxyl functional groups can be quantified with ^{31}P NMR [170]. ^{31}P NMR spectra

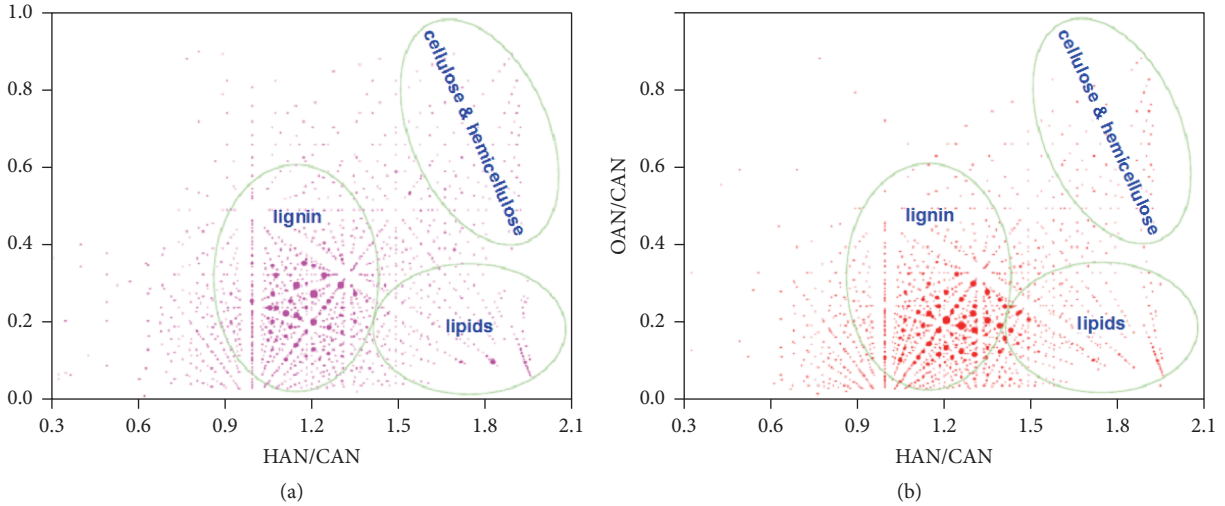

FIGURE 4: van Krevelen diagrams of O_n class species by negative-ion ESI FT-ICR MS analysis [28].

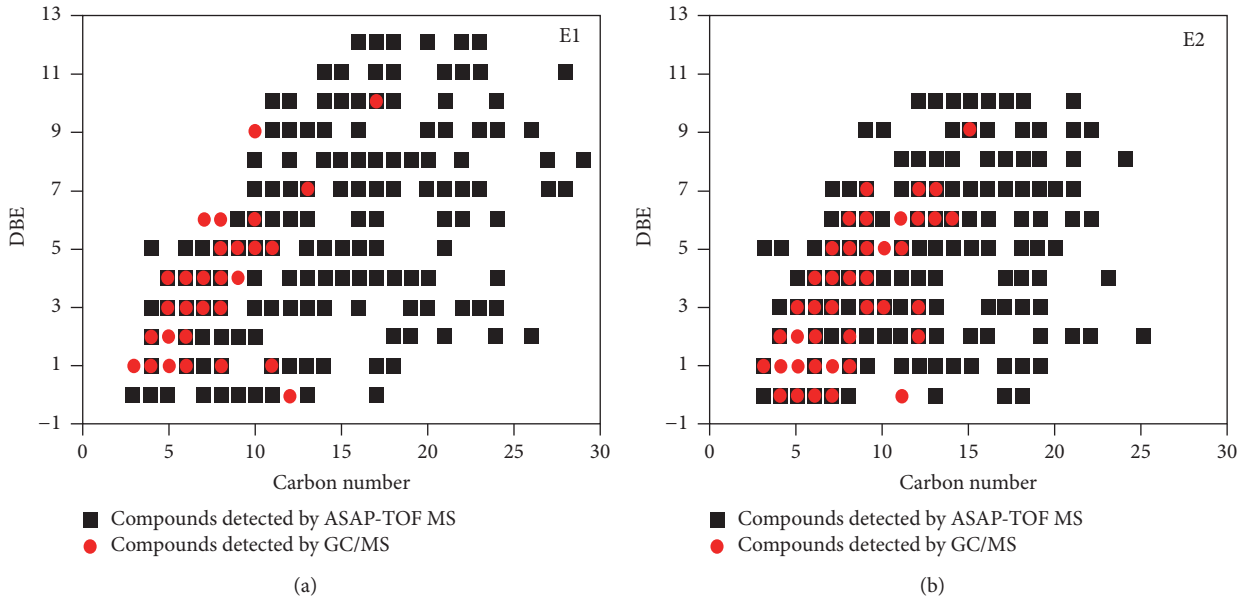

FIGURE 5: DBE versus carbon number of *n*-hexane and CCl_4 extractable species in a rice husk biooil using atmospheric solids analysis probe mass spectrometry [29].

of derived phosphites could also give clear evidence for oxidation of phenolics and lignins to quinines [171–173].

2D NMR provides more detailed information on the overview of functional groups and the corresponding quantitative results in biooils without considering MW [174]. Contents of chemical bonds in biooils, such as C-C, C-O, and C-H bonds, could be quantified with 1D NMR and 2D NMR [175]. 2D NMR and solid state 2D NMR have been proven versatile techniques for the structural analysis of lignin and biomass [176, 177]. Heteronuclear single-quantum correlation-nuclear magnetic resonance (HSQC-NMR) was used to characterize the types of C-H bonds and their presence in different moieties of compounds in biooils [32, 57, 75, 164]. 2D ^{1}H-^{13}C HSQC-NMR was successfully used in the characterization of pyrolytic sugars in fractions of biooil by providing different C-H types in aliphatic, guaiacol, and ferulate structures [32] (see Figure 8). Pyrolysis induces a variety of structural changes to lignin in addition to reduction in MW. In the structural characterization of lignin extracted from the biooil produced by fast pyrolysis of switchgrass *(Panicum virgatum)*, the results of 2D ^{1}H-^{13}C HSQC-NMR analysis showed the absence of γ-methylene hydrogens from β-O-4 linkages, implying rearrangements in the propyl linking chains. Ferulate and hydroxyl phenol esters are still present with lower concentrations in pyrolyzed lignin compared to unpyrolyzed switchgrass lignin [56]. The ^{1}H-^{13}C heteronuclear multiple-bond correlation (HMBC-NMR) spectrum showed that β-O-4 linkages, ferulate esters, and guaiacyl ether linkages remained together, indicating significant difference from the pyrolyzed material [56].

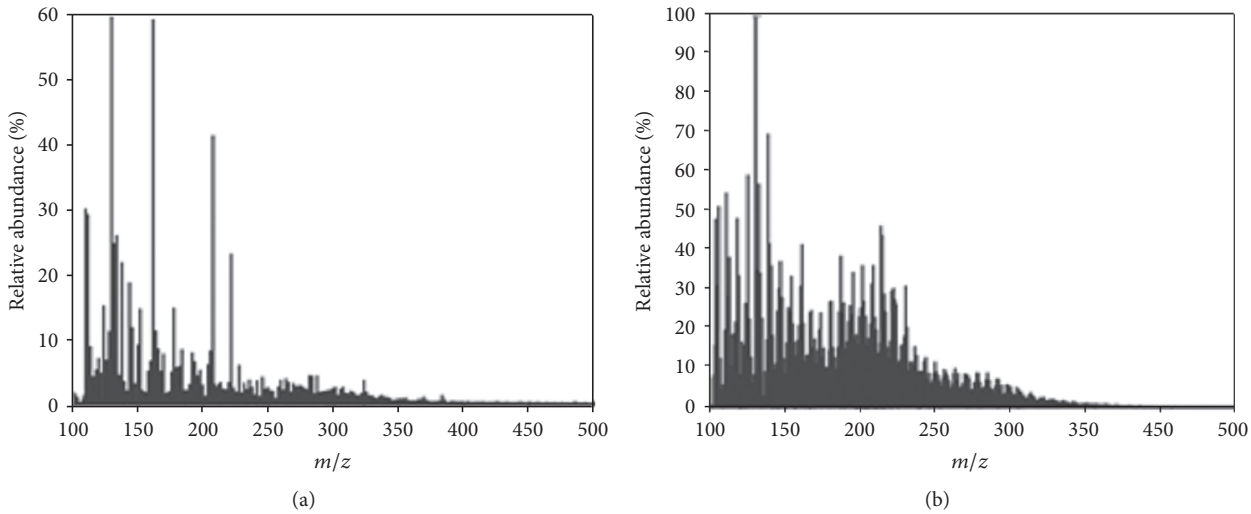

Figure 6: Negative-ion ESI-MS (a) and negative-ion APCI-MS spectra (b) of pyrolysis biooil (Orbitrap Elite; $m/\Delta m_{50}$ = 480,000 at m/z 400) [30].

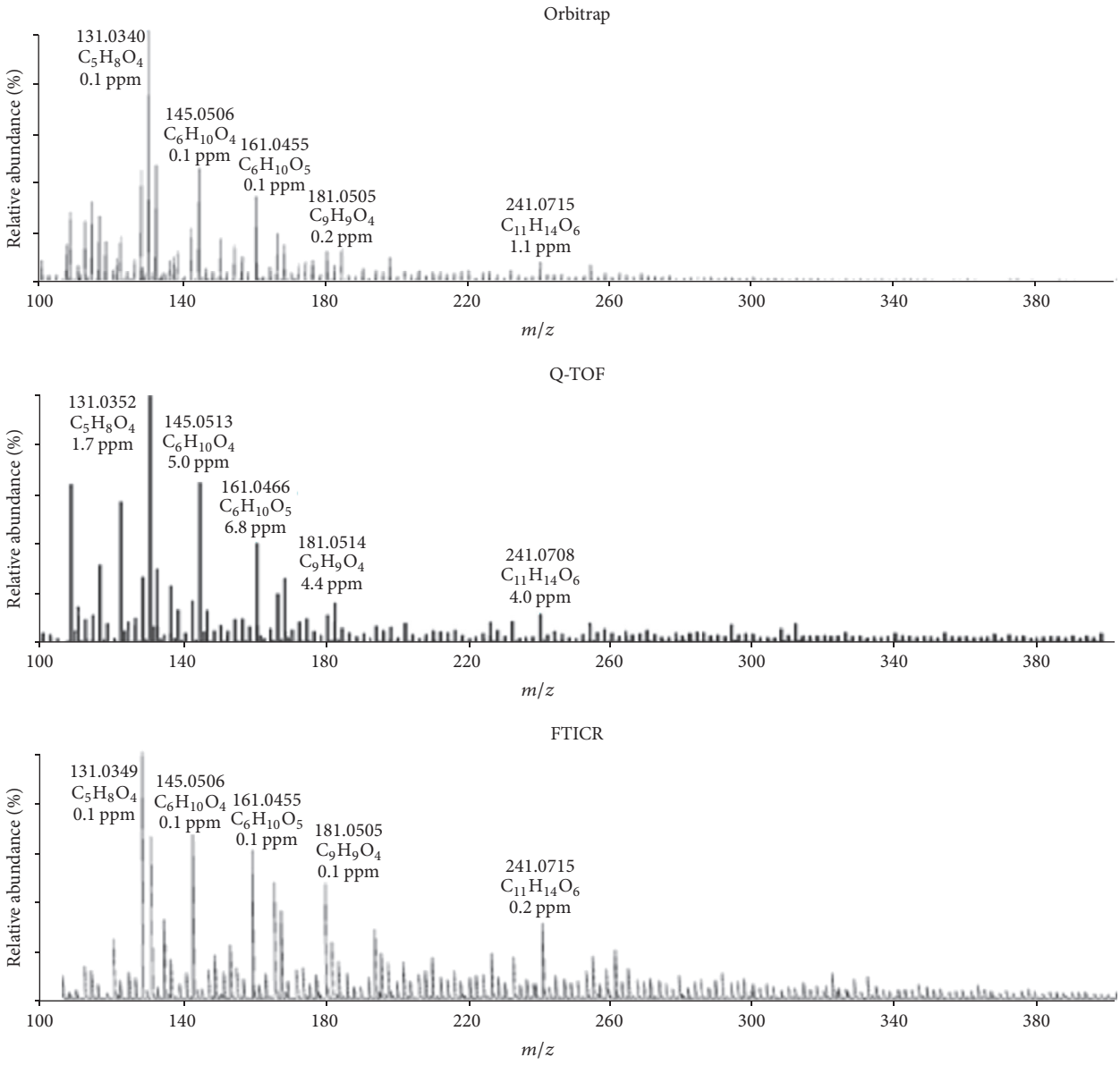

Figure 7: High resolution mass spectra (negative ESI source) of red oak biooils obtained using Orbitrap, Q-TOF, and FT-ICR, respectively [31].

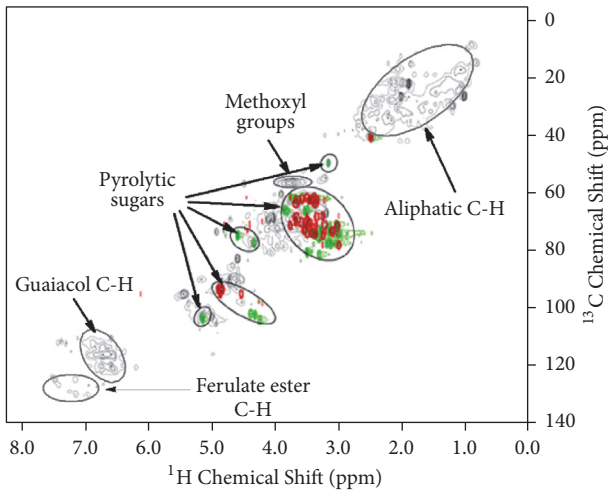

Figure 8: Typical assignments of biooil and various sugar standards in 2D ^{1}H-^{13}C HSQC spectra. Gray: biooil; red: sugar monomers including glucose, galactose, mannose, xylose, and arabinose; green: anhydrosugars including levoglucosan, cellobiosan, and cellotriosan [32].

5. Conclusion and Suggestion

Conventional spectrometric and chromatographic techniques have been applied for the common compositional analysis of biooil allowing detailed determination of its components. FTIR and NMR analyses treat the samples as a whole and provide information on the chemical functional groups and types of chemical bonds. By using conventional HPLC and GC techniques coupled to various detectors, primary identification, and classification of the partial components in biooil with appropriate polarity, MW and boiling point could be obtained. By the combination of pretreatments of sample prior to the chromatographic or spectrometric analyses, the identification of species could be significantly increased. However, more detailed and comprehensive results could not be obtained due to their inherent respective detective limitation, separation capacity, and resolving power of species. The significant development and progress in the comprehensive, hyphenated chromatographic, and spectrometric techniques, such as GC × GC, LC × LC, and 2D NMR, coupled with various MS detectors, have improved the characterization of components in biooil. HRMSs, such as Orbitrap MS, Q-TOFMS, and FT-ICR MS, have been proven effective techniques for the detailed elucidation of components in biooils and complex unknown structures.

With the development of analytical strategies by combining conventional and comprehensive spectrometric and chromatographic techniques, as well as different kinds of HRMSs, significant advancements have been brought for the complete characterization of components in biooils.

Conflicts of Interest

The authors declare that they have no conflicts of interest.

Acknowledgments

This work was supported by the Fundamental Research Funds for the Central Universities (Grant 2014QNA83), the National Natural Science Foundation of China (Grant nos. 21506250, 21676293, and 51604271), and the Natural Science Foundation of Jiangsu Province (Grant no. BK20150182).

References

[1] J. Conti, P. Holtberg, J. Diefenderfer, A. LaRose, J. T. Turnure, and L. Westfall, "International Energy Outlook 2016 With Projections to 2040," Tech. Rep., U.S. Energy InformationAdministration, Washington, DC, USA, 2016.

[2] J. Philp, "Balancing the bioeconomy: Supporting biofuels and bio-based materials in public policy," *Energy & Environmental Science*, vol. 8, no. 11, pp. 3063–3068, 2015.

[3] D. Mohan, C. U. Pittman Jr., and P. H. Steele, "Pyrolysis of wood/biomass for bio-oil: a critical review," *Energy & Fuels*, vol. 20, no. 3, pp. 848–889, 2006.

[4] T. N. Pham, D. Shi, and D. E. Resasco, "Evaluating strategies for catalytic upgrading of pyrolysis oil in liquid phase," *Applied Catalysis B: Environmental*, vol. 145, pp. 10–23, 2014.

[5] A. Dutta, A. Sahir, E. Tan et al., "Process Design and Economics for the Conversion of Lignocellulosic Biomass to Hydrocarbon Fuels. Thermochemical Research Pathways with In Situ and Ex Situ Upgrading of Fast Pyrolysis Vapors," Tech. Rep. NREL/TP-5100-62455, Richland, WA, USA, 2015.

[6] R. C. Brown and T. R. Brown, *Biorenewable Resources: Engineering New Products from Agriculture*, Iowa State Press, Ames, Iowa, USA, 2014.

[7] S. V. Vassilev, D. Baxter, L. K. Andersen, and C. G. Vassileva, "An overview of the chemical composition of biomass," *Fuel*, vol. 89, no. 5, pp. 913–933, 2010.

[8] S. V. Vassilev, D. Baxter, L. K. Andersen, C. G. Vassileva, and T. J. Morgan, "An overview of the organic and inorganic phase composition of biomass," *Fuel*, vol. 94, pp. 1–33, 2012.

[9] S.-Y. No, "Application of bio-oils from lignocellulosic biomass to transportation, heat and power generation - A review," *Renewable & Sustainable Energy Reviews*, vol. 40, pp. 1108–1125, 2014.

[10] T. Stedile, L. Ender, H. F. Meier, E. L. Simionatto, and V. R. Wiggers, "Comparison between physical properties and chemical composition of bio-oils derived from lignocellulose and triglyceride sources," *Renewable & Sustainable Energy Reviews*, vol. 50, pp. 92–108, 2015.

[11] H. Kuo, B. Hou, and A. Huang, "The influences of the gas fluidization velocity on the properties of bio-oils from fluidized bed pyrolyzer with in-line distillation," *Applied Energy*, vol. 194, pp. 279–286, 2017.

[12] G. Kabir and B. H. Hameed, "Recent progress on catalytic pyrolysis of lignocellulosic biomass to high-grade bio-oil and bio-chemicals," *Renewable & Sustainable Energy Reviews*, vol. 70, pp. 945–967, 2017.

[13] N. S. Shamsul, S. K. Kamarudin, and N. A. Rahman, "Conversion of bio-oil to bio gasoline via pyrolysis and hydrothermal: A review," *Renewable & Sustainable Energy Reviews*, vol. 80, pp. 538–549, 2017.

[14] N. Bordoloi, R. Narzari, D. Sut, R. Saikia, R. S. Chutia, and R. Kataki, "Characterization of bio-oil and its sub-fractions from pyrolysis of Scenedesmus dimorphus," *Journal of Renewable Energy*, vol. 98, pp. 245–253, 2016.

[15] T. Wigley, A. C. K. Yip, and S. Pang, "A detailed product analysis of bio-oil from fast pyrolysis of demineralised and torrefied biomass," *Journal of Analytical and Applied Pyrolysis*, vol. 123, pp. 194–203, 2017.

[16] A. Oasmaa and C. Peacocke, *A Guide to Physical Property Characterisation of Biomassderived Fast Pyrolysis Liquids*, Espoo, FI: VTT Technical Research Center of Finland, 2001.

[17] M. Stas, D. Kubicka, J. Chudoba, and M. Pospisil, "Overview of analytical methods used for chemical characterization of pyrolysis bio-oil," *Energy & Fuels*, vol. 28, no. 1, pp. 385–402, 2014.

[18] P. K. Kanaujia, Y. K. Sharma, M. O. Garg, D. Tripathi, and R. Singh, "Review of analytical strategies in the production and upgrading of bio-oils derived from lignocellulosic biomass," *Journal of Analytical and Applied Pyrolysis*, vol. 105, pp. 55–74, 2014.

[19] S.-Z. Wang, X. Fan, A.-L. Zheng et al., "Evaluation of the Oxidation of Rice Husks with Sodium Hypochlorite Using Gas Chromatography-Mass Spectrometry and Direct Analysis in Real Time-Mass Spectrometry," *Analytical Letters*, vol. 47, no. 1, pp. 77–90, 2014.

[20] A. V. Bridgwater, "Principles and practice of biomass fast pyrolysis processes for liquids," *Journal of Analytical and Applied Pyrolysis*, vol. 51, no. 1, pp. 3–22, 1999.

[21] Y. Lu, X.-Y. Wei, J.-P. Cao et al., "Characterization of a bio-oil from pyrolysis of rice husk by detailed compositional analysis and structural investigation of lignin," *Bioresource Technology*, vol. 116, pp. 114–119, 2012.

[22] H. Hassan, J. K. Lim, and B. H. Hameed, "Recent progress on biomass co-pyrolysis conversion into high-quality bio-oil," *Bioresource Technology*, vol. 221, pp. 645–655, 2016.

[23] J. Lehto, A. Oasmaa, Y. Solantausta, M. Kytö, and D. Chiaramonti, "Review of fuel oil quality and combustion of fast pyrolysis bio-oils from lignocellulosic biomass," *Applied Energy*, vol. 116, pp. 178–190, 2014.

[24] A. Oasmaa and P. Cordner, *Properties and Fuel Use of Biomass-derived Fast Pyrolysis Liquids: A Guide*, VTT Technical Research Center of Finland, Espoo, Finland, 2010.

[25] M. Castellví Barnés, J.-P. Lange, G. Van Rossum, and S. R. A. Kersten, "A new approach for bio-oil characterization based on gel permeation chromatography preparative fractionation," *Journal of Analytical and Applied Pyrolysis*, vol. 113, article 3445, pp. 444–453, 2015.

[26] R. V. S. Silva, A. Casilli, A. L. Sampaio et al., "The analytical characterization of castor seed cake pyrolysis bio-oils by using comprehensive GC coupled to time of flight mass spectrometry," *Journal of Analytical and Applied Pyrolysis*, vol. 106, pp. 152–159, 2014.

[27] B. Dhungana, C. Becker, B. Zekavat, T. Solouki, W. C. Hockaday, and C. K. Chambliss, "Characterization of slow-pyrolysis bio-oils by high-resolution mass spectrometry and ion mobility spectrometry," *Energy & Fuels*, vol. 29, no. 2, pp. 744–753, 2015.

[28] H.-L. Yan, Z.-M. Zong, Z.-K. Li, and X.-Y. Wei, "Characterization of bio-oils from the alkanolyses of sweet sorghum stalk by electrospray ionization Fourier transform ion cyclotron resonance mass spectrometry," *Fuel*, vol. 160, pp. 596–604, 2015.

[29] X. Fan, J.-L. Zhu, A.-L. Zheng et al., "Rapid characterization of heteroatomic molecules in a bio-oil from pyrolysis of rice husk using atmospheric solids analysis probe mass spectrometry," *Journal of Analytical and Applied Pyrolysis*, vol. 115, pp. 16–23, 2015.

[30] M. Staš, J. Chudoba, D. Kubička, and M. Pospíšil, "Chemical characterization of pyrolysis bio-oil: Application of orbitrap mass spectrometry," *Energy & Fuels*, vol. 29, no. 5, pp. 3233–3240, 2015.

[31] E. A. Smith, S. Park, A. T. Klein, and Y. J. Lee, "Bio-oil analysis using negative electrospray ionization: Comparative study of high-resolution mass spectrometers and phenolic versus sugaric components," *Energy & Fuels*, vol. 26, no. 6, pp. 3796–3802, 2012.

[32] Y. Yu, Y. W. Chua, and H. Wu, "Characterization of Pyrolytic Sugars in Bio-Oil Produced from Biomass Fast Pyrolysis," *Energy & Fuels*, vol. 30, no. 5, pp. 4145–4149, 2016.

[33] Y. Lu, X.-Y. Wei, F.-J. Liu et al., "Evaluation of an upgraded bio-oil from the pyrolysis of rice husk by acidic resin-catalyzed esterification," *Energy Sources, Part A: Recovery, Utilization, and Environmental Effects*, vol. 36, no. 6, pp. 575–581, 2014.

[34] M. Saber, B. Nakhshiniev, and K. Yoshikawa, "A review of production and upgrading of algal bio-oil," *Renewable & Sustainable Energy Reviews*, vol. 58, pp. 918–930, 2016.

[35] P. Duan, C. Zhang, F. Wang et al., "Activated carbons for the hydrothermal upgrading of crude duckweed bio-oil," *Catalysis Today*, vol. 274, pp. 73–81, 2016.

[36] I. Graca, J. M. Lopes, H. S. Cerqueira, and M. F. Ribeiro, "Bio-oils upgrading for second generation biofuels," *Industrial & Engineering Chemistry Research*, vol. 52, no. 1, pp. 275–287, 2013.

[37] Y. Liu, Z. Li, J. J. Leahy, and W. Kwapinski, "Catalytically upgrading bio-oil via esterification," *Energy & Fuels*, vol. 29, no. 6, pp. 3691–3698, 2015.

[38] Q. Guo, M. Wu, K. Wang, L. Zhang, and X. Xu, "Catalytic hydrodeoxygenation of algae bio-oil over bimetallic Ni-Cu/ZrO2 catalysts," *Industrial & Engineering Chemistry Research*, vol. 54, no. 3, pp. 890–899, 2015.

[39] H. Lee, Y.-M. Kim, I.-G. Lee et al., "Recent advances in the catalytic hydrodeoxygenation of bio-oil," *Korean Journal of Chemical Engineering*, vol. 33, no. 12, pp. 3299–3315, 2016.

[40] Z. Si, X. Zhang, C. Wang, L. Ma, and R. Dong, "An overview on catalytic hydrodeoxygenation of pyrolysis oil and its model compounds," *Journal of Catalysis*, vol. 7, no. 6, pp. 169–190, 2017.

[41] X. Li, G. Chen, C. Liu, W. Ma, B. Yan, and J. Zhang, "Hydrodeoxygenation of lignin-derived bio-oil using molecular sieves supported metal catalysts: A critical review," *Renewable & Sustainable Energy Reviews*, vol. 71, pp. 296–308, 2017.

[42] R. Lodeng, L. Hannevold, H. Bergem, and M. Stöcker, "The role of catalysis for the sustainable production of bio-fuels and bio-chemicals," *Focus on Catalysts*, vol. 2013, no. 11, p. 8, 2013.

[43] A. R. Ardiyanti, R. H. Venderbosch, W. Yin, and H. J. Heeres, *Catalytic Hydrogenation for Biomass Valorization*, RSC Publishing, UK, 2015.

[44] C. M. Michailof, K. G. Kalogiannis, T. Sfetsas, D. T. Patiaka, and A. A. Lappas, "Advanced analytical techniques for bio-oil characterization," *Wiley Interdisciplinary Reviews: Energy and Environment*, vol. 5, no. 6, pp. 614–639, 2016.

[45] R. Bayerbach and D. Meier, "Characterization of the water-insoluble fraction from fast pyrolysis liquids (pyrolytic lignin). Part IV: Structure elucidation of oligomeric molecules," *Journal of Analytical and Applied Pyrolysis*, vol. 85, no. 1-2, pp. 98–107, 2009.

[46] X. Fan, X.-Y. Wei, and Z.-M. Zong, "Application of gas chromatography/mass spectrometry in studies on separation and identification of organic species in coals," *Fuel*, vol. 109, pp. 28–32, 2013.

[47] J. M. Jarvis, A. M. McKenna, R. N. Hilten, K. C. Das, R. P. Rodgers, and A. G. Marshall, "Characterization of pine pellet and peanut hull pyrolysis bio-oils by negative-ion electrospray ionization fourier transform ion cyclotron resonance mass spectrometry," *Energy & Fuels*, vol. 26, no. 6, pp. 3810–3815, 2012.

[48] P. K. Kanaujia, Y. K. Sharma, U. C. Agrawal, and M. O. Garg, "Analytical approaches to characterizing pyrolysis oil from biomass," *TrAC - Trends in Analytical Chemistry*, vol. 42, pp. 125–136, 2013.

[49] K. M. Yenkie, W. Wu, R. L. Clark, B. F. Pfleger, T. W. Root, and C. T. Maravelias, "A roadmap for the synthesis of separation networks for the recovery of bio-based chemicals: Matching biological and process feasibility," *Biotechnology Advances*, vol. 34, no. 8, pp. 1362–1383, 2016.

[50] J. Zuber, M. M. Kroll, P. Rathsack, and M. Otto, "Gas Chromatography/atmospheric pressure chemical ionization-fourier transform ion cyclotron resonance mass spectrometry of pyrolysis oil from german brown coal," *International Journal of Analytical Chemistry*, vol. 2016, Article ID 5960916, 12 pages, 2016.

[51] A. Imran, E. A. Bramer, K. Seshan, and G. Brem, "High quality bio-oil from catalytic flash pyrolysis of lignocellulosic biomass over alumina-supported sodium carbonate," *Fuel Processing Technology*, vol. 127, pp. 72–79, 2014.

[52] N. Sudasinghe, J. R. Cort, R. Hallen, M. Olarte, A. Schmidt, and T. Schaub, "Hydrothermal liquefaction oil and hydrotreated product from pine feedstock characterized by heteronuclear two-dimensional NMR spectroscopy and FT-ICR mass spectrometry," *Fuel*, vol. 137, pp. 60–69, 2014.

[53] J. E. Szulejko, Y.-H. Kim, and K.-H. Kim, "Method to predict gas chromatographic response factors for the trace-level analysis of volatile organic compounds based on the effective carbon number concept," *Journal of Separation Science*, vol. 36, no. 20, pp. 3356–3365, 2013.

[54] R. M. Santos, A. O. Santos, E. M. Sussuchi, J. S. Nascimento, A. S. Lima, and L. S. Freitas, "Pyrolysis of mangaba seed: Production and characterization of bio-oil," *Bioresource Technology*, vol. 196, pp. 43–48, 2015.

[55] Y. Elkasabi, C. A. Mullen, M. A. Jackson, and A. A. Boateng, "Characterization of fast-pyrolysis bio-oil distillation residues and their potential applications," *Journal of Analytical and Applied Pyrolysis*, vol. 114, pp. 179–186, 2015.

[56] M. Fortin, M. Mohadjer Beromi, A. Lai et al., "Structural Analysis of Pyrolytic Lignins Isolated from Switchgrass Fast-Pyrolysis Oil," *Energy & Fuels*, vol. 29, no. 12, pp. 8017–8026, 2015.

[57] H. Ben and A. J. Ragauskas, "Comparison for the compositions of fast and slow pyrolysis oils by NMR characterization," *Bioresource Technology*, vol. 147, pp. 577–584, 2013.

[58] J. Joseph, M. J. Rasmussen, J. P. Fecteau et al., "Compositional Changes to Low Water Content Bio-oils during Aging: An NMR, GC/MS, and LC/MS Study," *Energy & Fuels*, vol. 30, no. 6, pp. 4825–4840, 2016.

[59] A. Croce, E. Battistel, S. Chiaberge, S. Spera, S. Reale, and F. De Angelis, "Mass Spectrometry and Nuclear Magnetic Resonance Spectroscopy Study of Carbohydrate Decomposition by Hydrothermal Liquefaction Treatment: A Modeling Approach on Bio-oil Production from Organic Wastes," *Energy & Fuels*, vol. 29, no. 9, pp. 5847–5856, 2015.

[60] A. Undri, M. Abou-Zaid, C. Briens et al., "A simple procedure for chromatographic analysis of bio-oils from pyrolysis," *Journal of Analytical and Applied Pyrolysis*, vol. 114, pp. 208–221, 2015.

[61] F. Y. S. Choi, P. A. Johnston, R. C. Brown, B. H. Shanks, and K.-H. Lee, "Detailed characterization of red oak-derived pyrolysis oil: Integrated use of GC, HPLC, IC, GPC and Karl-Fischer," *Journal of Analytical and Applied Pyrolysis*, vol. 110, pp. 147–154, 2014.

[62] M. R. Rover, P. A. Johnston, B. P. Lamsal, and R. C. Brown, "Total water-soluble sugars quantification in bio-oil using the phenol-sulfuric acid assay," *Journal of Analytical and Applied Pyrolysis*, vol. 104, pp. 194–201, 2013.

[63] E. D. Christensen, G. M. Chupka, J. Luecke et al., "Analysis of oxygenated compounds in hydrotreated biomass fast pyrolysis oil distillate fractions," *Energy & Fuels*, vol. 25, no. 11, pp. 5462–5471, 2011.

[64] E. Hoekstra, W. P. M. Van Swaaij, S. R. A. Kersten, and K. J. A. Hogendoorn, "Fast pyrolysis in a novel wire-mesh reactor: Decomposition of pine wood and model compounds," *Chemical Engineering Journal*, vol. 187, pp. 172–184, 2012.

[65] M. Sarrut, A. Corgier, G. Crétier, A. Le Masle, S. Dubant, and S. Heinisch, "Potential and limitations of on-line comprehensive reversed phase liquid chromatography×supercritical fluid chromatography for the separation of neutral compounds: An approach to separate an aqueous extract of bio-oil," *Journal of Chromatography A*, vol. 1402, pp. 124–133, 2015.

[66] A.-N. Huang, C.-P. Hsu, B.-R. Hou, and H.-P. Kuo, "Production and separation of rice husk pyrolysis bio-oils from a fractional distillation column connected fluidized bed reactor," *Powder Technology*, 2016.

[67] J. L. Heelan, B. C. Gates, S. E. Ebeler, and D. E. Block, "Catalytic conversion of biofuel components: Product analysis by multidetector gas chromatography," *Energy & Fuels*, vol. 29, no. 3, pp. 1801–1811, 2015.

[68] T. M. Almeida, M. D. Bispo, A. R. T. Cardoso et al., "Preliminary studies of bio-oil from fast pyrolysis of coconut fibers," *Journal of Agricultural and Food Chemistry*, vol. 61, no. 28, pp. 6812–6821, 2013.

[69] U. Moralı, N. Yavuzel, and S. Şensöz, "Pyrolysis of hornbeam (Carpinus betulus L.) sawdust: Characterization of bio-oil and bio-char," *Bioresource Technology*, vol. 221, pp. 682–685, 2016.

[70] S. Gutierrez Sama, A. Desprez, G. Krier et al., "Study of the Aggregation of Metal Complexes with Asphaltenes Using Gel Permeation Chromatography Inductively Coupled Plasma High-Resolution Mass Spectrometry," *Energy & Fuels*, vol. 30, no. 9, pp. 6907–6912, 2016.

[71] J. A. Murray, "Qualitative and quantitative approaches in comprehensive two-dimensional gas chromatography," *Journal of Chromatography A*, vol. 1261, pp. 58–68, 2012.

[72] I. D. V. Torri, V. Paasikallio, C. S. Faccini et al., "Bio-oil production of softwood and hardwood forest industry residues through fast and intermediate pyrolysis and its chromatographic characterization," *Bioresource Technology*, vol. 200, pp. 680–690, 2016.

[73] G. Purcaro, L. Barp, M. Beccaria, and L. S. Conte, "Characterisation of minor components in vegetable oil by comprehensive gas chromatography with dual detection," *Food Chemistry*, vol. 212, pp. 730–738, 2016.

[74] N. S. Tessarolo, R. V. S. Silva, G. Vanini et al., "Characterization of thermal and catalytic pyrolysis bio-oils by high-resolution techniques: 1H NMR, GC × GC-TOFMS and FT-ICR MS,"

Journal of Analytical and Applied Pyrolysis, vol. 117, pp. 257–267, 2016.

[75] C. Michailof, T. Sfetsas, S. Stefanidis, K. Kalogiannis, G. Theodoridis, and A. Lappas, "Quantitative and qualitative analysis of hemicellulose, cellulose and lignin bio-oils by comprehensive two-dimensional gas chromatography with time-of-flight mass spectrometry," *Journal of Chromatography A*, vol. 1369, pp. 147–160, 2014.

[76] N. S. Tessarolo, R. C. Silva, G. Vanini et al., "Assessing the chemical composition of bio-oils using FT-ICR mass spectrometry and comprehensive two-dimensional gas chromatography with time-of-flight mass spectrometry," *Microchemical Journal*, vol. 117, pp. 68–76, 2014.

[77] L. L. P. Van Stee, J. Beens, R. J. J. Vreuls, and U. A. T. Brinkman, "Comprehensive two-dimensional gas chromatography with atomic emission detection and correlation with mass spectrometric detection: Principles and application in petrochemical analysis," *Journal of Chromatography A*, vol. 1019, no. 1-2, pp. 89–99, 2003.

[78] A. Kloekhorst, J. Wildschut, and H. J. Heeres, "Catalytic hydrotreatment of pyrolytic lignins to give alkylphenolics and aromatics using a supported Ru catalyst," *Catalysis Science & Technology*, vol. 4, no. 8, pp. 2367–2377, 2014.

[79] A.-L. Zheng, X. Fan, F.-J. Liu et al., "Characterization of Zhundong subbituminous coal by time-of-flight mass spectrometry equipped with atmospheric pressure photoionization ion source," *Fuel Processing Technology*, vol. 117, pp. 60–65, 2014.

[80] J.-L. Zhu, X. Fan, X.-Y. Wei et al., "Molecular characterization of heteroatomic compounds in a high-temperature coal tar using three mass spectrometers," *Fuel Processing Technology*, vol. 138, pp. 65–73, 2015.

[81] D. F. Gurka, S. Pyle, and R. Titus, "Environmental Applications of Gas Chromatography/Atomic Emission Detection," *Analytical Chemistry*, vol. 69, no. 13, pp. 2411–2417, 1997.

[82] M. Wang, X. Fan, X.-Y. Wei et al., "Characterization of the oxidation products of Shengli lignite using mass spectrometers with 'hard', 'soft' and ambient ion sources," *Fuel*, vol. 183, pp. 115–122, 2016.

[83] P. V. Abdelnur, B. G. Vaz, J. D. Rocha, M. B. B. De Almeida, M. A. G. Teixeira, and R. C. L. Pereira, "Characterization of bio-oils from different pyrolysis process steps and biomass using high-resolution mass spectrometry," *Energy & Fuels*, vol. 27, no. 11, pp. 6646–6654, 2013.

[84] X. Fan, Y.-R. Yu, J.-L. Xia et al., "Analysis of soluble components in coals and interpretations for the complex mass spectra," *Rapid Communications in Mass Spectrometry*, vol. 31, no. 6, pp. 503–508, 2017.

[85] M. R. Djokic, T. Dijkmans, G. Yildiz, W. Prins, and K. M. Van Geem, "Quantitative analysis of crude and stabilized bio-oils by comprehensive two-dimensional gas-chromatography," *Journal of Chromatography A*, vol. 1257, pp. 131–140, 2012.

[86] T. Sfetsas, C. Michailof, A. Lappas, Q. Li, and B. Kneale, "Qualitative and quantitative analysis of pyrolysis oil by gas chromatography with flame ionization detection and comprehensive two-dimensional gas chromatography with time-of-flight mass spectrometry," *Journal of Chromatography A*, vol. 1218, no. 21, pp. 3317–3325, 2011.

[87] P. Q. Tranchida, S. Salivo, F. A. Franchina, and L. Mondello, "Flow-modulated comprehensive two-dimensional gas chromatography combined with a high-resolution time-of-flight mass spectrometer: A proof-of-principle study," *Analytical Chemistry*, vol. 87, no. 5, pp. 2925–2930, 2015.

[88] J.-L. Xia, X. Fan, C.-Y. You, X.-Y. Wei, Y.-P. Zhao, and J.-P. Cao, "Sequential ultrasonic extraction of a Chinese coal and characterization of nitrogen-containing compounds in the extracts using high-performance liquid chromatography with mass spectrometry," *Journal of Separation Science*, vol. 39, no. 13, pp. 2491–2498, 2016.

[89] S. Grundas, A. Arenillas, and J. Á. Menéndez, "Microwave heating applied to pyrolysis," in *Advances in Induction and Microwave Heating of Mineral and Organic Materials*, 752, p. 723, InTech, Croatia, 2011.

[90] S. M. Abdul Aziz, R. Wahi, Z. Ngaini, and S. Hamdan, "Bio-oils from microwave pyrolysis of agricultural wastes," *Fuel Processing Technology*, vol. 106, pp. 744–750, 2013.

[91] R. J. M. Westerhof, D. W. F. Brilman, M. Garcia-Perez, Z. Wang, S. R. G. Oudenhoven, and S. R. A. Kersten, "Stepwise fast pyrolysis of pine wood," *Energy & Fuels*, vol. 26, no. 12, pp. 7263–7273, 2012.

[92] A. Zheng, Z. Zhao, S. Chang, Z. Huang, F. He, and H. Li, "Effect of torrefaction temperature on product distribution from two-staged pyrolysis of biomass," *Energy & Fuels*, vol. 26, no. 5, pp. 2968–2974, 2012.

[93] A. A. Salema and F. N. Ani, "Pyrolysis of oil palm empty fruit bunch biomass pellets using multimode microwave irradiation," *Bioresource Technology*, vol. 125, pp. 102–107, 2012.

[94] Q. Bu, H. Lei, L. Wang et al., "Renewable phenols production by catalytic microwave pyrolysis of Douglas fir sawdust pellets with activated carbon catalysts," *Bioresource Technology*, vol. 142, pp. 546–552, 2013.

[95] Q. Bu, H. Lei, L. Wang et al., "Bio-based phenols and fuel production from catalytic microwave pyrolysis of lignin by activated carbons," *Bioresource Technology*, vol. 162, pp. 142–147, 2014.

[96] M. Auta, L. M. Ern, and B. H. Hameed, "Fixed-bed catalytic and non-catalytic empty fruit bunch biomass pyrolysis," *Journal of Analytical and Applied Pyrolysis*, vol. 107, pp. 67–72, 2014.

[97] C. Peng, G. Zhang, J. Yue, and G. Xu, "Pyrolysis of lignin for phenols with alkaline additive," *Fuel Processing Technology*, vol. 124, pp. 212–221, 2014.

[98] J.-S. Kim, "Production, separation and applications of phenolic-rich bio-oil - A review," *Bioresource Technology*, vol. 178, pp. 90–98, 2015.

[99] W.-H. Yan, P.-G. Duan, F. Wang, and Y.-P. Xu, "Composition of the bio-oil from the hydrothermal liquefaction of duckweed and the influence of the extraction solvents," *Fuel*, vol. 185, pp. 229–235, 2016.

[100] Y. Wei, H. Lei, L. Wang et al., "Liquid-liquid extraction of biomass pyrolysis bio-oil," *Energy & Fuels*, vol. 28, no. 2, pp. 1207–1212, 2014.

[101] S. Wang, Y. Wang, Q. Cai, X. Wang, H. Jin, and Z. Luo, "Multi-step separation of monophenols and pyrolytic lignins from the water-insoluble phase of bio-oil," *Separation and Purification Technology*, vol. 122, pp. 248–255, 2014.

[102] P. K. Rout, M. K. Naik, S. N. Naik, V. V. Goud, L. M. Das, and A. K. Dalai, "Supercritical CO 2 fractionation of bio-oil produced from mixed biomass of wheat and wood sawdust," *Energy & Fuels*, vol. 23, no. 12, pp. 6181–6188, 2009.

[103] S. Naik, V. V. Goud, P. K. Rout, and A. K. Dalai, "Supercritical CO2 fractionation of bio-oil produced from wheat-hemlock biomass," *Bioresource Technology*, vol. 101, no. 19, pp. 7605–7613, 2010.

[104] J. Wang, H. Cui, S. Wei et al., "Separation of Biomass Pyrolysis Oil by Supercritical CO2 Extraction," *Smart Grid and Renewable Energy*, vol. 01, no. 02, pp. 98–107, 2010.

[105] M. D. Matovic, "High-efficiency separation of bio-oil," in *Biomass Now – Sustainable Growth and Use*, 418, p. 401, InTech, Croatia, 2013.

[106] T. Cheng, Y. Han, Y. Zhang, and C. Xu, "Molecular composition of oxygenated compounds in fast pyrolysis bio-oil and its supercritical fluid extracts," *Fuel*, vol. 172, pp. 49–57, 2016.

[107] S. Czernik and A. V. Bridgwater, "Overview of applications of biomass fast pyrolysis oil," *Energy & Fuels*, vol. 18, no. 2, pp. 590–598, 2004.

[108] S. Wang, Y. Gu, Q. Liu et al., "Separation of bio-oil by molecular distillation," *Fuel Processing Technology*, vol. 90, no. 5, pp. 738–745, 2009.

[109] Y. Wang, S. Wang, F. Leng, J. Chen, L. Zhu, and Z. Luo, "Separation and characterization of pyrolytic lignins from the heavy fraction of bio-oil by molecular distillation," *Separation and Purification Technology*, vol. 152, pp. 123–132, 2015.

[110] Z. Guo, S. Wang, Y. Gu, G. Xu, X. Li, and Z. Luo, "Separation characteristics of biomass pyrolysis oil in molecular distillation," *Separation and Purification Technology*, vol. 76, no. 1, pp. 52–57, 2010.

[111] S. Kumar, J. P. Lange, G. Van Rossum, and S. R. A. Kersten, "Bio-oil fractionation by temperature-swing extraction: Principle and application," *Biomass & Bioenergy*, vol. 83, pp. 96–104, 2015.

[112] N. Özbay, B. B. Uzun, E. A. Varol, and A. E. Pütün, "Comparative analysis of pyrolysis oils and its subfractions under different atmospheric conditions," *Fuel Processing Technology*, vol. 87, no. 11, pp. 1013–1019, 2006.

[113] B. B. Uzun, A. E. Pütün, and E. Pütün, "Rapid pyrolysis of olive residue. 1. Effect of heat and mass transfer limitations on product yields and bio-oil compositions," *Energy & Fuels*, vol. 21, no. 3, pp. 1768–1776, 2007.

[114] S. Yorgun and D. Yildiz, "Slow pyrolysis of paulownia wood: Effects of pyrolysis parameters on product yields and bio-oil characterization," *Journal of Analytical and Applied Pyrolysis*, vol. 114, pp. 68–78, 2015.

[115] N. Bordoloi, R. Narzari, R. S. Chutia, T. Bhaskar, and R. Kataki, "Pyrolysis of Mesua ferrea and Pongamia glabra seed cover: Characterization of bio-oil and its sub-fractions," *Bioresource Technology*, vol. 178, pp. 83–89, 2015.

[116] F. Zeng, W. Liu, H. Jiang, H.-Q. Yu, R. J. Zeng, and Q. Guo, "Separation of phthalate esters from bio-oil derived from rice husk by a basification-acidification process and column chromatography," *Bioresource Technology*, vol. 102, no. 2, pp. 1982–1987, 2011.

[117] M. R. Rover, P. A. Johnston, L. E. Whitmer, R. G. Smith, and R. C. Brown, "The effect of pyrolysis temperature on recovery of bio-oil as distinctive stage fractions," *Journal of Analytical and Applied Pyrolysis*, vol. 105, pp. 262–268, 2014.

[118] S. Kumar, J.-P. Lange, G. Van Rossum, and S. R. A. Kersten, "Liquefaction of lignocellulose: Do basic and acidic additives help out?" *Chemical Engineering Journal*, vol. 278, pp. 99–104, 2015.

[119] U. Morali and S. Şensöz, "Pyrolysis of hornbeam shell (Carpinus betulus L.) in a fixed bed reactor: Characterization of bio-oil and bio-char," *Fuel*, vol. 150, pp. 672–678, 2015.

[120] S. Zhou, D. Mourant, C. Lievens, Y. Wang, C. Li, and M. Garcia-Perez, "Effect of sulfuric acid concentration on the yield and properties of the bio-oils obtained from the auger and fast pyrolysis of Douglas Fir," *Fuel*, vol. 104, pp. 536–546, 2013.

[121] S.-S. Liaw, S. Zhou, H. Wu, and M. Garcia-Perez, "Effect of pretreatment temperature on the yield and properties of bio-oils obtained from the auger pyrolysis of Douglas fir wood," *Fuel*, vol. 103, pp. 672–682, 2013.

[122] N. Thegarid, G. Fogassy, Y. Schuurman et al., "Second-generation biofuels by co-processing catalytic pyrolysis oil in FCC units," *Applied Catalysis B: Environmental*, vol. 145, pp. 161–166, 2014.

[123] Z. Li, S. Kelkar, L. Raycraft et al., "A mild approach for bio-oil stabilization and upgrading: Electrocatalytic hydrogenation using ruthenium supported on activated carbon cloth," *Green Chemistry*, vol. 16, no. 2, pp. 844–852, 2014.

[124] L. Zhang, R. Yin, Y. Mei, R. Liu, and W. Yu, "Characterization of crude and ethanol-stabilized bio-oils before and after accelerated aging treatment by comprehensive two-dimensional gas-chromatography with time-of-flight mass spectrometry," *Journal of the Energy Institute*, vol. 90, no. 4, pp. 646–659, 2017.

[125] H. Ben and A. J. Ragauskas, "Heteronuclear single-quantum correlation-nuclear magnetic resonance (HSQC-NMR) fingerprint analysis of pyrolysis oils," *Energy & Fuels*, vol. 25, no. 12, pp. 5791–5801, 2011.

[126] C. Lievens, D. Mourant, M. He, R. Gunawan, X. Li, and C.-Z. Li, "An FT-IR spectroscopic study of carbonyl functionalities in bio-oils," *Fuel*, vol. 90, no. 11, pp. 3417–3423, 2011.

[127] F. Xu, Y. Xu, R. Lu, G.-P. Sheng, and H.-Q. Yu, "Elucidation of the thermal deterioration mechanism of bio-oil pyrolyzed from rice husk using fourier transform infrared spectroscopy," *Journal of Agricultural and Food Chemistry*, vol. 59, no. 17, pp. 9243–9249, 2011.

[128] B. S. Souza, A. P. D. Moreira, and A. M. R. F. Teixeira, "TG-FTIR coupling to monitor the pyrolysis products from agricultural residues," *Journal of Thermal Analysis and Calorimetry*, vol. 97, no. 2, pp. 637–642, 2009.

[129] D. Chen, J. Zhou, and Q. Zhang, "Effects of torrefaction on the pyrolysis behavior and bio-oil properties of rice husk by using TG-FTIR and Py-GC/MS," *Energy & Fuels*, vol. 28, no. 9, pp. 5857–5863, 2014.

[130] Z. Ma, Q. Sun, J. Ye, Q. Yao, and C. Zhao, "Study on the thermal degradation behaviors and kinetics of alkali lignin for production of phenolic-rich bio-oil using TGA-FTIR and Py-GC/MS," *Journal of Analytical and Applied Pyrolysis*, vol. 117, pp. 116–124, 2016.

[131] F. Stankovikj and M. Garcia-Perez, "TG-FTIR Method for the Characterization of Bio-oils in Chemical Families," *Energy & Fuels*, vol. 31, no. 2, pp. 1689–1701, 2017.

[132] S. Wu, D. Shen, J. Hu, R. Xiao, and H. Zhang, "TG-FTIR and Py-GC-MS analysis of a model compound of cellulose-glyceraldehyde," *Journal of Analytical and Applied Pyrolysis*, vol. 101, pp. 79–85, 2013.

[133] J. E. Szulejko and K.-H. Kim, "Re-evaluation of effective carbon number (ECN) approach to predict response factors of 'compounds lacking authentic standards or surrogates' (CLASS) by thermal desorption analysis with GC-MS," *Analytica Chimica Acta*, vol. 851, no. C, pp. 14–22, 2014.

[134] S.-J. Oh, G.-G. Choi, and J.-S. Kim, "Characteristics of bio-oil from the pyrolysis of palm kernel shell in a newly developed two-stage pyrolyzer," *Energy*, vol. 113, pp. 108–115, 2016.

[135] G.-G. Choi, S.-J. Oh, S.-J. Lee, and J.-S. Kim, "Production of bio-based phenolic resin and activated carbon from bio-oil and biochar derived from fast pyrolysis of palm kernel shells," *Bioresource Technology*, vol. 178, pp. 99–107, 2015.

[136] Y.-H. Kim, K.-H. Kim, J. E. Szulejko, M.-S. Bae, and R. J. C. Brown, "Experimental validation of an effective carbon number-based approach for the gas chromatography-mass spectrometry quantification of 'compounds lacking authentic standards or surrogates'," *Analytica Chimica Acta*, vol. 830, pp. 32–41, 2014.

[137] R. E. Murphy, M. R. Schure, and J. P. Foley, "Effect of sampling rate on resolution in comprehensive two-dimensional liquid chromatography," *Analytical Chemistry*, vol. 70, no. 8, pp. 1585–1594, 1998.

[138] A. Mostafa, M. Edwards, and T. Górecki, "Optimization aspects of comprehensive two-dimensional gas chromatography," *Journal of Chromatography A*, vol. 1255, pp. 38–55, 2012.

[139] T. Cordero-Lanzac, R. Palos, J. M. Arandes et al., "Stability of an acid activated carbon based bifunctional catalyst for the raw bio-oil hydrodeoxygenation," *Applied Catalysis B: Environmental*, vol. 203, pp. 389–399, 2017.

[140] G. S. Groenewold, K. M. Johnson, S. C. Fox et al., "Pyrolysis Two-Dimensional GC-MS of Miscanthus Biomass: Quantitative Measurement Using an Internal Standard Method," *Energy & Fuels*, vol. 31, no. 2, pp. 1620–1630, 2017.

[141] B. Onorevoli, M. E. Machado, C. Dariva et al., "A one-dimensional and comprehensive two-dimensional gas chromatography study of the oil and the bio-oil of the residual cakes from the seeds of Crambe abyssinica," *Industrial Crops and Products*, vol. 52, pp. 8–18, 2014.

[142] M. S. A. Moraes, M. V. Migliorini, F. C. Damasceno et al., "Qualitative analysis of bio oils of agricultural residues obtained through pyrolysis using comprehensive two dimensional gas chromatography with time-of-flight mass spectrometric detector," *Journal of Analytical and Applied Pyrolysis*, vol. 98, pp. 51–64, 2012.

[143] C. Tessini, N. Müller, C. Mardones, D. Meier, A. Berg, and D. Von Baer, "Chromatographic approaches for determination of low-molecular mass aldehydes in bio-oil," *Journal of Chromatography A*, vol. 1219, pp. 154–160, 2012.

[144] S. S. Kaki, T. Jabeen, J. R. C. Reddy et al., "Isolation and physicochemical characterization of Butea parviflora seed oil," *Grasas y Aceites*, vol. 67, no. 3, 2016.

[145] M. B. Reena, S. R. Y. Reddy, and B. R. Lokesh, "Changes in triacylglycerol molecular species and thermal properties of blended and interesterified mixtures of coconut oil or palm oil with rice bran oil or sesame oil," *European Journal of Lipid Science and Technology*, vol. 111, no. 4, pp. 346–357, 2009.

[146] I. François and P. Sandra, "Comprehensive supercritical fluid chromatography × reversed phase liquid chromatography for the analysis of the fatty acids in fish oil," *Journal of Chromatography A*, vol. 1216, no. 18, pp. 4005–4012, 2009.

[147] A. Le Masle, D. Angot, C. Gouin et al., "Development of on-line comprehensive two-dimensional liquid chromatography method for the separation of biomass compounds," *Journal of Chromatography A*, vol. 1340, pp. 90–98, 2014.

[148] D. Tomasini, F. Cacciola, F. Rigano et al., "Complementary analytical liquid chromatography methods for the characterization of aqueous phase from pyrolysis of lignocellulosic biomasses," *Analytical Chemistry*, vol. 86, no. 22, pp. 11255–11262, 2014.

[149] E. A. Smith and Y. J. Lee, "Petroleomic analysis of bio-oils from the fast pyrolysis of biomass: Laser desorption ionization-linear ion trap-orbitrap mass spectrometry approach," *Energy & Fuels*, vol. 24, no. 9, pp. 5190–5198, 2010.

[150] Y. Liu, Q. Shi, Y. Zhang et al., "Characterization of red pine pyrolysis bio-oil by gas chromatography-mass spectrometry and negative-ion electrospray ionization Fourier transform ion cyclotron resonance mass spectrometry," *Energy & Fuels*, vol. 26, no. 7, pp. 4532–4539, 2012.

[151] R. Olcese, V. Carré, F. Aubriet, and A. Dufour, "Selectivity of bio-oils catalytic hydrotreatment assessed by petroleomic and GC*GC/MS-FID analysis," *Energy & Fuels*, vol. 27, no. 4, pp. 2135–2145, 2013.

[152] S. Chiaberge, I. Leonardis, T. Fiorani, P. Cesti, S. Reale, and F. D. Angelis, "Bio-oil from waste: A comprehensive analytical study by soft-ionization FTICR mass spectrometry," *Energy & Fuels*, vol. 28, no. 3, pp. 2019–2026, 2014.

[153] M. M. Sanguineti, N. Hourani, M. Witt, S. M. Sarathy, L. Thomsen, and N. Kuhnert, "Analysis of impact of temperature and saltwater on Nannochloropsis salina bio-oil production by ultra high resolution APCI FT-ICR MS," *Algal Research*, vol. 9, pp. 227–235, 2015.

[154] S.-Z. Wang, X. Fan, A.-L. Zheng et al., "Evaluation of atmospheric solids analysis probe mass spectrometry for the analysis of coal-related model compounds," *Fuel*, vol. 117, pp. 556–563, 2014.

[155] M. Staš, J. Chudoba, M. Auersvald et al., "Application of orbitrap mass spectrometry for analysis of model bio-oil compounds and fast pyrolysis bio-oils from different biomass sources," *Journal of Analytical and Applied Pyrolysis*, vol. 124, pp. 230–238, 2017.

[156] E. Alsbou and B. Helleur, "Direct infusion mass spectrometric analysis of bio-oil using ESI-Ion-trap MS," *Energy & Fuels*, vol. 28, no. 1, pp. 578–590, 2014.

[157] H. K. Reddy, T. Muppaneni, S. Ponnusamy et al., "Temperature effect on hydrothermal liquefaction of Nannochloropsis gaditana and Chlorella sp.," *Applied Energy*, vol. 165, pp. 943–951, 2016.

[158] P. Rathsack, "Analysis of pyrolysis liquids obtained from the slow pyrolysis of a German brown coal by comprehensive gas chromatography mass spectrometry," *Fuel*, vol. 191, pp. 312–321, 2017.

[159] J. Liu, X.-Y. Wei, D.-D. Zhang et al., "Characterization of heteroatom-containing species in the soluble portion from the ethanolysis of the extraction residue from Xinghe lignite by electrospray ionization Fourier transform ion cyclotron resonance mass spectrometry," *Fuel*, vol. 173, pp. 222–229, 2016.

[160] N. Koike, S. Hosokai, A. Takagaki et al., "Upgrading of pyrolysis bio-oil using nickel phosphide catalysts," *Journal of Catalysis*, vol. 333, pp. 115–126, 2016.

[161] V. V. Lobodin, L. Nyadong, B. M. Ruddy et al., "DART Fourier transform ion cyclotron resonance mass spectrometry for analysis of complex organic mixtures," *International Journal of Mass Spectrometry*, vol. 378, Article ID 15276, pp. 186–192, 2015.

[162] J. M. Jarvis, D. S. Page-Dumroese, N. M. Anderson, Y. Corilo, and R. P. Rodgers, "Characterization of fast pyrolysis products generated from several western USA woody species," *Energy & Fuels*, vol. 28, no. 10, pp. 6438–6446, 2014.

[163] Y. Bi, G. Wang, Q. Shi, C. Xu, and J. Gao, "Compositional changes during hydrodeoxygenation of biomass pyrolysis oil," *Energy & Fuels*, vol. 28, no. 4, pp. 2571–2580, 2014.

[164] B. E. Hartman and P. G. Hatcher, "Hydrothermal liquefaction of isolated cuticle of Agave americana and Capsicum annuum: Chemical characterization of petroleum-like products," *Fuel*, vol. 156, pp. 225–233, 2015.

[165] C. F. Wang, X. Fan, F. Zhang et al., "Characterization of humic acids extracted from a lignite and interpretation for the mass spectra," *RSC Advances*, vol. 7, no. 33, pp. 20677–20684, 2017.

[166] D. P. Cole, E. A. Smith, D. Dalluge et al., "Molecular characterization of nitrogen-containing species in switchgrass bio-oils at various harvest times," *Fuel*, vol. 111, pp. 718–726, 2013.

[167] D. P. Cole and Y. J. Lee, "Effective evaluation of catalytic deoxygenation for in situ catalytic fast pyrolysis using gas chromatography-high resolution mass spectrometry," *Journal of Analytical and Applied Pyrolysis*, vol. 112, pp. 129–134, 2015.

[168] C. A. Mullen, G. D. Strahan, and A. A. Boateng, "Characterization of various fast-pyrolysis bio-oils by NMR spectroscopy," *Energy & Fuels*, vol. 23, no. 5, pp. 2707–2718, 2009.

[169] C. Mattsson, S.-I. Andersson, T. Belkheiri et al., "Using 2D NMR to characterize the structure of the low and high molecular weight fractions of bio-oil obtained from LignoBoost™ kraft lignin depolymerized in subcritical water," *Biomass & Bioenergy*, vol. 95, pp. 364–377, 2016.

[170] C. Díaz-Urrutia, B. B. Hurisso, P. M. P. Gauthier, B. Sedai, R. D. Singer, and R. T. Baker, "Catalytic aerobic oxidation of lignin-derived bio-oils using oxovanadium and copper complex catalysts and ionic liquids," *Journal of Molecular Catalysis A: Chemical*, vol. 423, pp. 414–422, 2016.

[171] B. Biannic, J. J. Bozell, and T. Elder, "Steric effects in the design of Co-Schiff base complexes for the catalytic oxidation of lignin models to para-benzoquinones," *Green Chemistry*, vol. 16, no. 7, pp. 3635–3642, 2014.

[172] R. Y. Nsimba, C. A. Mullen, N. M. West, and A. A. Boateng, "Structure-property characteristics of pyrolytic lignins derived from fast pyrolysis of a lignin rich biomass extract," *ACS Sustainable Chemistry & Engineering*, vol. 1, no. 2, pp. 260–267, 2013.

[173] Y. Pu, S. Cao, and A. J. Ragauskas, "Application of quantitative 31P NMR in biomass lignin and biofuel precursors characterization," *Energy & Environmental Science*, vol. 4, no. 9, pp. 3154–3166, 2011.

[174] P. Giraudeau, "Quantitative 2D liquid-state NMR," *Magnetic Resonance in Chemistry*, vol. 52, no. 6, pp. 259–272, 2014.

[175] H. Ben and A. J. Ragauskas, "In situ NMR characterization of pyrolysis oil during accelerated aging," *ChemSusChem*, vol. 5, no. 9, pp. 1687–1693, 2012.

[176] Y. Le Brech, L. Delmotte, J. Raya, N. Brosse, R. Gadiou, and A. Dufour, "High resolution solid state 2D NMR analysis of biomass and biochar," *Analytical Chemistry*, vol. 87, no. 2, pp. 843–847, 2015.

[177] J. I. Santos, R. Martín-Sampedro, Ú. Fillat et al., "Evaluating lignin-rich residues from biochemical ethanol production of wheat straw and olive tree pruning by FTIR and 2d-NMR," *International Journal of Polymer Science*, vol. 2015, Article ID 314891, 11 pages, 2015.

Hindawi
International Journal of Analytical Chemistry
Volume 2017, Article ID 7305682, 9 pages
https://doi.org/10.1155/2017/7305682

Research Article

Detailed Componential Characterization of Extractable Species with Organic Solvents from Wheat Straw

Yong-Chao Lu,[1] Yao Lu,[2,3] Zhao-Lin Lu,[2] and Xian-Yong Wei[3]

[1]*School of Basic Education Sciences, Xuzhou Medical University, Xuzhou 221004, China*
[2]*Advanced Analysis & Computation Center, China University of Mining & Technology, Xuzhou 221116, China*
[3]*Key Laboratory of Coal Processing and Efficient Utilization, Ministry of Education, China University of Mining & Technology, Xuzhou 221116, China*

Correspondence should be addressed to Yao Lu; luyimao@163.com

Received 17 March 2017; Revised 25 July 2017; Accepted 18 September 2017; Published 1 November 2017

Academic Editor: Nilusha Sudasinghe

Componential analysis of extractives is important for better understanding the structure and utilization of biomass. In this investigation, wheat straw (WS) was extracted with petroleum ether (PE) and carbon disulfide (CS_2) sequentially, to afford extractable fractions EF_{PE} and EF_{CS2}, respectively. Detailed componential analyses of EF_{PE} and EF_{CS2} were carried out with Fourier transform infrared (FTIR) spectroscopy, gas chromatography/mass spectrometry (GC/MS), X-ray photoelectron spectroscopy (XPS), transmission electron microscopy (TEM), energy dispersive spectrometry (EDS), and electron probe microanalysis (EPMA). Total extractives were quantified 4.96% by weight compared to the initial WS sample. FTIR and GC/MS analyses results showed that PE was effective for the extraction of ketones and waxes derived compounds; meanwhile CS_2 preferred ketones and other species with higher degrees of unsaturation. Steroids were enriched into EF_{PE} and EF_{CS2} with considerable high relative contents, namely, 64.52% and 79.58%, respectively. XPS analysis showed that most of the C atoms in extractives were contained in the structures of C-C, C-COOR, and C-O. TEM-EDS and EPMA analyses were used to detect trace amount elements, such as Al, Si, P, S, Cl, and Ca atoms. Detailed characterization of extractable species from WS can provide more information on elucidation of extractives in biomass.

1. Introduction

Biomass has been considered to be a promising feedstock for fuels and chemicals production to substitute fossil resources [1, 2]. The main components of lignocellulosic biomass are cellulose, hemicellulose, and lignin, accounting for 60–90% of entire dry weight; other components include extractives, protein, and pectin. Thermochemical or biological techniques [1, 3] have been carried out aiming at the conversion of biomass for strategic utilization. Biomass-based fuels, such as bioethanol, biogas, biodiesel, and biooil, have been used as complementary fuels for decades; meanwhile, various value-added chemicals, such as furans, aldehydes, ketones, and aromatics, so-called platform compounds, can also be produced in biorefinery plants [1–3].

Extractives are natural nonstructured nonpolymer components in biomass and are capable of being extracted with water and organic solvents [4]. Chemically, extractives cover a wide range of species, such as aliphatic hydrocarbons, alcohols, acids, fats, terpenes, steroids, resin acids, rosin, phenols, waxes, glycosides, quinines, and proteins, accounting for 5–30% of dry weight of biomass [4]. The components of the extractives from biomass vary significantly [5] according to the family, genera, and species and even the location, part, age, and season.

Although the extractives are considered to be nonstructural substances with low contents, they play an important role in the attractive forces of adjacent biomass particles [6] by providing weak H-bonding and van der Waal's forces [7, 8]. Furthermore, extractives may affect subsequent characterization, further degradation processes, and even the utilization of carbohydrates and lignin in biomass. For example, due to incomplete removal in the extraction, residual extractives will precipitate together with insoluble lignin, leading to

an overestimation of lignin content [9]. In pulping process, serious pitch problem may arise if extractives are not removed effectively; for example, sterols and waxes are insoluble and will deposit in alkaline solutions [5]. In thermochemical conversion of biomass, extractives are decomposed under lower temperature avoiding significant influence on product properties. However, extractives can catalyze the reactions involved in the pyrolysis of biomass [10] and additional products derived from extractives can alter the distribution of the final products [11]. Furthermore, some extractives are potentially toxic to microorganisms which would negatively influence the biochemical conversion of biomass [12]. Therefore, it is necessary to remove them prior to downstream analysis or handling of biomass [13].

The removal of extractives depends heavily on the solvents and conditions used. Generally, water and ethanol extractives contain organic acids, inorganic substances, waxes, nonstructural sugars, and so forth. [14, 15]. Hot water can extract tannins and phenolics effectively from biomass [16–18], while ethanol, acetone, and dichloromethane can remove phytosterols and lipophilic extractives from wood significantly, but leaving fatty acid esters with considerable amounts [11]. Petroleum ether (PE) and carbon disulfide (CS_2) are organic solvents with low polarities. They can extract alkanes, waxes, benzene-ring containing compounds (BRCCs), fatty acids, and organonitrogen compounds (ONCs) effectively from degraded biomass samples [19–22]. Typical components in extractives can also be enriched in the extraction fractions. PE is effective for the removal of alkanes and waxes in stalks [19] and for the extraction of BRCCs in biooil produced from pyrolysis of rice husk [20]. CS_2 was reported to have strong π-π interaction with fatty acids [21] and ONCs in the extraction [22].

A systematic study showed that wheat straw (WS) was more readily depolymerized with the oxidation of NaOCl aqueous solution after sequential extraction with several organic solvents [23]. Oxidative degradation of organic components in WS might be hindered by extractives to some extent. In order to explore more information on the extraction process, in this investigation, PE and CS_2 were used as the solvents in the sequential extraction of WS, and detailed characterization of the extraction fractions was carried out. Fourier transform infrared (FTIR) spectroscopy, as a routine technique for analysis of organic substances, was used to determine functional groups in extraction fractions. Difference between WS and extracted WS in their components could be clearly presented. The volatile species in extractives were identified and characterized with gas chromatography/mass spectrometry (GC/MS). GC/MS is a frequently used technique to identify compounds based on the high effective chromatographic separation of species with different volatilities. Mass spectrometer provides high resolution for charged fragments derived from molecules. FTIR and GC/MS are convenient and reliable methods for the analysis of complex samples, such as the degradation products from biomass and coals [24, 25]. The chemical states of elements contained in extractives were assayed by X-ray photoelectron spectroscopy (XPS). Binding types between atoms can be assigned by calculated binding energy.

Table 1: Proximate and ultimate analyses (wt.%) of WS.

Proximate analysis			Ultimate analysis				
M_{ad}	A_d	V_{daf}	C	H	O*	N	S
8.0	8.2	70.2	42.3	6.6	50.2	0.3	0.6

*By difference: M_{ad}, moisture on air dried basis; A_d, ash on dry basis; V_{daf}, volatile matter on dry and ash-free basis.

Though it is very expensive to conduct, XPS analysis is useful in understanding the composition of samples by providing fundamental structural information [26, 27]. Transmission electron microscopy (TEM) coupled with energy dispersive spectrometry (EDS) and electron probe microanalysis (EPMA) were employed for the determination of abundance of organic/inorganic atoms in the extraction fractions. TEM-EDS method provides accurate qualitative and quantitative analyses for elements with atomic number from 4 (Be) to 92 (U). The costs of TEM-EDS and EPMA analyses are higher than FTIR and GC/MS analyses since they contain relatively more expensive instruments. They were more often used in elemental analysis of inorganic materials, such as semiconductors and cells. In recent years, EDS was used in the characterization of lignite and its alkali extracted residue [28]. Very few reports were issued on the analysis of inorganic matters derived from biomass [29, 30].

2. Experimental

2.1. Materials. WS was purchased from Xuzhou, Jiangsu Province, China. It was washed with distilled water for several times to remove sandy soil and then dried in sunlight for more than two months. Then the dried WS was chopped into small pieces and pulverized to pass through an 80-mesh sieve (<180 μm) followed by desiccation in a vacuum drying oven at 80°C for 48 h. Table 1 shows the proximate and ultimate analyses of the dried WS sample. PE and CS_2 were of analytical purity and distilled at their boiling points under atmospheric pressure with a Büchi R-134 rotary evaporator to avoid contaminative impurities.

2.2. Extraction. 50.0 g WS sample and 500 mL PE were added to a 1 L beaker, magnetically stirred at 25°C for 1 h, and then placed in a thermostatic ultrasonic bath set at 25°C for about 6 h. The mixture was filtrated to afford a filter cake EFC_1 and a filtrate EF_{PE1}. Then the EFC_1 was extracted by another 500 mL of PE with the same procedure previously used, affording a filter cake EFC_2 and a filtrate EF_{PE2}. The two filtrates were combined together to afford a solution EF_{PE}. EFC_2 was dried in a vacuum drying oven at 40°C for 48 h to remove the solvent to a constant weight (±0.01 g). The amount of extractives extracted by PE was calculated as the weight loss based on the initial dried WS.

Then EFC_2 was extracted by CS_2 with the same procedure used for PE to afford a solution EF_{CS2} and a filter cake EFC_4. The same drying conditions were used for EFC_4. The amount of extractives extracted by CS_2 was calculated as the weight loss based on the difference between EFC_2 and EFC_4. EF_{PE} and EF_{CS2} were concentrated to remove the

solvents drastically by using a Büchi R-134 rotary evaporator while keeping the solvent temperature at 40°C under vacuum distillation condition. The dried extractives from EF_{PE} and EF_{CS2} were stored in a desiccator at 25°C.

2.3. FTIR Analysis. The WS sample, extraction residue EFC_4, and the extractives from EF_{PE} and EF_{CS2} were analyzed with a Nicolet Magna IR-560 FTIR spectrometer using KBr pellet method. The spectra were recorded by collecting 50 scans at a resolution of 8 cm^{-1} in reflectance mode with a measuring region of 4000–500 cm^{-1}.

2.4. GC/MS Analysis. The extractives were analyzed with a Hewlett-Packard 6890/5973 GC/MS system equipped with a HP-5MS capillary column (cross link 5% PH ME siloxane, 60 m × 0.25 mm *i.d.*, 0.25 μm film thickness) and a quadrupole analyzer. The compounds were ionized by electron ionization under 70 eV. Quadrupole mass analyzer was used to obtain the mass spectra. Helium was used as the carrier gas with a flow rate at 1.0 mL/min. The column was heated first at a rate of 5°C/min from 60°C to 150°C and then at a rate of 7°C/min from 150°C to 300°C (and held at 300°C for 40 min). Both injector and detector temperatures were set at 300°C. The scanned mass range was 30–500 *m/z*. The reproducibility of quantitative analysis for the species was conducted by duplicated injection of the samples. The data were acquired and processed using Chemstation software together with GC/MS system. The species were identified by comparing mass spectra with National Institute of Standards and Technology (NIST) library data according to fragmentation rules of organic species under electron ionization condition.

2.5. XPS Analysis. The XPS analysis was performed on an ESCALAB 250Xi system (Thermo-Fisher, USA). The source gun type was Al K Alpha, and spot size was 900 μm. Data were recorded by collecting 30 scans in 20 min with pass energy at 20.0 eV. Survey scan was conducted within the range 0–1000 eV. Peak fitting was used for the spectra to the assignment of different chemical bonds according to specific binding energy.

2.6. TEM-EDS Analysis. EF_{PE} sample was dispersed with ethanol, then sprayed with carbon film and loaded on 300-mesh copper grids under sonic condition for 10 min, and then dried under lamp. TEM analysis was performed on a Tecnai G^2 F20 electron microscope (FEI, USA) at an accelerating voltage of 200 kV and linked to an X-ray analysis system (Oxford EDS 6767). Determination of C atoms was interfered by carbon film introduced in the preparation of the sample. O element was not taken into consideration in the TEM-EDS analysis since previous methods provided detailed results. Inorganic elements with trace amounts in extractives were assayed, such as Al, Si, P, S, Cl, and Ca atoms.

2.7. EPMA Analysis. In order to find more information on the elemental composition of EF_{PE} and to verify the results obtained with TEM-EDS analysis, EPMA analysis was carried out, especially concentrating on K, Na, Mg, S, and Ca elements. The analysis was conducted on an 8050G system (Shimadzu, Japan). Schottky emission mode was used, and the accelerating voltage was 15 kV.

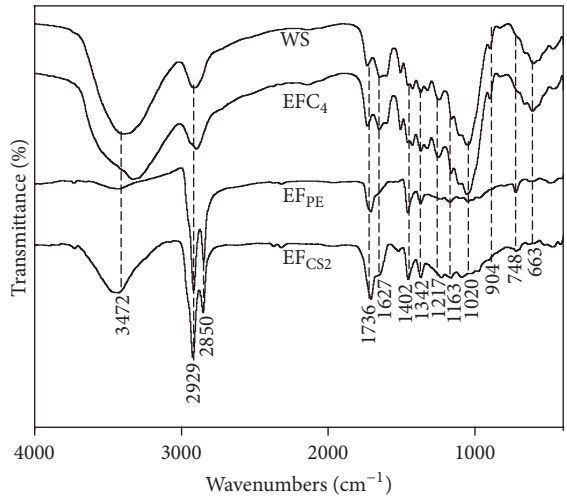

FIGURE 1: FTIR analysis of WS, EFC_4, EF_{PE}, and EF_{CS2}.

3. Results and Discussions

3.1. Extraction Yields. The dried EFC_4 lost 2.48 g comparing to the WS sample, indicating that the extractives accounted for 4.96% of the starting material. PE and CS_2 were removed completely with a rotary evaporator under reduced pressure. The weights of extractives from EF_{PE} and EF_{CS2} were 1.66 g and 0.82 g, respectively. Waxes and BRCCs could be concentrated into EF_{PE} because PE was effective for dewaxing of stalks [19] and for the extracting of BRCCs [20]. Species containing double bond or triple-bond, such as fatty acids, aldehydes, ketones, and ONCs, could be enriched into EF_{CS2} due to their strong π-π interaction with CS_2 [21, 22].

3.2. FTIR Analysis. Significant differences were observed in the FTIR spectra of WS sample, EF_{PE}, EF_{CS2}, and EFC_4, as shown in Figure 1. Wide and strong peaks around 3200–3700 cm^{-1} were attributed to the vibration of -OH; for example, peaks 3450–3650 cm^{-1} and 3200–3400 cm^{-1} were assigned to free and associated -OH, respectively. Except for EFC_4, all the other three samples showed wide peak around 3500 cm^{-1}, implying the presence of species containing free -OH. There was an interesting transformation of absorbance peak before and after the extraction, that is, from free -OH to associated -OH. Species containing free -OH in extractives can be extracted from WS sample with PE and CS_2, sequentially. Free -OH containing species were enriched in EF_{CS2} rather than EF_{PE}. Peak around 3300–3500 cm^{-1} in the spectrum of EF_{CS2} could also be attributed to the vibration of -NH, implying the presence of ONCs [22]. However, in spectrum of EF_{PE}, only a weak peak was obtained within this range. Peaks around 2929 cm^{-1} and 2850 cm^{-1} were attributed to the stretching of $-CH_2-$ and $-CH_3$, implying the presence of alkanes, waxes, aliphatics, and so forth. Fine

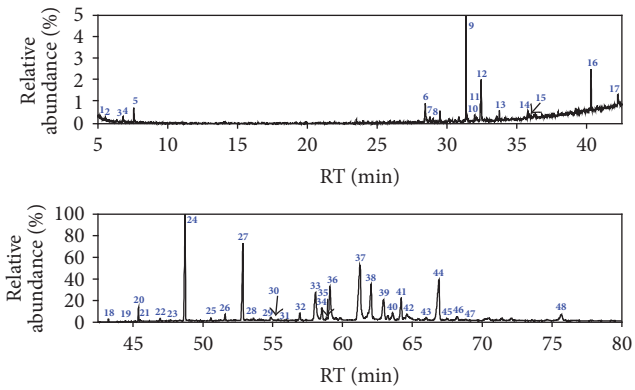

Figure 2: TICs of EF_{PE} from WS.

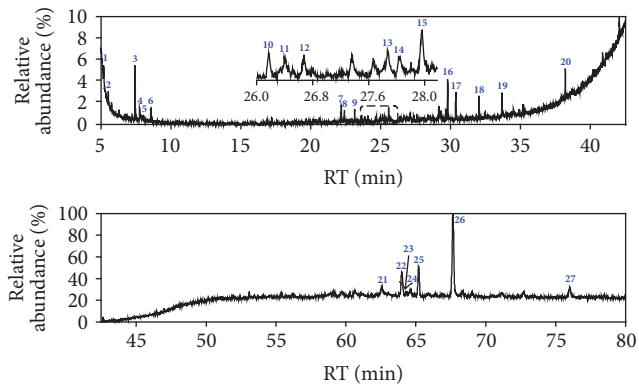

Figure 3: TICs of EF_{CS2} from WS.

structures of spectra were only observed for the two extracts, namely, EF_{PE} and EF_{CS2}, implying the selectivity of these two solvents for -CH_2- and -CH_3 containing species. The intense peaks around 1736 cm^{-1} and 1627 cm^{-1} were attributed to the vibration of C=O, indicating the presence of aldehydes, ketones, carboxylic acids, esters, and so forth [31]. All the four samples contained the peak at 1736 cm^{-1} with similar intensity. However, the peaks at 1627 cm^{-1} were weaker in spectra of EF_{PE} and EF_{CS2}. Peak around 1402 cm^{-1} could be assigned to the bending of C-H in aliphatics, O-H in carboxylic acids, C-O-H in alcohols, and so forth. This peak was common in each spectrum of samples. Peaks around 1736 cm^{-1}, 1627 cm^{-1}, and 1402 cm^{-1} could also be assigned to characteristic absorption of ONCs, namely, amide I and II bands and -NO_2 stretching, respectively [22]. Peaks at 1163 cm^{-1}, 1020 cm^{-1}, and 663 cm^{-1} were assigned to stretching of C-O-C and in-plane bending of aromatic C-H, which were observed obviously in the spectra of WS and EFC_4. The C-O-C structure can be found in almost all kinds of hemicelluloses and cellulose in biomass and the aromatic C-H present in lignins. In the spectra of EF_{PE} and EF_{CS2}, peaks around 748 cm^{-1} were attributed to the stretching of -CH_2- in waxes and aliphatics [32]. The difference between WS and EFC_4 spectra was difficult to figure out; meanwhile EF_{PE} and EF_{CS2} shared very similar spectrum. Significant differences between the two groups (WS/EFC_4 and EF_{PE}/EF_{CS2}) lie in peaks around 3200–3700 cm^{-1} and 1020 cm^{-1}, indicating different states of -OH and presence of aromatic C-H.

3.3. GC/MS Analysis of the Species in the Extracts. In total, 48 and 27 compounds were identified in EF_{PE} and EF_{CS2}, respectively, with GC/MS analysis. The total ionic chromatograms (TICs) were presented in Figures 2 and 3, respectively. These species can be classified into alkanes, alkenes, arenes, alcohols, furan, aldehydes, ketones, ONCs, carboxylic acid (CA), esters, and others, as listed in Tables S1 and S2 (see Supplementary Material available online at https://doi.org/10.1155/2017/7305682). Double bond equivalent (DBE) was calculated for each species identified in EF_{PE} and EF_{CS2}; and the plot of DBE versus carbon number was used to demonstrate the degrees of unsaturation of compounds, shown in Figure 4. From the plot, one can

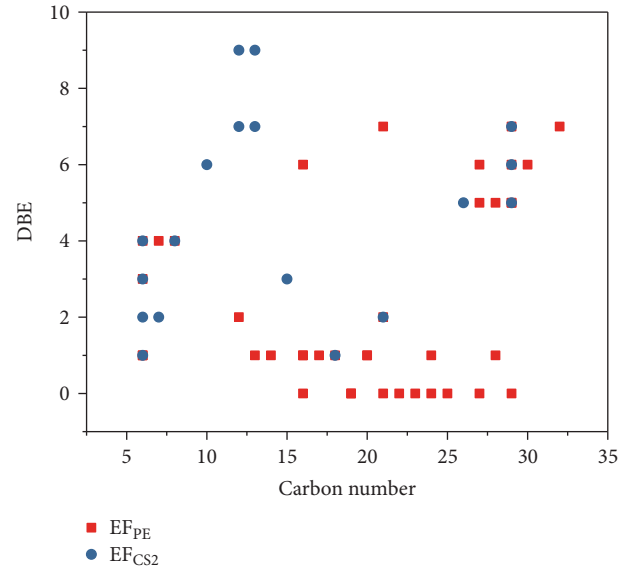

Figure 4: The relationship between DBE and carbon number for compounds identified in EF_{PE} and EF_{CS2}.

observe that compounds were roughly divided into two groups in these two samples, namely, lower DBE group and higher DBE group. CS_2 favors species with higher DBEs and less carbon numbers, while species with more carbon numbers and lower DBEs were enriched in PE.

Various long-chain alkanes, alkenes, and aldehydes derived from waxes were identified, which could be extracted easily by PE [19]. Two arenes were identified in EF_{PE} (**1** and **3**). Eight alkanes with carbon numbers ranging from 16 to 29 were detected. All the 5 alcohols identified were sterols. Only one furan was identified, that is, 2,5-dimethylfuran **(2)**, which could be derived from cellulose and hemicelluloses [33]. For the contents of the classes of compounds identified in EF_{PE}, ketones, alkanes, alcohols, and ONCs were abundant, as shown in Figure 5. Ketones were the most abundant species in EF_{PE}. Besides alkanones (**11** and **12**) and furanone **(16)**, abundance sterones were identified (**35**, **39–42**, **44–46,** and **48**). Sterols and sterones are typical species in extractives with considerable amounts, which can be extracted easily with

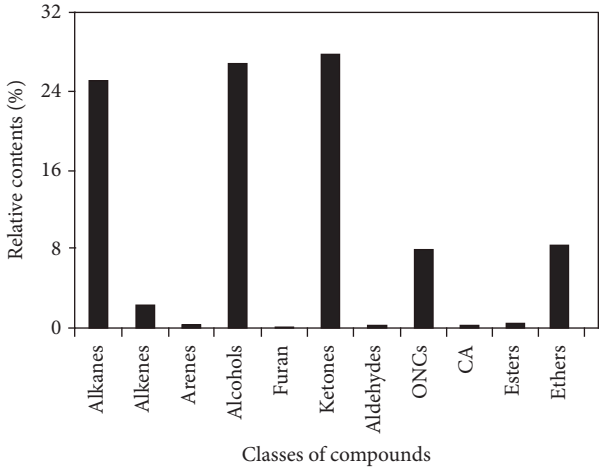

Figure 5: Relative contents of classes of compounds identified in EF_{PE}.

solvents. Extractives were considered as potential material for production of medicine for pharmaceutical utilization based on the steroids components, such as sterols and sterones [34]. Sterones tablets containing testosterone, norethindrone, methandienone, and so forth have been used for treatment of many diseases. There were 17 steroids identified in the EF_{PE}, accounting for about 64.52% in relative content, such as cholests and stigmasts. Among them, the most abundant were 22,23-dihydrostigmasterol **(37)** and stigmastane-3,6-dione **(44)**. *N*,4-Dimethylbenzenesulfonamide **(6)** was the only one sulfur-containing species identified. Two of the esters identified, namely, butyl methyl phthalate **(10)** and dipropyl phthalate **(13)**, might be impurities coming from the GC/MS system with plastic or rubber devices or contaminants introduced in the process of sample preparation [35].

Compounds identified in EF_{CS2} with GC/MS analysis can be classified into arenes, alcohols, furans, ONC, ketones, and esters, as listed in Table S2. Neither alkanes nor alkenes were identified in the EF_{CS2}, and no species that could be derived from waxes were found. Besides benzene **(1)** and xylene **(5)**, acenaphthene **(9)** and 9H-fluorene **(14)** were identified and grouped into the arenes. All the three alcohols identified were steroids (**15**, **21,** and **23**). 2,5-Dimethylfuran **(2)** and dibenzofuran **(11)** may be derived from the hemicellulose and lignin, respectively. Similar with EF_{PE}, ketones were the most abundant class identified in EF_{CS2} and could be classified further into alkanones (**3** and **16**), cycloalkanone **(6)**, furanone **(20)**, alkenone **(8),** and sterones **(24–27)**. Seven steroids were identified in the EF_{CS2} with relative content of 79.58%. The four phthalates identified (**7**, **13**, **17,** and **18**) might not be the components in the extractives, which could be considered as impurities or contaminants [35]. The relative contents of the classes of compounds identified in EF_{CS2} were shown in Figure 6. Ketones, esters, and alcohols were the three most abundant classes.

3.4. XPS Analysis. As displayed in Figure 7, 101.8 eV, 284.1 eV, and 531.9 eV were attributed to Si 2*p*, C 1*s*, and O 1*s* [36], respectively, implying the presence of the Si-, C-, and O-containing species in EF_{PE}. Peak fittings for C 1*s* and Si 2*p* were conducted (see (b) and (c) in Figure 7) and the resulting peaks were assigned for different chemical bonds indicating the status of C, O, and Si atoms according to their special binding energy (BE), as shown in Table 2. The full width at half maximum (FWHM) of each chemical bond was also calculated. According to the atomic percentage for specific chemical bond, C atoms contained in C-C bond accounted for 48.54% indicating the presence of high amount of long-chain aliphatic species, such as alkanes, waxes, and/or steroids, which is consistent with the componential analysis by GC/MS. C-COOR containing species could be attributed to fatty acids and esters holding 25.29% of C atoms. Other types of C atoms were in C-O, C=O, and O-C=O structures [36]. Si-O bond was divided into two bonds in peak fitting, namely, 102.1 eV and 102.7 eV, which could be assigned to Si_2O_3 and SiO_2, respectively. XPS is a surface-sensitive technique by providing accurate qualitative and quantitative analyses of elemental composition, chemical state, and electronic state of the elements in a sample. It can be used as complementary method along with FTIR and GC/MS analyses to characterize complex samples derived from biomass.

Table 2: Chemical statuses of C and Si atoms in EF_{PE} analyzed with XPS.

Chemical bond	BE (eV)	FWHM (eV)	Area	Atomic (%)
C-C	284.9	1.01	34722.3	48.54
C-COOR	285.3	0.98	18089.1	25.29
C-O	286.4	1.42	8333.9	11.66
-C=O	287.9	1.13	1899.8	2.66
O-C=O	289.1	1.01	1779.9	2.49
Si-O	102.1	0.91	166.8	0.38
	102.7		85.1	0.01

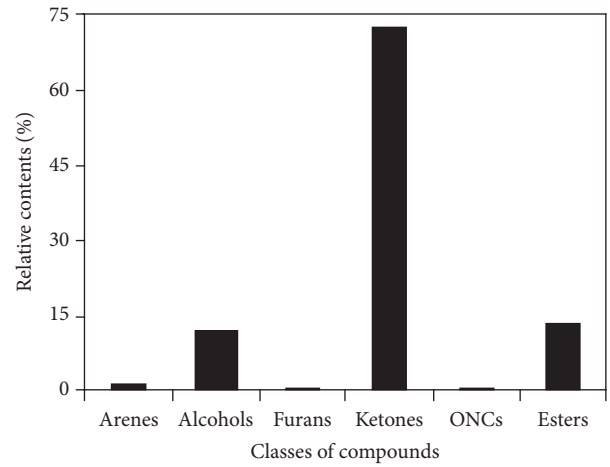

Figure 6: Relative contents of classes of compounds identified in EF_{CS2}.

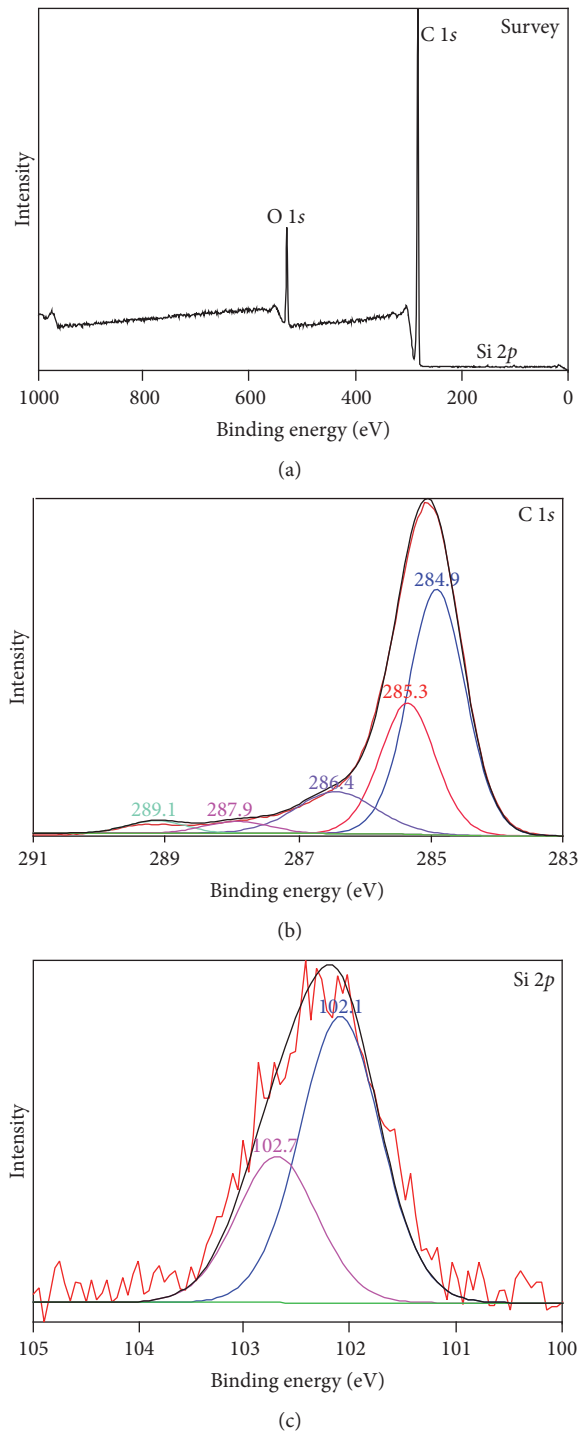

Figure 7: XPS analysis of EF_{PE}. ((a) survey scan of the sample; (b) peak fitting of the C 1*s*; and (c) peak fitting of the Si 2*p*.)

3.5. TEM-EDS Analysis. As shown in Figure S1 (Supporting Information), two areas (Areas 1 and 2) were selected for the scanning and determining elements with TEM-EDS in EF_{PE}. Data were collected from six points in each area. Carbon film was used in the sample preparation, and it would interfere with the identification of C atoms. C and O elements were not considered in the detection with TEM-EDS analysis.

Table 3: TEM-EDS analysis of elements and their percentages of weight (wt.%) in EF_{PE}.

Areas	Data points	Al (K)	Si (K)	P (K)	S (K)	Cl (K)	Ca (K)
1	1	32.64	Nd	28.54	30.67	8.12	Nd
	2	3.11	4.78	Nd	Nd	Nd	92.09
	3	3.60	16.91	Nd	0.36	Nd	79.11
	4	10.72	15.50	Nd	Nd	Nd	73.77
	5	Nd	75.96	10.70	Nd	13.32	Nd
	6	Nd	61.01	6.53	11.06	21.39	Nd
	Average	8.35	29.03	7.63	7.02	7.14	40.83
2	1	3.65	16.96	Nd	38.71	5.43	35.22
	2	Nd	4.85	0.33	46.20	Nd	48.60
	3	Nd	47.59	49.64	Nd	Nd	2.76
	4	Nd	49.74	9.59	19.68	9.20	11.76
	5	13.09	Nd	Nd	37.81	Nd	49.08
	6	Nd	61.88	21.15	16.96	Nd	Nd
	Average	2.79	30.17	13.45	26.56	2.44	24.57

Nd: not detected.

Al, Si, P, S, Cl, and Ca atoms were counted on the data point of EF_{PE} and the results were listed in Table 3. Ca, Si, and S atoms were counted with higher intensities for both areas, which may present in inorganic materials or complexes. Si is known as beneficial element for wheat straw [37, 38]. Morphological silica materials, such as SiO_2, can be obtained by thermochemical treatments [39]. Phytoliths are the main forms of Si uptaken by wheat straw [40]. Then the Si-containing species deposit within different intracellular and extracellular structures. Ca atoms were detected in the extractives with comparable accounts to Si. Calcium oxalate is another main component in phytoliths [41, 42] together with Si-containing species. The concentration of Si in WS ranges from 1.5 to 12 g/kg [43], while Ca content in WS is around 5.6 g/kg [44]. Current application of the Ca and Si in biomass was concentrated on the production of ash and further for the preparation of value-added materials, such as catalyst [45]. By using organic solvents in the extraction, namely, PE and CS_2, only trace amounts of Si and Ca were extracted since most of them were in their inorganic forms. S atoms were also counted with similar amounts to Si and Ca atoms near Area 2. The content of S in WS was in the range of 0.1–0.7% (air dried basis) [46, 47]. Sulfur atom is building block of some proteins and a key ingredient in the formation of chlorophyll. Most of the sulfur is assimilated by the roots in the form of SO_4^{2-}. Then it is stored in the form of sulfate and metabolized and/or incorporated into organic structures. It was reported that almost all the sulfur in rice hull occurs in organic form [48]. However, only one sulfur-containing compound was detected in GC/MS analysis of extracts (*N*,4-dimethylbenzenesulfonamide in EF_{PE}, see Table S1 in Supporting Information). In biomass, most of Al, P, and Cl atoms are in their inorganic forms. Among them, the existence of P atoms could be attributed to phosphate in biomass. Phosphate fertilizer is important for the growth of plants and will be stored mainly in the form of phosphate.

In order to obtain more accurate information of inorganic substances, more data points should be collected; however, due to the intrinsic limitation of TEM-EDS analysis, only qualitative and semiquantitative results can be obtained. The detection of inorganic substances with trace amounts relies on the progress of in situ analytical techniques with higher resolutions. Meanwhile, enlarging the number of data points is necessary to achieve more accurate and representative analytical results.

3.6. EPMA Analysis. Similar qualitative results for trace amount of elements were obtained by EPMA. Eight data points were selected for EF_{PE}. Sample image and net intensities for C, Na, Mg, Si, S, K, and Ca atoms of each data point were presented in Figure S2 (Supporting Information). In EPMA, metal elements K, Na, and Mg were identified well in the EF_{PE}. Metal ions are usually in the forms of oxides presented in ash after the combustion of biomass [49]. K and Na atoms, in their forms of cations, are crucially important nutrients affecting most of the biochemical and physiological processes to promote plant growth and metabolism [50, 51]. Mg is one of the most important nutrients to plants. It provides the central ions of chlorophyll to accomplish photosynthesis in plants and is involved in many enzyme activities and the structural stabilization of tissues [52]. Due to intrinsic restriction, similar with TEM-EDS analysis, EPMA provides qualitative and semiquantitative results of inorganic elements.

4. Conclusions

The PE and CS_2 extractable extractives were weighted up to 4.96% of initial WS material. Detailed componential characterization of the extractives was carried out by FTIR, GC/MS, TEM-EDS, EPMA, and XPS. FTIR and GC/MS analyses can be treated as universal techniques used in the compositional characterization of complex samples containing various organic species. PE and CS_2 were proved to be effective solvents for extraction of waxes, ketones, esters, and ONCs. Among the detected compounds with GC/MS, ketones were the most abundant species in the two extraction fractions. Other classes of species were alkanes, alkenes, alcohols, aldehydes, ONCs, and so forth. Considerable amounts of steroids especially sterones were identified. This kind of species could be used for medicine production. Trace amounts of atoms including Ca, Si, K, Cl, Na, and S were counted with EDS in extractives. EPMA provided similar results with TEM-EDS analysis. Chemical bonds and their abundances were assigned for C, O, and Si by using XPS analysis. Most of the C atoms in the species of extractives were contained in the structures of C-C, C-COOR, and C-O. Si atoms could be assigned in Si-O structures contained in Si_2O_3 and SiO_2.

FTIR analysis can be used to determine the functional group changes in the sample before and after extraction, and GC/MS analysis is suitable for the detection of volatile organic species providing more accurate information of individuals. These two techniques were used conventionally and effectively in the compositional analysis of complex samples. TEM-EDS and EPMA analyses are nondestructive techniques providing detailed information on the composition of elements and the contents of various atoms, especially for inorganic elements rather than C atoms. By calculating the BEs of atoms in specific chemical bonds, XPS analysis can provide fundamental structural information that is useful for understanding the composition of complex samples. Generally, the later three analytical methods are more expensive than the former two. Based on the intrinsic properties of the samples in this investigation, FTIR, GC/MS, and XPS were recommended methods used in industries. Comprehensive understanding of the composition of extractives and other complex samples relies on the combination of the advanced analytical techniques.

Conflicts of Interest

The authors declare that they have no conflicts of interest.

Acknowledgments

This work was supported by the Fundamental Research Funds for the Central Universities (Grant 2014QNA83), the National Natural Science Foundation of China (Grant no. 21506250), and the Natural Science Foundation of Jiangsu Province (Grant no. BK20150182).

References

[1] H. M. Morgan, Q. Bu, J. Liang et al., "A review of catalytic microwave pyrolysis of lignocellulosic biomass for value-added fuel and chemicals," *Bioresource Technology*, vol. 230, pp. 112–121, 2017.

[2] T. Kan, V. Strezov, and T. J. Evans, "Lignocellulosic biomass pyrolysis: a review of product properties and effects of pyrolysis parameters," *Renewable & Sustainable Energy Reviews*, vol. 57, pp. 1126–1140, 2016.

[3] S. S. Ail and S. Dasappa, "Biomass to liquid transportation fuel via Fischer Tropsch synthesis - Technology review and current scenario," *Renewable & Sustainable Energy Reviews*, vol. 58, pp. 267–286, 2016.

[4] J. B. Sluiter, R. O. Ruiz, C. J. Scarlata, A. D. Sluiter, and D. W. Templeton, "Compositional analysis of lignocellulosic feedstocks. 1. Review and description of methods," *Journal of Agricultural and Food Chemistry*, vol. 58, no. 16, pp. 9043–9053, 2010.

[5] S. H. Ghaffar and M. Fan, "An aggregated understanding of physicochemical properties and surface functionalities of wheat straw node and internode," *Industrial Crops and Products*, vol. 95, pp. 207–215, 2017.

[6] N. P. K. Nielsen, D. J. Gardner, and C. Felby, "Effect of extractives and storage on the pelletizing process of sawdust," *Fuel*, vol. 89, no. 1, pp. 94–98, 2010.

[7] W. Stelte, J. K. Holm, A. R. Sanadi, S. Barsberg, J. Ahrenfeldt, and U. B. Henriksen, "A study of bonding and failure mechanisms in fuel pellets from different biomass resources," *Biomass & Bioenergy*, vol. 35, no. 2, pp. 910–918, 2011.

[8] Z. Liu, A. Quek, and R. Balasubramanian, "Preparation and characterization of fuel pellets from woody biomass, agro-residues and their corresponding hydrochars," *Applied Energy*, vol. 113, pp. 1315–1322, 2014.

[9] S. Burkhardt, L. Kumar, R. Chandra, and J. Saddler, "How effective are traditional methods of compositional analysis in providing an accurate material balance for a range of softwood derived residues?" *Biotechnology for Biofuels*, vol. 6, no. 1, pp. 90–99, 2013.

[10] E. Ranzi, M. Corbetta, F. Manenti, and S. Pierucci, "Kinetic modeling of the thermal degradation and combustion of biomass," *Chemical Engineering Science*, vol. 110, pp. 2–12, 2014.

[11] E. Mészáros, E. Jakab, and G. Várhegyi, "TG/MS, Py-GC/MS and THM-GC/MS study of the composition and thermal behavior of extractive components of Robinia pseudoacacia," *Journal of Analytical and Applied Pyrolysis*, vol. 79, no. 1-2, pp. 61–70, 2007.

[12] W. Peng, Q. Xue, and M. Ohkoshi, "Immune effects of extractives on bamboo biomass self-plasticization," *Pakistan Journal of Pharmaceutical Sciences*, vol. 27, no. 4, pp. 991–999, 2014.

[13] A. Sluiter, R. Ruiz, C. Scarlata, J. Sluiter, and D. Templeton, *Determination of Extractives in Biomass*, National Renewable Energy Laboratory, Golden, CO., http://www.nrel.gov/biomass/pdfs/42619.pdf/.

[14] S.-F. Chen, R. A. Mowery, C. J. Scarlata, and C. K. Chambliss, "Compositional analysis of water-soluble materials in corn stover," *Journal of Agricultural and Food Chemistry*, vol. 55, no. 15, pp. 5912–5918, 2007.

[15] A. Garcia-Maraver, D. Salvachúa, M. J. Martínez, L. F. Diaz, and M. Zamorano, "Analysis of the relation between the cellulose, hemicellulose and lignin content and the thermal behavior of residual biomass from olive trees," *Waste Management*, vol. 33, no. 11, pp. 2245–2249, 2013.

[16] R. C. Sun and J. Tomkinson, "Comparative study of organic solvent-soluble and water-soluble lipophilic extractives from wheat straw 2: Spectroscopic and thermal analysis," *Journal of Wood Science*, vol. 48, no. 3, pp. 222–226, 2002.

[17] R. C. Sun and J. Tomkinson, "Comparative study of organic solvent and water-soluble lipophilic extractives from wheat straw I: Yield and chemical composition," *Journal of Wood Science*, vol. 49, no. 1, pp. 47–52, 2003.

[18] R. C. Sun, D. Salisbury, and J. Tomkinson, "Chemical composition of lipophilic extractives released during the hot water treatment of wheat straw," *Bioresource Technology*, vol. 88, no. 2, pp. 95–101, 2003.

[19] W. Zhao, Z. Zong M, J. Lin et al., "Dewaxing from stalks with petroleum ether by different methods," *Energy & Fuels*, vol. 21, no. 2, pp. 1165–1168, 2007.

[20] Y. Lu, X.-Y. Wei, J.-P. Cao et al., "Characterization of a bio-oil from pyrolysis of rice husk by detailed compositional analysis and structural investigation of lignin," *Bioresource Technology*, vol. 116, pp. 114–119, 2012.

[21] M.-J. Ding, Z.-M. Zong, Y. Zong et al., "Isolation and identification of fatty acid amides from Shengli coal," *Energy & Fuels*, vol. 22, no. 4, pp. 2419–2421, 2008.

[22] Y. Lu, X.-Y. Wei, Z.-M. Zong et al., "Organonitrogen compounds identified in degraded wheat straw by oxidation in a sodium hypochlorite aqueous solution," *Fuel*, vol. 109, pp. 61–67, 2013.

[23] Y. Lu, *Sequential oxidation of rice husk, wheat straw and their extraction residues [Ph. D. Thesis]*, China University of Mining & Technology, 2013.

[24] L. Feng, G. Zhao, Y. Zhao, M. Zhao, and J. Tang, "Construction of the molecular structure model of the Shengli lignite using TG-GC/MS and FTIR spectrometry data," *Fuel*, vol. 203, pp. 924–931, 2017.

[25] F. Wei, J. Cao P, X. Zhao Y et al., "Nitrogen evolution during fast pyrolysis of sewage sludge under inert and reductive atmospheres," *Energy & Fuels*, vol. 31, no. 7, pp. 7191–7196, 2017.

[26] G. Jiang, G. A. Husseini, L. L. Baxter, and M. R. Linford, "Analysis of straw by X-ray Photoelectron Spectroscopy," *Surface Science Spectra*, vol. 11, no. 2, pp. 91–96, 2004.

[27] D.-Y. Xu, J. Jin, Y. Yan et al., "Characterization of biochar by X-ray photoelectron spectroscopy and 13C nuclear magnetic resonance," *Guang Pu Xue Yu Guang Pu Fen Xi/Spectroscopy and Spectral Analysis*, vol. 34, no. 12, pp. 3415–3418, 2014.

[28] C. Wang F, X. Fan, F. Zhang et al., "Characterization of humic acids extracted from a lignite and interpretation for the mass spectra," *RSC Advances*, vol. 7, pp. 20677–20684, 2017.

[29] M. Gopi Kiran, K. Pakshirajan, and G. Das, "Heavy metal removal using sulfate-reducing biomass obtained from a lab-scale upflow anaerobic-packed bed reactor," *Journal of Environmental Engineering*, vol. 142, no. 9, article C4015010, 2016.

[30] L. Xu, X. Zheng, H. Cui, Z. Zhu, J. Liang, and J. Zhou, "Equilibrium, kinetic, and thermodynamic studies on the adsorption of cadmium from aqueous solution by modified biomass ash," *Bioinorganic Chemistry and Applications*, vol. 2017, Article ID 3695604, 9 pages, 2017.

[31] Z. Hao, J. Cao, Y. Wu et al., "Preparation of porous carbon sphere from waste sugar solution for electric double-layer capacitor," *Journal of Power Sources*, vol. 361, pp. 249–258, 2017.

[32] T. Attard M, C. McElroy R, and J. Hunt A, "Economic assessment of supercritical CO2 extraction of waxes as part of a maize stover biorefinery," *International Journal of Molecular Sciences*, vol. 16, pp. 17546–17564, 2015.

[33] I. Delidovich, K. Leonhard, and R. Palkovits, "Cellulose and hemicellulose valorisation: An integrated challenge of catalysis and reaction engineering," *Energy & Environmental Science*, vol. 7, no. 9, pp. 2803–2830, 2014.

[34] E. William N, K. Alan D, and Steroids., "Pharmacology, complications, and practice delivery issue," *The Ochsner Journal*, vol. 14, no. 2, article 4052587, 2014.

[35] B. O. Keller, J. Sui, A. B. Young, and R. M. Whittal, "Interferences and contaminants encountered in modern mass spectrometry," *Analytica Chimica Acta*, vol. 627, no. 1, pp. 71–81, 2008.

[36] H. Bubert, J. Lambert, and P. Burba, "Structural and elemental investigations of isolated aquatic humic substances using X-ray photoelectron spectroscopy," *Fresenius' Journal of Analytical Chemistry*, vol. 368, no. 2-3, pp. 274–280, 2000.

[37] C. Atik and S. Ates, "Mass balance of silica in straw from the perspective of silica reduction in straw pulp," *Bioresources*, vol. 7, no. 3, pp. 3274–3282, 2012.

[38] S. Neu, J. Schaller, and E. G. Dudel, "Silicon availability modifies nutrient use efficiency and content, C:N:P stoichiometry, and productivity of winter wheat (Triticum aestivum L.)," *Scientific Reports*, vol. 7, article 40829, 2017.

[39] H. A. Alyosef, D. Schneider, S. Wassersleben et al., "Meso/macroporous silica from miscanthus, cereal remnant pellets, and wheat straw," *ACS Sustainable Chemistry & Engineering*, vol. 3, no. 9, pp. 2012–2021, 2015.

[40] M. Gocke, W. Liang, M. Sommer, and Y. Kuzyakov, "Silicon uptake by wheat: Effects of Si pools and pH," *Journal of Plant Nutrition and Soil Science*, vol. 176, no. 4, pp. 551–560, 2013.

[41] V. Pérez Cuadra and P. Hermann, "Characterization and macropattern of calcium oxalate phytoliths in Argentinean endemic species of Chenopodioideae (Amaranthaceae)," *Quaternary International*, vol. 287, pp. 83–88, 2013.

[42] M. Pierantoni, R. Tenne, V. Brumfeld et al., "Plants and light manipulation: the integrated mineral system in okra leaves," *Advanced Science*, vol. 4, no. 5, article 16000416, 2017.

[43] B. S. Tubana, T. Babu, and L. E. Datnoff, "A review of silicon in soils and plants and its role in us agriculture: History and future perspectives," *Soil Science*, vol. 181, no. 9-10, pp. 393–411, 2016.

[44] D. Buraczyńska and F. Ceglarek, "Previous crop value of post-harvest residues and straw of spring wheat, field pea and their mixtures for winter triticale part I. Weight and chemical composition of post-harvest residues and straw," *Acta Scientiarum Polonorum, Agricultura*, vol. 10, no. 2, pp. 3–18, 2011.

[45] I. R. Shaikh, R. A. Shaikh, A. A. Shaikh et al., "H-ZSM-5 zeolite synthesis by sourcing silica from the wheat husk Ash: characterization and application as a versatile heterogeneous catalyst in organic transformations including some multicomponent reactions," *Journal of Catalysts*, vol. 2015, Article ID 805714, 14 pages, 2015.

[46] B. Wang, Y. Huang, and J. Zhang, "Sulfur distribution during hydrothermal liquefaction of lignite, wheat straw and plastic waste in sub-critical water," *China Petroleum Processing and Petrochemical Technology*, vol. 17, no. 1, pp. 24–30, 2015.

[47] P. E. A. Debiagi, C. Pecchi, G. Gentile et al., "Extractives extend the applicability of multistep kinetic scheme of biomass pyrolysis," *Energy & Fuels*, vol. 29, no. 10, pp. 6544–6555, 2015.

[48] L. Deng and D. Che, "Chemical, electrochemical and spectral characterization of water leachates from biomass," *Industrial & Engineering Chemistry Research*, vol. 51, no. 48, pp. 15710–15719, 2012.

[49] L. Wang, G. Skjevrak, J. E. Hustad, and Ø. Skreiberg, "Investigation of biomass ash sintering characteristics and the effect of additives," *Energy & Fuels*, vol. 28, no. 1, pp. 208–218, 2014.

[50] M. Nieves-Cordones, F. R. Al Shiblawi, and H. Sentenac, "Roles and transport of sodium and potassium in plants," *Metal Ions in Life Sciences*, vol. 16, pp. 291–324, 2016.

[51] M. Yamada, C. Kuroda, and H. Fujiyama, "Function of sodium and potassium in growth of sodium-loving Amaranthaceae species," *Soil Science & Plant Nutrition*, vol. 62, no. 1, pp. 20–26, 2016.

[52] W. Guo, H. Nazim, Z. Liang, and D. Yang, "Magnesium deficiency in plants: An urgent problem," *The Crop Journal*, vol. 4, no. 2, pp. 83–91, 2016.

Hindawi
International Journal of Analytical Chemistry
Volume 2017, Article ID 4763937, 8 pages
https://doi.org/10.1155/2017/4763937

Research Article

Separation Process of Fine Coals by Ultrasonic Vibration Gas-Solid Fluidized Bed

Shuai Wang,[1] Yaqun He,[1,2] Hua Wei,[1] and Weining Xie[1]

[1]*Advanced Analysis and Computation Center, China University of Mining and Technology, Xuzhou 221116, China*
[2]*School of Chemical Engineering and Technology, China University of Mining and Technology, Xuzhou, Jiangsu 221116, China*

Correspondence should be addressed to Yaqun He; yqhe_cumt@126.com

Received 16 March 2017; Revised 7 May 2017; Accepted 25 May 2017; Published 6 August 2017

Academic Editor: Xun Hu

Ultrasonic vibration gas-solid fluidized bed was proposed and introduced to separate fine coals (0.5–0.125 mm fraction). Several technological methods such as XRF, XRD, XPS, and EPMA were used to study the composition of heavy products to evaluate the separation effect. Results show that the ultrasonic vibration force field strengthens the particle separation process based on density when the vibration frequency is 35 kHz and the fluidization number is 1.8. The ash difference between the light and heavy products and the recovery of combustible material obtain the maximum values of 47.30% and 89.59%, respectively. The sulfur content of the heavy product reaches the maximum value of 6.78%. Chemical state analysis of sulfur shows that organic sulfur (-C-S-), sulfate-sulfur (-SO_4), and pyrite-sulfur (-S_2) are confirmed in the original coal and heavy product. Organic sulfur (-C-S-) is mainly concentrated in the light product, and pyrite-sulfur (-S_2) is significantly enriched in the heavy product. The element composition, phase composition, backscatter imagery, and surface distribution of elements for heavy product show concentration of high-density minerals including pyrite, quartz, and kaolinite. Some harmful elements such as F, Pb, and As are also concentrated in the heavy product.

1. Introduction

Coal is an important primary energy source worldwide, especially in China. In China, coal-fired power is predominant in the production of the Chinese electric power and accounts for more than 70% [1]. Coal contains appreciable quantity of inorganic minerals and harmful elements, such as sulfur, lead, arsenic, and mercury; these minerals and elements can be transformed into inhalable particles, acid rain, and other pollutants and can be discharged into the atmosphere during coal combustion [2], thereby resulting in serious pollution to the atmosphere and large economic losses [3–6]. Thus, desulfurization and deashing of coal prior to combustion are important to prevent fog haze weather.

Although lump coals are separated prior to milling to remove large pieces of waste rock, fine waste rocks containing harmful elements inlay in the coal are not always removed. If coal is sufficiently crushed to fine particles, then the mineral particles can be fully dissociated from the coal. Such condition is favorable to the separation process. Fine coals are currently separated mainly by flotation, which can effectively separate <0.5 mm fraction coal [7–9]. The development of cyclonic-static microbubble flotation column and new reagent systems has enabled good results of low-rank coal separation [9–13]. However, the flotation process consumes large amounts of water, and its development in arid regions is limited by water resource deficiency. Thus, high-efficiency dry separation technology of fine coals should be investigated.

Dry separation technologies, especially the separation technology of the gas-solid fluidized bed, are currently used to separate coal [14–19]. For example, air dense medium fluidized bed is used to effectively separate coal of 50−6 mm size fraction [20–24]. Xu and Zhu [25] examined the influence of vibration parameter on the fluidization characteristics of fine materials. Luo et al. [26] separated coal of 6−1 mm size fraction by use of air dense medium fluidized bed and analyze the particle force condition. Yang et al. [27, 28] used

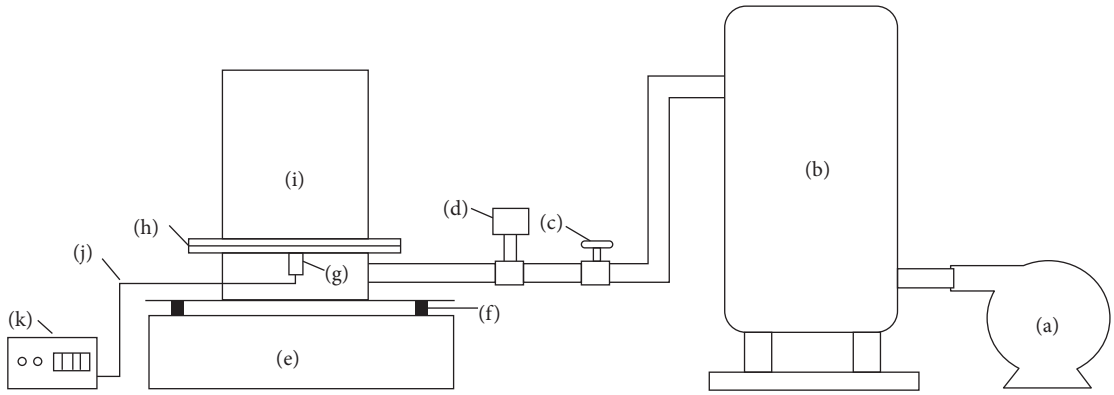

Figure 1: Schematic diagram of the experimental system: (a) roots blower; (b) air reservoir; (c) air valve; (d) vortex flow meter; (e) pedestal; (f) spring; (g) ultrasonic transducer; (h) air distribution plate; (i) fluidized bed; (j) cable; (k) ultrasonic power supply.

vibrated fluidized bed to separate coal of 6–3 and 3–1 mm size fractions without a dense medium. These abovementioned dry separation methods can effectively separate >0.5 mm fraction coal but present difficulty in separating <0.5 mm fraction coal and exhibit many limitations. Thus, new dry separation methods to deal with fine coal of <0.5 mm fraction should be explored.

This study investigated the separation process of the 0.5–0.125 mm fraction coal with ultrasonic vibration gas-solid fluidized bed. The composition of products under different experimental conditions was studied by advanced analysis and test methods to evaluate the separation results.

2. Materials and Methods

2.1. Sampling and Experimental Device. The 0.5–0.125 mm fraction coal was chosen to study the separation process. The ash content of the coal was 36.21%, and its sulfur content reached 2.82%. The coal was obviously of high sulfur content. The schematic of experimental system is shown in Figure 1. The system included air supply and separation systems. The air supply system included a roots blower, an air reservoir, a rotor flow meter, and an air valve. The separation system included a gas-solid fluidized bed and an ultrasonic vibration device. The fluidized bed was made of organic glass (radius of 75 mm and height of 300 mm), and the ultrasonic vibration device included one ultrasonic transducer and one ultrasonic power supply. The ultrasonic transducer was fixed to the bottom of the air distribution plate. The air came from the blower and enters the fluidized bed through the pipe, air reservoir, rotor flow meter, and air distributor. The vibration force field came from the ultrasonic vibrator, which was controlled by ultrasonic generator. The height of the static bed containing the material was 100 mm. The product was divided into five layers, and the thickness ratio of each layer from upper to lower was 1 : 1 : 1 : 1 : 1.

To obtain high-density mineral as pure as possible, the product of the fifth layer was collected as the heavy product, whereas that in the upper four layers was collected as the light product. The ash contents of light and heavy products were measured. The recovery of combustible material was calculated using (1) to estimate the separation effect.

$$E = \gamma_j \times \left(\frac{100 - \mathrm{Ad}_j}{100 - \mathrm{Ad}_y} \right) \times 100\%, \quad (1)$$

where E is the recovery of combustible material; γ_j is the yield of light product; Ad_j and Ad_y are the ash contents of the light product and raw coal, respectively.

2.2. XRF Analysis. X-ray fluorescence spectrometer (XRF, S8 Tiger, Bruker, Germany) was applied to the sulfur content analysis for different products to study the separation effect at different experimental conditions. The XRF worked at 20 kV–60 kV and 10 mA–100 mA; the collimator angle was 0.23°.

2.3. XRD Analysis. The phase composition analysis was run with an X-ray diffractometer (XRD, D8 Advance, Bruker, Germany) for heavy product from separation process with a voltage of 40 kV and a current of 30 mA. XRD data were recorded in a scanning mode from the detective angle of 3°–90° with the step of 0.01945° (step) and the scanning speed of 0.1 s/step.

2.4. XPS Analysis. X-ray photoelectron spectrometer (XPS, ESCALAB 250Xi, Thermo Fisher, America) with Al Ka radiation (hv = 1486.6 eV) and a 900 μm light spot size was used to analyze the chemical state of sulfur in the coal.

2.5. EPMA Analysis. Field emission electron probe microanalyzer (EPMA, 8050G, Shimadzu, Japan) was applied to the microstructure, backscatter imaging, and area distribution of element analysis for the heavy products. The beam size was Min, the BC electric current was 10–100 nA, and the testing voltage was 15 kV.

3. Results and Discussion

3.1. Effect of Operating Parameters on Separation. The separation results in Figure 2 present the influence of vibration

Table 1: Sulfur content of each layer of product.

Layer number	Sulfur content/%					
	0 Hz	20 kHz	25 kHz	30 kHz	35 kHz	40 kHz
First layer	1.52	1.38	1.35	1.33	1.26	1.48
Second layer	2.11	1.96	1.93	1.86	1.82	1.98
Third layer	2.23	2.18	2.26	2.14	2.22	2.08
Forth layer	2.26	2.32	2.35	2.28	2.25	2.29
Fifth layer	6.56	6.75	6.73	6.68	6.89	6.77

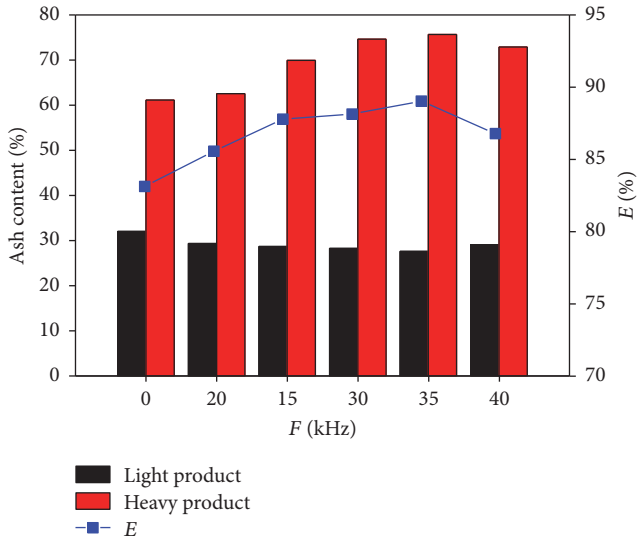

Figure 2: Separation results at different vibration frequency.

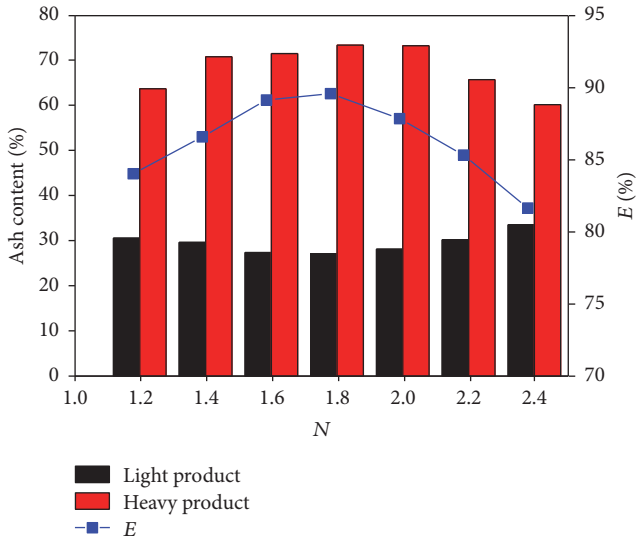

Figure 3: Separation results at different fluidization number.

frequency ranging from 20 kHz to 40 kHz and no vibration at a fluidization number of 1.6 and a separation time of 30 s. The ash difference between the light and heavy products and the recovery of combustible material are all minimal at 29.08% and 83.13%, respectively, under no vibration condition. With the increase in vibration frequency from 20 kHz to 35 kHz, the ash difference between the light and heavy products and the recovery of combustible material increase and reach the maximum values of 47.07% and 89.04%, respectively, at 35 kHz. After 35 kHz, the ash difference and the recovery of combustible material decrease. Thus, the addition of ultrasonic vibration field intensifies the separation process of fine coal under different densities.

Table 1 shows the sulfur content of each layer of product at different vibration frequencies. Sulfur is mainly concentrated in the fifth layer, the contents of which are all above 6%, and the maximum value is 6.89% when the vibration frequency is 35 kHz. On the contrary, the sulfur contents of the first layer at different vibration frequencies are low at below 1.6%. The minimum value is 1.26% when the vibration frequency is 35 kHz.

Figure 3 shows the separation results obtained at different fluidization numbers at a vibration frequency of 35 kHz and at a fluidizing time of 30 s. At low fluidization number, the bed liquidity is poor and the resistance to particle sedimentation is high. Thus, the separation of the coal and high-density minerals becomes difficult. With the increase in the fluidization number, the bed fluidity and the separation effect also increase. The ash difference between the light and heavy products and the recovery of combustible material obtain the maximum values of 47.30% and 89.59%, respectively, when the fluidization number is 1.8. Thereafter, the separation effect decreases with the further increase in the fluidization number. The reason is that the bed stability is destroyed because of the increase in gas velocity, thereby leading to serious back mixing between the light and heavy products.

Table 2 shows the sulfur content of each layer of product at different fluidization numbers. Similarly, sulfur is mainly concentrated in the fifth layer, and the maximum value is 6.78% when the fluidization number is 1.8. The sulfur contents of the first layer are all below 2.0%, and the minimum value is 1.22% when the fluidization number is 2.0.

3.2. Component Analysis of Products. The results of the main element content analysis of the original coal and light and heavy products are shown in Table 3. In the light product, the contents of magnesium, calcium, iron, silicon, aluminum, and sulfur decrease compared with those in the original coal. On the contrary, these contents obviously increase in the heavy product, especially those of sulfur and iron.

The XPS spectra of sulfur in different samples are shown in Figure 4, and the content of sulfur in different chemical

Table 2: Sulfur content of each layer of product.

Layer number	Sulfur content/%						
	1.2	1.4	1.6	1.8	2.0	2.2	2.4
First layer	2.12	1.76	1.34	1.25	1.22	1.58	2.25
Second layer	2.23	2.03	1.92	1.78	1.80	1.89	2.28
Third layer	2.33	2.38	2.02	1.84	1.92	2.44	2.96
Forth layer	2.45	2.27	2.13	2.10	2.15	2.53	3.12
Fifth layer	5.36	6.15	6.33	6.78	6.59	5.62	4.98

Table 3: Elemental composition of different samples.

Sample name	Element content/%						
	MgO	CaO	Fe_2O_3	Al_2O_3	SiO_2	S	P
Original coal	0.16	2.74	2.02	11.91	13.06	2.43	0.021
Light product	0.10	0.61	0.63	9.76	12.07	1.66	0.022
Heavy product	0.58	2.03	3.68	20.38	39.28	6.78	0.029

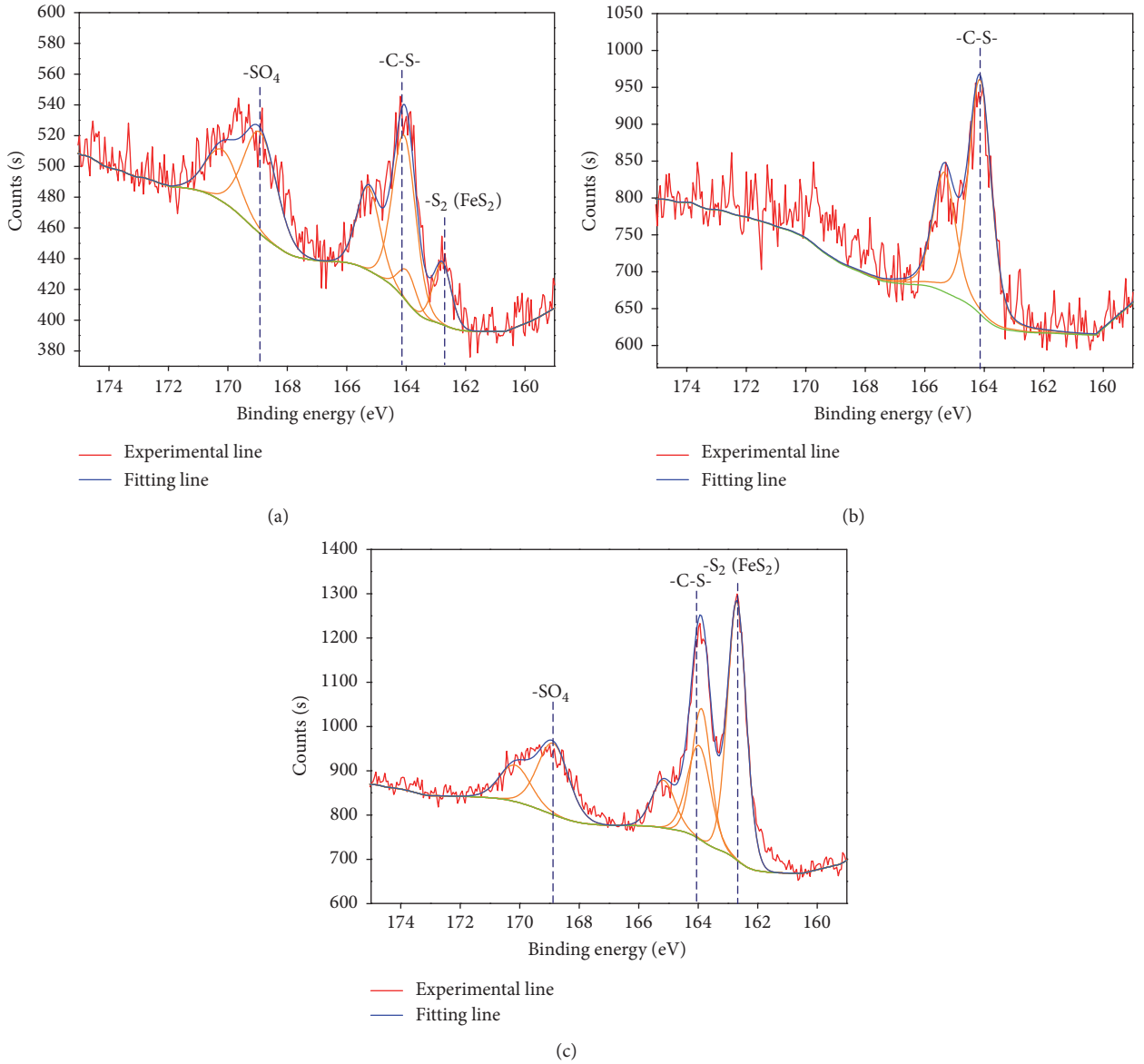

Figure 4: X-ray photoelectron spectroscopy spectra of the coal: (a) original coal; (b) light product; (c) heavy product.

Table 4: Content of sulfur in different chemical states.

Name	Original coal		Heavy product	
	Peak BE	Atomic%	Peak BE	Atomic%
$-SO_4$	168.91	40.75	168.88	24.03
-C-S-	164.06	45.75	163.97	23.43
$-S_2$	162.78	13.5	162.7	52.54

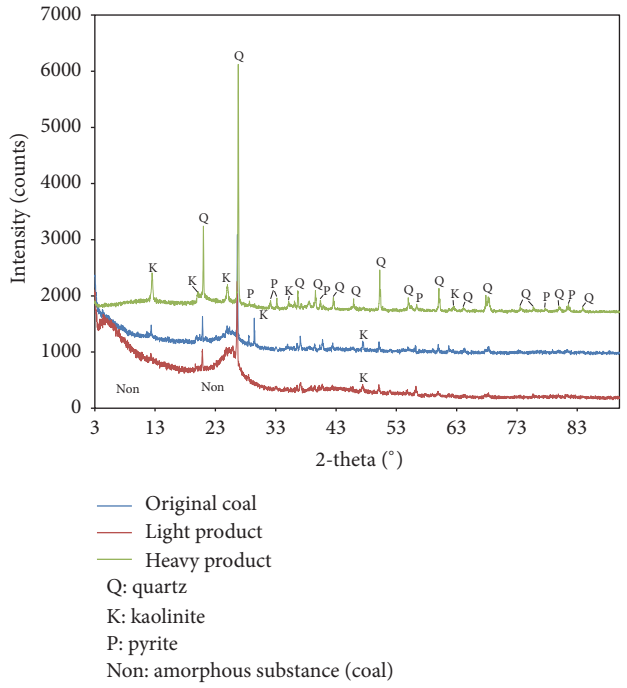

Figure 5: X-ray diffraction of the different samples.

states is shown in Table 4. Organic sulfur (-C-S-), sulfate-sulfur ($-SO_4$), and pyrite-sulfur ($-S_2$) are confirmed in the original coal and heavy product by their binding energies, whereas mainly organic sulfur (-C-S-) exists in the light product. In the original coal, the contents of $-SO_4$, -C-S-, and $-S_2$ are 40.75, 45.75, and 13.5 at.%, respectively. The contents are 24.03, 23.43, and 52.54 at.% in the heavy product. According to the peak area, the pyrite and sulfate are evidently enriched in the heavy product.

Figure 5 shows the XRD analysis results for the original coal and light and heavy products. The wide and dispersion diffraction peaks of the light product show obvious amorphous characteristics, and the original coal exhibits a few sharp diffraction peaks of mineral. At the same time, the heavy product presents obvious crystal characteristics due to the appearance of several sharp diffraction peaks. Apart from a few amorphous minerals (coals), numerous high-density minerals such as quartz, kaolinite, and pyrite are enriched in the heavy product.

The backscatter imagery and surface distribution of elements in heavy product are shown in Figure 6. In the backscatter imagery, high-density particles with high average atomic number are bright, especially the particles that contain iron. The main elements in the heavy product are Si, Al, and Ca. In other words, aluminosilicate minerals are the main minerals in the heavy product. In addition, sulfur and iron exist in the heavy product. The distribution of sulfur is also the same as that of iron, thereby indicating that S exists in the form of pyrite. Therefore, pyrite has been separated during the separation experiment.

The backscatter imagery of different minerals in heavy product by qualitative analysis is shown in Figure 7. Obviously, high-density minerals such as pyrite, quartz, kaolinite, chalcopyrite, gypsum, and iron oxide are effectively separated in the separation process.

Some harmful elements such as Pb, As, and F are also found in the heavy product by qualitative analysis as shown in Figure 8. These particles contain harmful elements that are generally distributed in large particles with tiny sizes. In addition, S and Fe always appear in the same particle containing the abovementioned harmful elements. This condition means that pyrite is the important medium for those elements. Thus, removal of pyrite is the key to the desulfurization and detoxification of fine coal.

4. Conclusion

The 0.5–0.125 mm fraction fine coal is separated effectively by ultrasonic vibration gas-solid fluidized bed. After adding the ultrasonic vibration force field, the particle separation process based on density is strengthened, and the best result appears when the vibration frequency is 35 kHz. The ash difference between the light and heavy products and the recovery of combustible material reach the maximum values of 47.07% and 89.04%, respectively. Airflow velocity significantly influences the separation. When the fluidization number is low, the bed liquidity is poor and the resistance to particle sedimentation is high. Conversely, the bed stability is destroyed and the back mixing between the light and heavy products occurs, thereby hindering the separation. When the vibration frequency is 35 kHz and the fluidization number is 1.8, the ash difference between the light and heavy products and the recovery of combustible material obtain the maximum values of 47.30% and 89.59%, respectively. Sulfur is mainly concentrated in the heavy product, and the content reaches the maximum value of 6.78%.

The XPS results show that -C-S-, $-SO_4$, and $-S_2$ exist in the original coal and heavy product; however, the content of $-S_2$ in the heavy product is higher than that in the original coal. On the contrary, -C-S- mainly exists in the light product. According to the peak area, pyrite and sulfate are evidently enriched in the heavy product. The XRF and XRD results also show that several high-density minerals such as quartz, kaolinite, and pyrite are enriched in the heavy product. Some harmful elements such as F, Pb, and As are also found in the heavy product by EPMA. These elements are generally distributed in large particles with tiny sizes. Therefore, fine coal is effectively separated by the proposed method and thus the target of desulfurization and deashing by ultrasonic vibration gas-solid fluidized bed is realized.

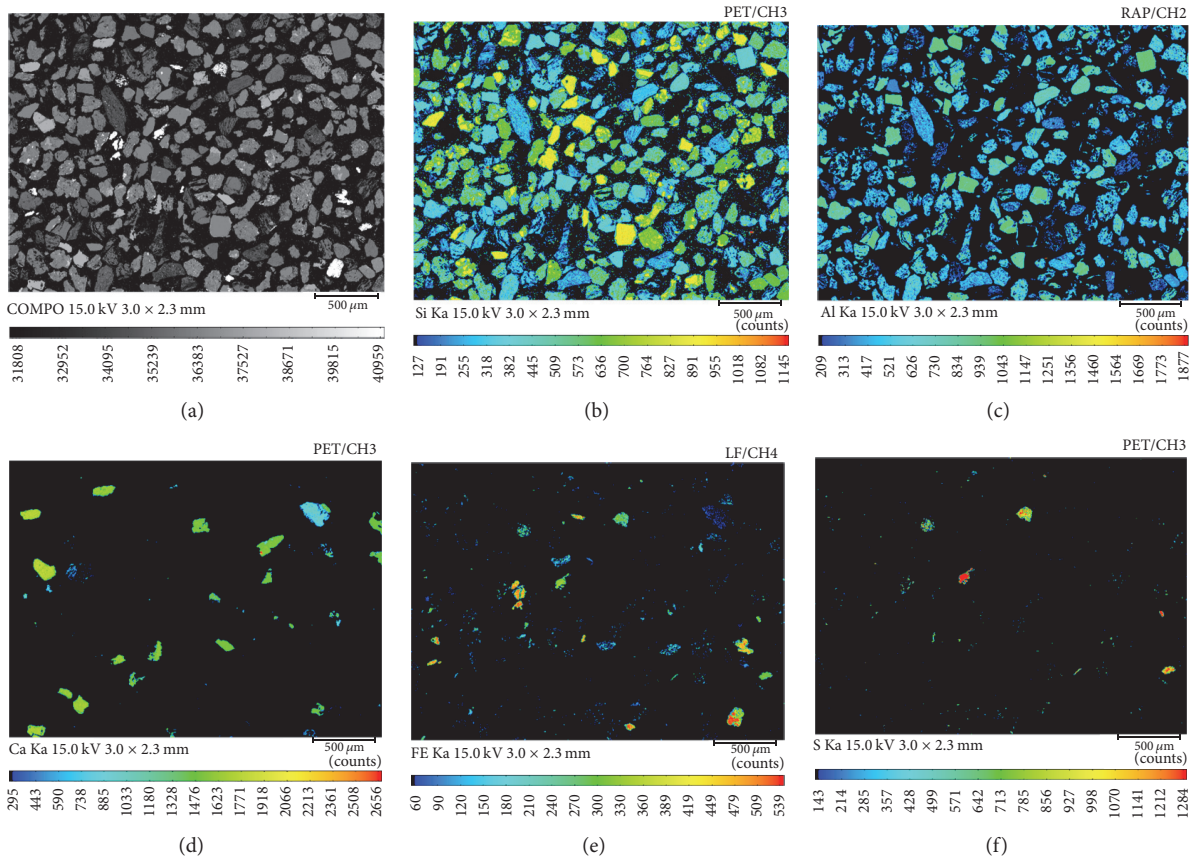

Figure 6: Surface distribution of elements in heavy product: (a) backscatter imagery of heavy product; (b) Si; (c) Al; (d) Ca; (e) Fe; (f) S.

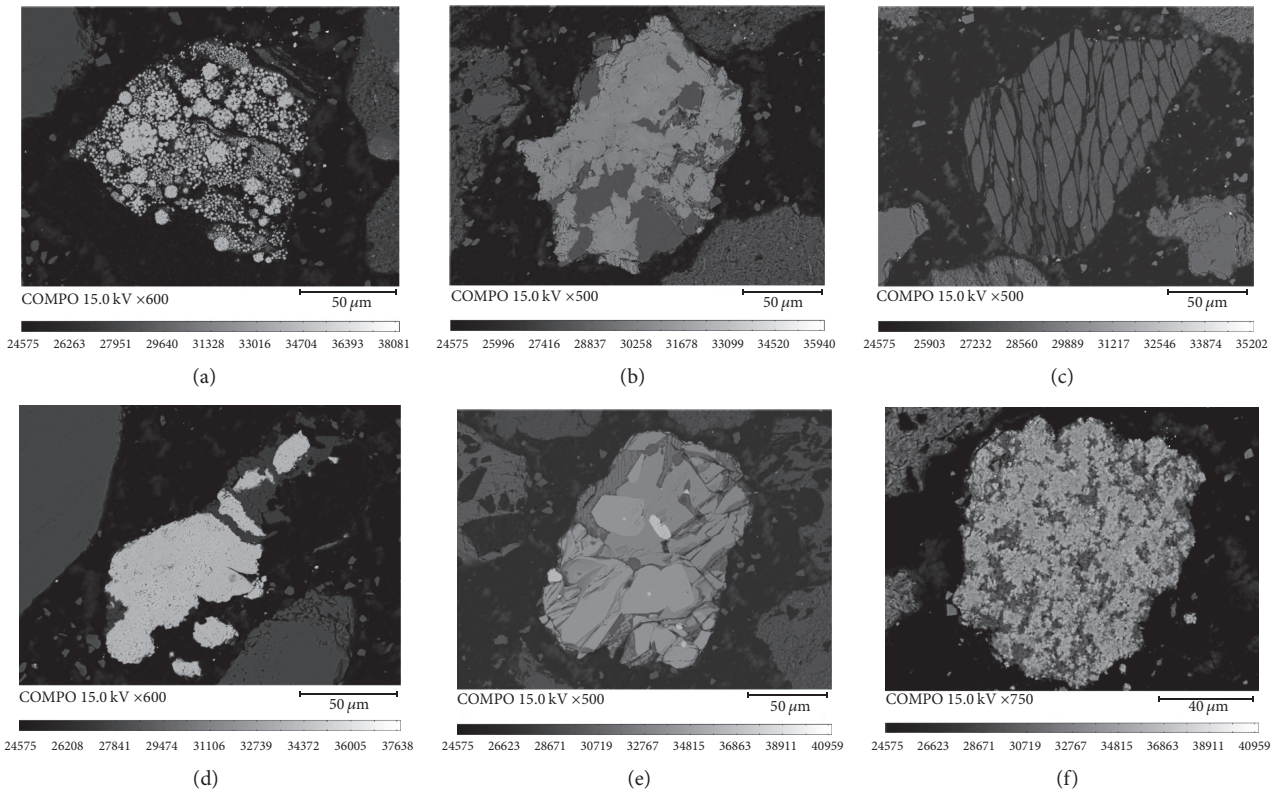

Figure 7: Backscatter imagery of different mineral in heavy product: (a) pyrite; (b) quartz; (c) kaolinite; (d) iron oxide; (e) chalcopyrite; (f) gypsum.

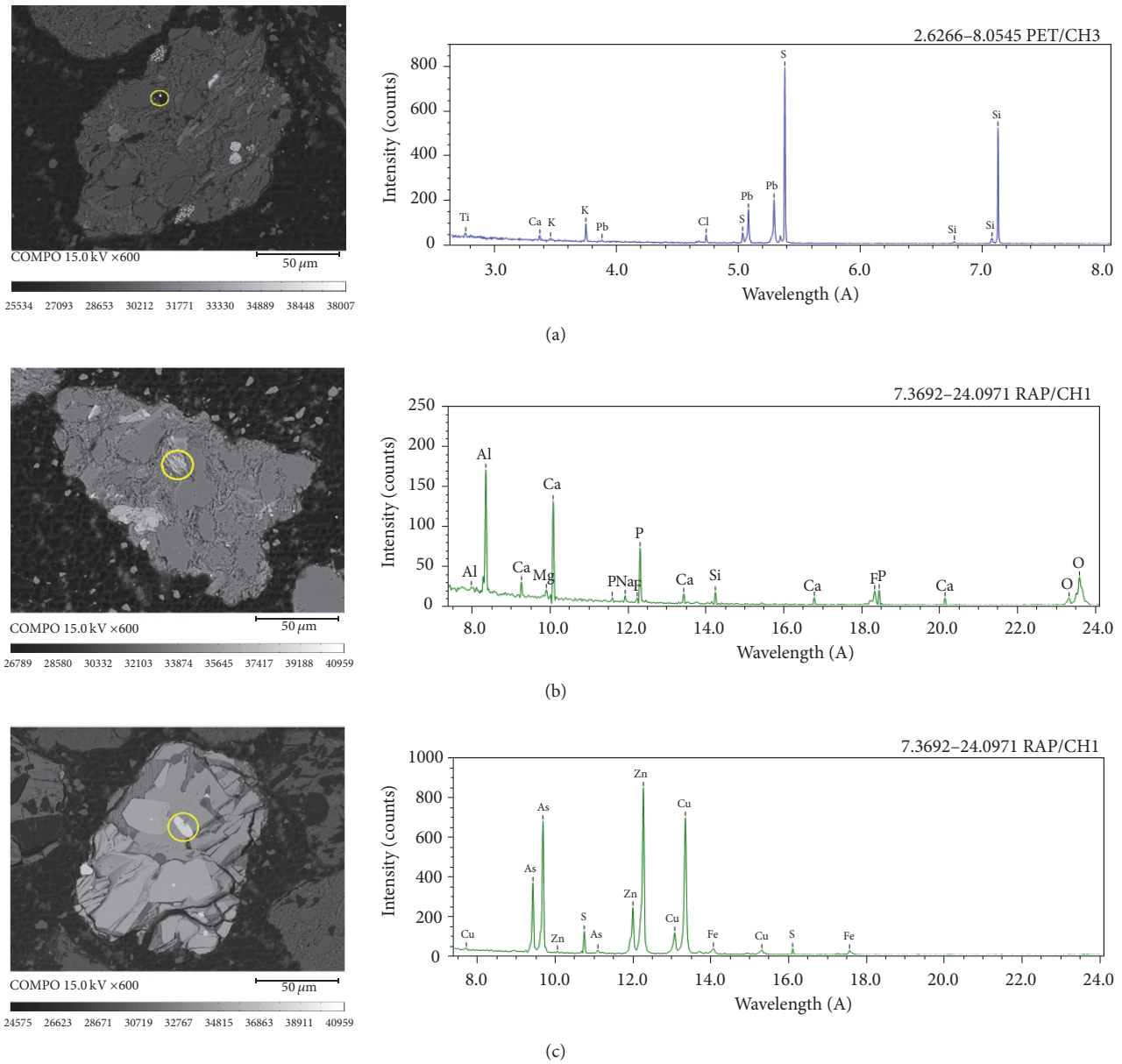

Figure 8: Qualitative analysis of particles containing harmful elements: (a) lead particle; (b) fluoride particle; (c) arsenic particle.

Conflicts of Interest

The authors declare that there are no conflicts of interest regarding the publication of this paper.

Acknowledgments

This project received funding from the National Natural Science Foundation of China (51404267 and 51574234). The authors would like to acknowledge the Advanced Analysis and Computation Center of China University of Mining and Technology for their technical support.

References

[1] W.-N. Xie, Y.-Q. He, Y.-H. Zhang et al., "Simulation study of the energy-size reduction of MPS vertical spindle pulverizer," *Fuel*, vol. 139, pp. 180–189, 2015.

[2] Q. Zhang, Z. Shen, J. Cao et al., "Variations in PM2.5, TSP, BC, and trace gases (NO_2, SO_2, and O_3) between haze and non-haze episodes in winter over Xi'an, China," *Atmospheric Environment*, vol. 112, pp. 64–71, 2015.

[3] H. F. Zhang, J. Hu, Y. X. Qi et al., "Emission characterization, environmental impact, and control measure of PM2.5 emitted from agricultural crop residue burning in China," *Journal of Cleaner Production*, vol. 149, pp. 629–635, 2017.

[4] Y. L. Zhang and F. Cao, "Is it time to tackle PM2.5 air pollutions in China from biomass-burning emissions?" *Environmental Pollution*, vol. 202, pp. 217–219, 2015.

[5] X. Fan, G.-F. Liu, Z.-M. Zong et al., "Ni-and Pd/C-catalyzed hydrodenitrogenation of isoquinoline," *Energy Sources, Part A: Recovery, Utilization and Environmental Effects*, vol. 37, no. 1, pp. 55–60, 2015.

[6] X. Fan, G.-F. Liu, Z.-M. Zong et al., "Mechanism for catalytic hydrodenitrogenation of isoquinoline," *Fuel Processing Technology*, vol. 106, pp. 661–665, 2013.

[7] Y. W. Xing, X. H. Xu, X. H. Gui, Y. J. Cao, and M. D. Xu, "Effect of kaolinite and montmorillonite on fine coal flotation," *Fuel*, vol. 195, pp. 284–289, 2017.

[8] K. B. Tankersley, L. A. Owen, N. P. Dunning et al., "Microflotation removal of coal contaminants from archaeological radiocarbon samples from Chaco Canyon, New Mexico, USA," *Journal of Archaeological Science: Reports*, vol. 12, pp. 66–73, 2017.

[9] K. Jiang, J. E. Dickinson, and K. P. Galvin, "Two-stage fast flotation of coal tailings using reflux flotation," *Minerals Engineering*, vol. 98, pp. 151–160, 2016.

[10] Y. Xing, X. Gui, Y. Cao, D. Wang, and H. Zhang, "Clean low-rank-coal purification technique combining cyclonic-static microbubble flotation column with collector emulsification," *Journal of Cleaner Production*, 2015.

[11] X. Gui, Y. Xing, G. Rong, Y. Cao, and J. Liu, "Interaction forces between coal and kaolinite particles measured by atomic force microscopy," *Powder Technology*, vol. 301, pp. 349–355, 2016.

[12] W. Xia, J. Yang, and C. Liang, "A short review of improvement in flotation of low rank/oxidized coals by pretreatments," *Powder Technology*, vol. 237, pp. 1–8, 2013.

[13] J.-L. Xia, X. Fan, C.-Y. You, X.-Y. Wei, Y.-P. Zhao, and J.-P. Cao, "Sequential ultrasonic extraction of a Chinese coal and characterization of nitrogen-containing compounds in the extracts using high-performance liquid chromatography with mass spectrometry," *Journal of Separation Science*, vol. 39, no. 13, pp. 2491–2498, 2016.

[14] S. Wang, Y. He, J. He, L. Ge, and Q. Liu, "Experiment and simulation on the pyrite removal from the recirculating load of pulverizer with a dilute phase gas-solid fluidized bed," *International Journal of Mining Science and Technology*, vol. 23, no. 2, pp. 301–305, 2013.

[15] S. A. Macpherson, S. M. Iveson, and K. P. Galvin, "Density based separations in the Reflux Classifier with an air-sand dense-medium and vibration," *Minerals Engineering*, vol. 23, no. 2, pp. 74–82, 2010.

[16] J. Oshitani, T. Kawahito, M. Yoshida, K. Gotoh, and G. V. Franks, "The influence of the density of a gas-solid fluidized bed on the dry dense medium separation of lump iron ore," *Minerals Engineering*, vol. 24, no. 1, pp. 70–76, 2011.

[17] J. He, Y. Zhao, Z. Luo, Y. He, and C. Duan, "Numerical simulation and experimental verification of bubble size distribution in an air dense medium fluidized bed," *International Journal of Mining Science and Technology*, vol. 23, no. 3, pp. 387–393, 2013.

[18] L. Dong, Y. Zhao, C. Duan, Z. Luo, B. Zhang, and X. Yang, "Characteristics of bubble and fine coal separation using active pulsing air dense medium fluidized bed," *Powder Technology*, vol. 257, pp. 40–46, 2014.

[19] Y. Q. He, H. F. Wang, C. L. Duan, and S. L. Song, "Airflow fields simulation on passive pulsing air classifiers," *Journal of the South African Institute of Ming and Metallurgy*, vol. 105, pp. 525–531, 2005.

[20] T. Lind, J. Hokkinen, and J. K. Jokiniemi, "Fine particle and trace element emissions from waste combustion - Comparison of fluidized bed and grate firing," *Fuel Processing Technology*, vol. 88, no. 7, pp. 737–746, 2007.

[21] M. Fan, Q. Chen, Y. Zhao, Z. L. Y. Guan, and B. Li, "Magnetically stabilized fluidized beds for fine coal separation," *Powder Technology*, vol. 123, no. 2-3, pp. 208–211, 2002.

[22] Y. Zhao, L. Tang, Z. Luo et al., "Experimental and numerical simulation studies of the fluidization characteristics of a separating gas-solid fluidized bed," *Fuel Processing Technology*, vol. 91, no. 12, pp. 1819–1825, 2010.

[23] Y. M. Zhao, X. J. Liu, K. L. Liu et al., "Fluidization characteristics of a gas-paigeite-powder bed to be utilized for dry coal beneficiation," *International Journal of Coal Preparation and Utilization*, vol. 31, no. 3-4, pp. 149–160, 2011.

[24] X. Fan, X.-Y. Wei, and Z.-M. Zong, "Application of gas chromatography/mass spectrometry in studies on separation and identification of organic species in coals," *Fuel*, vol. 109, pp. 28–32, 2013.

[25] C. Xu and J. Zhu, "Parametric study of fine particle fluidization under mechanical vibration," *Powder Technology*, vol. 161, no. 2, pp. 135–144, 2006.

[26] Z. Luo, Y. Zhao, X. Tao, M. Fan, Q. Chen, and L. Wei, "Progress in dry coal cleaning using air-dense medium fluidized beds," *International Journal of Coal Preparation and Utilization*, vol. 23, no. 1-2, pp. 13–20, 2003.

[27] X. Yang, Y. Zhao, Z. Luo, S. Song, C. Duan, and L. Dong, "Fine coal dry cleaning using a vibrated gas-fluidized bed," *Fuel Processing Technology*, vol. 106, pp. 338–343, 2013.

[28] X. Yang, Z. Fu, J. Zhao, E. Zhou, and Y. Zhao, "Process analysis of fine coal preparation using a vibrated gas-fluidized bed," *Powder Technology*, vol. 279, pp. 18–23, 2015.

Hindawi
International Journal of Analytical Chemistry
Volume 2017, Article ID 6953864, 12 pages
https://doi.org/10.1155/2017/6953864

Research Article

Geochemical Characteristics and Origins of the Crude Oil of Triassic Yanchang Formation in Southwestern Yishan Slope, Ordos Basin

Xiaoli Zhang,[1,2] Jinxian He,[1,2] Yande Zhao,[3] Hongchen Wu,[1,2] and Zeqiang Ren[1,2]

[1]*School of Resources and Geoscience, China University of Mining and Technology, Xuzhou 221116, China*
[2]*Key Laboratory of Coalbed Methane Resource and Reservoir Formation Process, Ministry of Education, China University of Mining and Technology, Xuzhou 221116, China*
[3]*Research Institute of Petroleum Exploration and Development, PetroChina Changqing Oilfield Company, Xi'an, Shanxi 710018, China*

Correspondence should be addressed to Xiaoli Zhang; xlzhang@cumt.edu.cn

Received 5 January 2017; Revised 26 April 2017; Accepted 28 May 2017; Published 2 July 2017

Academic Editor: Ya-He Zhang

Biomarker compounds that derived from early living organisms play an important role in oil and gas geochemistry and exploration since they can record the diagenetic evolution of the parent materials of crude oil and reflect the organic geochemical characteristics of crude oil and source rocks. To offer scientific basis for oil exploration and exploitation for study area, gas chromatography-mass spectrometry method is applied to study the biomarker compounds of crude oil in Southwestern Yishan Slope of Ordos Basin, through qualitatively and quantitatively analyzing separated materials. The crude oil of Yanchang Formation and the source rocks of Yan'an and Yanchang Formation were collected in order to systematically analyze the characteristics of the biomarker compounds in saturated hydrocarbon fractions and clarify the organic geochemical characteristics of crude oil. The distribution and composition of various types of hydrocarbon biomarker compounds in crude oil suggest that the parent materials of crude oil are composed of hydrobiont and terrigenous plants, and the crude oil is mature oil which is formed in the weak reducing fresh water environment. Oil source correlation results show that the crude oil of Yanchang Formation in Yishan Slope is sourced from the source rocks of Chang 7 subformation.

1. Introduction

Biomarker compounds that occur in sedimentary organic matter are derived from early living organisms and are stable in the evolution of organic matters. They record the complex organic compounds of original biological parent materials. The maturity of the chromatographic-mass spectrometry technology has ensured the important position of biomarker compounds in oil and gas geochemistry and exploration. Biomarker compounds with characteristic stereochemical structures and rich information have both inheritance and variability in the evolution process of organisms, sedimentary organic matter, oil, and gas. Although the biomarker compounds in crude oil are low in abundance, they are diversified in types and extensive in distribution. Some biomarker compounds with very good specificity and strong mark function are of important significance in judging the source, depositional environment, and maturity of organic matter and studying oil source correlation and hydrocarbon migration [1]. Gas chromatography-mass spectrometry (GC-MS) analysis techniques is the most important method to study the biomarker compounds.

The Ordos Basin as the second largest petroliferous sedimentary basin in China can be divided into six secondary structural units. As the largest secondary structural unit in the Ordos Basin (Figure 1), Yishan Slope is the focus for oil and gas exploration and development in the basin. Triassic Yanchang Formation is the major exploration target in the basin, which is divided into ten oil groups (Chang 1 to Chang 10 from top to bottom) by oil and gas exploration department. Important breakthroughs have been made in the exploration and development of the crude oil in the Ordos Basin and

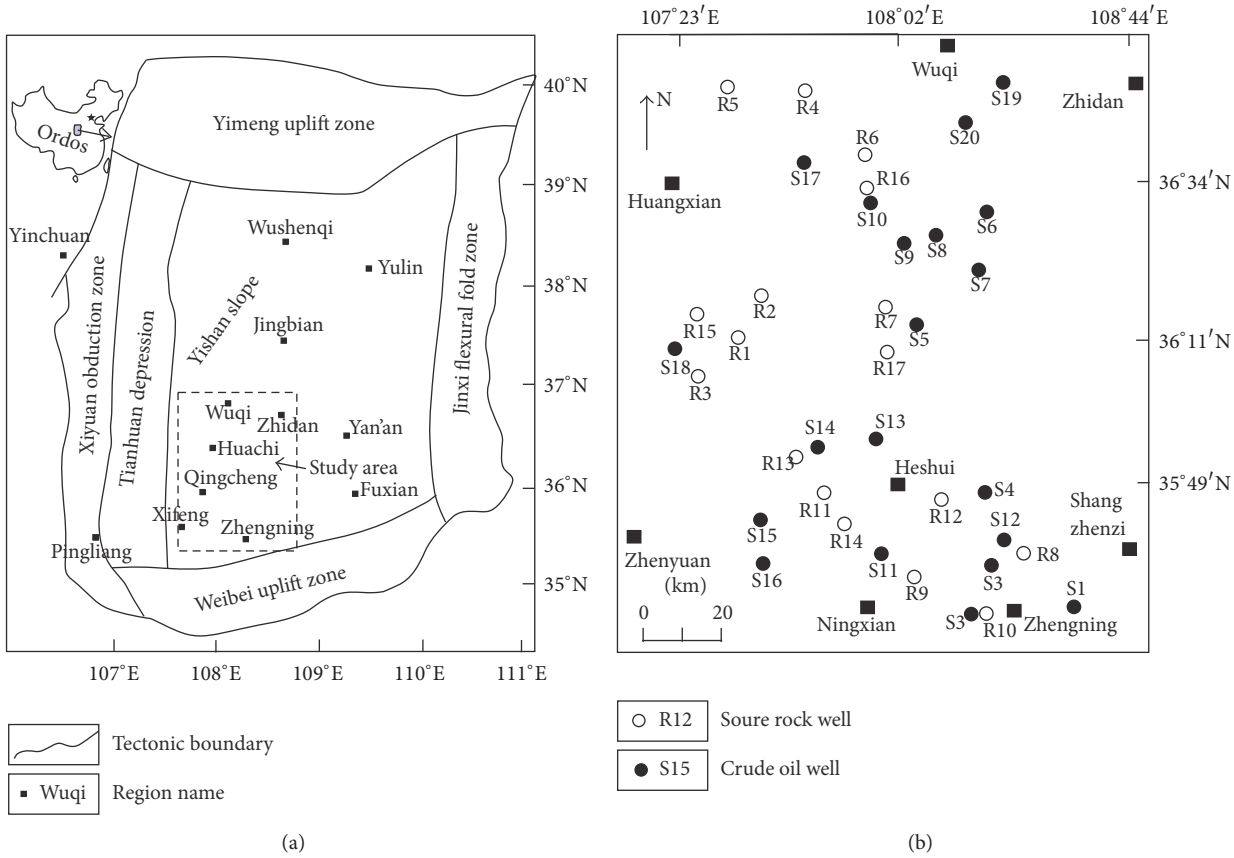

Figure 1: Tectonic units of the Ordos Basin and locations of crude oil and source rock samples.

good achievements have been gained in the geochemical study of Mesozoic crude oil [2–7]. However, because of the scattered geochemical study and uneven distribution of the oil groups of source rock samples [8–11], a systematic study on the geochemistry with abundant samples of crude oil and source rock distributed reasonably in Yanchang Formations is necessary.

In this study, the crude oil samples of Chang 1 to Chang 10 and the source rock samples of Jurassic Yan'an Formation and Yanchang Formation Chang 4 + 5, Chang 6, 7, 8, and Chang 9 were systematically collected to study the geochemistry of crude oil and discuss parent material characteristics, formation environment, and maturity of crude oil, which can provide geochemical evidence for the study on hydrocarbon accumulation.

2. Sampling and Experimentation

2.1. Sampling. Crude oil samples of 20 wells and black mudstone samples of 17 wells were systematically collected from the Southwestern Yishan Slope, Ordos Basin. The well location is shown in Figure 1, and the data of group components of crude oil and source rock samples was shown in Table 1.

2.2. Experimentation

2.2.1. Soxhlet Extraction

Instrument. Soxhlet extractor is composed of three parts, including flask, extractor, and reflux condenser.

Experimental Conditions. The mudstone samples were ground to 100 mesh (0.150 mm) before extraction. 100 g of crushed mudstone, which weighed into a filter cartridge, was extracted using a Soxhlet apparatus. 300 mL chloroform and 2 pieces of red copper slices were added to the flask that was connected to extractor. The flask was heated in water-bath at a temperature of 78–82°C for extracting. Starting from the reflux of chloroform, extraction should last for 72 hours. After extraction, the flask was moved to water-bath kettle to concentrate the leaching liquor. Then, the funnel with degreasing cotton was used to filter. Eventually, the solvent was evaporated in oven at a constant temperature of 40°C until a constant weight.

2.2.2. Group Component Separation

Instrument. Glass chromatographic column.

Experimental Conditions. 15 mL n-hexane was added to 30 mg extract to dissolve for 12 hours. Then asphaltene was removed

Table 1: Data of group component of crude oil and source rock samples in Southwestern Yishan Slope.

	Sample number	Reservoir	Deep (m)	Asp (%)	Sat (%)	Aro (%)	non (%)	Sat/Aro	Asp + non (%)
Crude oil	S1	Chang 1	1614.2	1.39	65.18	8.95	24.47	7.28	25.86
	S2	Chang 2	1671.7	1.32	56.51	10.42	31.76	5.42	33.08
	S3	Chang 2	1652.0	2.04	59.49	7.43	31.04	8.01	33.08
	S4	Chang 2	1643.0	1.40	58.57	10.17	29.86	5.76	31.26
	S5	Chang 3	1673.6	2.12	60.52	10.44	26.93	5.80	29.04
	S6	Chang 3	1686.0	1.16	62.19	9.56	27.09	6.51	28.25
	S7	Chang 4 + 5	1732.6	0.38	67.41	6.01	26.20	11.21	26.57
	S8	Chang 4 + 5	1712.0	1.33	56.19	10.05	32.44	5.59	33.77
	S9	Chang 6	1753.7	2.56	64.48	9.93	23.02	6.49	25.59
	S10	Chang 6	1796.1	6.26	53.04	8.90	31.81	5.96	38.07
	S11	Chang 7	1843.3	1.90	65.44	6.56	26.10	9.97	28.00
	S12	Chang 7	1827.0	0.42	76.95	5.98	16.66	12.87	17.08
	S13	Chang 8	1948.4	3.01	43.75	11.99	41.25	3.65	44.26
	S14	Chang 8	1879.1	1.58	63.64	10.94	23.84	5.81	25.42
	S15	Chang 8	1919.4	2.10	64.42	7.55	25.92	8.53	28.03
	S16	Chang 8	1955.7	0.82	76.95	7.69	14.54	10.01	15.36
	S17	Chang 9	2078.5	0.71	67.97	5.58	25.74	12.19	26.45
	S18	Chang 9	1974.2	0.63	72.69	4.21	22.46	17.27	23.10
	S19	Chang 10	2218.7	3.94	62.02	10.39	23.64	5.97	27.59
	S20	Chang 10	2124.0	0.74	69.94	4.61	24.70	15.16	25.44
Source rock	R1	Yan 6	1381.4	42.02	15.88	20.58	21.52	0.77	63.54
	R2	Yan 7	1419.1	20.55	26.52	26.62	26.31	1.00	46.87
	R3	Yan 9	1423.5	4.80	53.67	15.19	26.33	3.53	31.13
	R4	Chang 4 + 5	1689.1	21.92	28.59	30.16	19.33	0.95	41.25
	R5	Chang 6	1730.0	16.50	48.32	20.08	15.10	2.41	31.60
	R6	Chang 8	1945.2	22.79	40.00	20.63	16.58	1.94	39.37
	R7	Chang 9	1970.6	6.97	36.39	30.27	26.37	1.20	33.34
	R8	Chang 7	1723.4	0.58	59.40	7.86	32.16	7.56	32.74
	R9	Chang 7	1746.8	2.12	62.21	8.98	26.69	6.93	28.81
	R10	Chang 7	1813.3	1.87	57.65	9.42	31.06	6.12	32.93
	R11	Chang 7	1837.6	3.51	60.43	9.41	26.65	6.42	30.16
	R12	Chang 7	1823.7	2.63	57.98	6.15	33.24	9.43	35.87
	R13	Chang 7	1786.5	0.94	63.31	11.92	23.83	5.31	24.77
	R14	Chang 7	1803.3	4.14	65.53	9.59	20.74	6.83	24.88
	R15	Chang 7	1867.2	2.05	58.32	9.48	30.15	6.15	32.20
	R16	Chang 7	1783.7	1.93	61.27	6.99	29.81	8.76	31.74
	R17	Chang 7	1795.6	0.73	56.82	5.37	37.08	10.59	37.81

Asp: asphaltene; Sat: saturated hydrocarbon; Aro: aromatic hydrocarbon; non: nonhydrocarbon; Sat/Aro: saturated hydrocarbon/aromatic hydrocarbon; Asp + non: asphaltene + nonhydrocarbon.

through filtration and the remaining solution without asphaltene was naturally volatilized to 2 mL. Transfer the 2 mL sample into a glass chromatographic column with 3 g silica gel (60 meshes) and 2 g alumina (100 meshes) in it. The saturated hydrocarbon fraction was collected after leaching with 20 mL n-hexane for four times; the aromatic fraction was collected after leaching with dichloromethane-n-hexane (2 : 1 by volume) and the nonhydrocarbon fractions were collected after leaching with anhydrous ethanol solution.

2.2.3. Chromatography-Mass Spectrometry (GC-MS) Test

Instrument. Agilent GC6890N/MS5973N.

Chromatograph Experimental Conditions. The injection volume is 0.2 μL. Split ratio is 30 : 1 and precolumn pressure is 11 standard atmospheric pressures. The chromatographic column is HP-5MS column (30 m × 0.32 mm) with the coating thickness of immobile phase is 0.25 μm and carrier

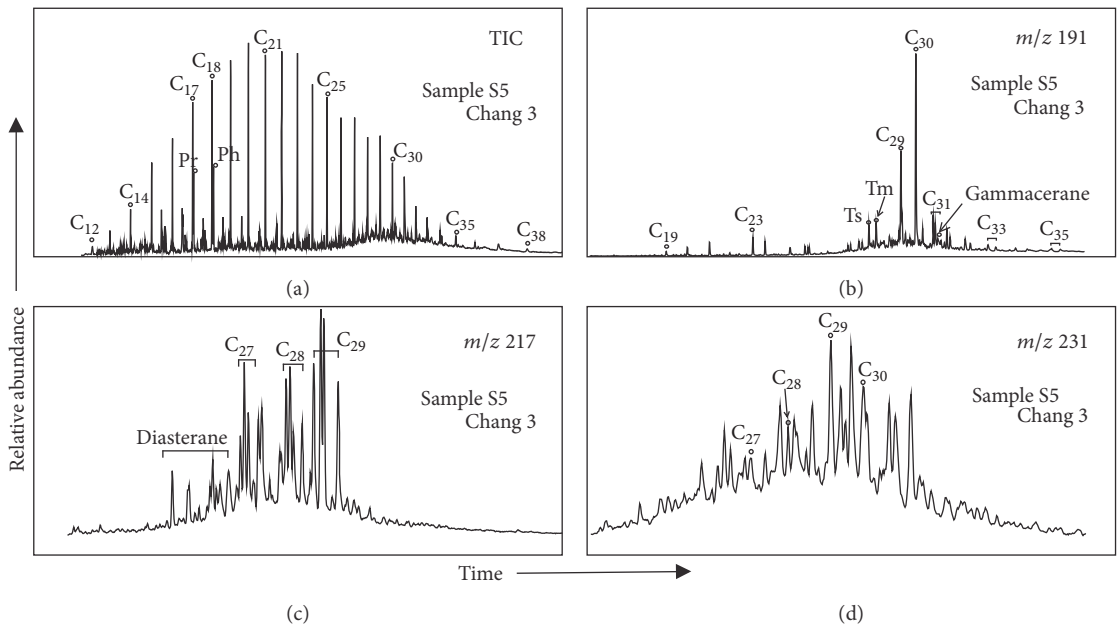

Figure 2: Representative chromatograms of n-alkanes (a), Terpanes (b), Steranes (c), and diasterane (d) of the crude oil of Yangchang Formation in Southwestern Yishan Slope.

gas is helium. The experimental temperature rises from 80°C to 300°C at a rate of 4°C/min and then keeps for 30 min.

Mass Spectrometry Experimental Conditions. EI ionization mode was adopted, with electron multiplication voltage of 900 V, scanning range of 18–690 AMV, ionization voltage of 70 eV, ion source temperature of 250°C, and GC/MS interface temperature of 300°C.

3. Results and Discussion

The biomarker compounds in the saturated hydrocarbon fraction of crude oil are high in abundance and have obvious characteristics. They are reliable indexes for the evaluation of crude oil, since they can stably reflect the depositional environment, the composition of raw material, the preservation condition, and the thermal evolution information of the parent material of crude oil. N-alkanes, isoprenoid alkanes, Steranes, and Terpanes are mainly used as saturated hydrocarbon biomarker compounds. Based on these parameters, the geochemical characteristics of crude oil can be reflected more comprehensively. Therefore, this paper focuses on the characteristics of n-alkanes, isoprene alkanes, Steranes, and Terpanes.

3.1. Characteristics of n-Alkanes and Isoprenoid Alkanes. The chromatographic features of n-alkane contain rich information about sedimentary environment, source composition, preservation condition, and thermal evolution [12–16]. N-alkanes are saturated straight-chain alkanes. The n-alkanes with different sources have different ranges of carbon numbers: the prepeak n-alkanes with C_{15}–C_{21} are mainly sourced from lower organism, while the postpeak n-alkanes with C_{23}–C_{35} are mainly sourced from higher organism. At diagenetic stage, deacidification exceeds reduction in oxidizing environment and the carbon number of hydrocarbons is one less than that of biological organic matter in the process of linear acids and alcohols converting to hydrocarbons and odd carbon advantage occurs in hydrocarbons. On the contrary, reduction takes dominance; even carbon advantage will appear. With the increase of maturity, carbon dominance gradually disappears and the ratio between prepeak and postpeak (OEP) approaches 1.

The acyclic isoprene alkanes are the paraffins composed of isoprenoid structural units. The compounds with low carbon number (lower than C_{20}) are phytane series compounds, which are the strong reduction products of the pigment in higher plants or photosynthetic bacteria. The phytate or phytane in the pigment material begins to form pristane under oxidation with the weakening of the reduction conditions. Accordingly, the ratio of pristane to phytane (Pr/Ph) can be used to determine the depositional environment. It is generally acknowledged that Pr/Ph < 0.5 signifies strong reducing sedimentary environment [17] and Pr/Ph = 0.5~1.0 and Pr/Ph = 1.0~2.0 suggest reducing and weak reducing-weak oxidizing environment, respectively, while Pr/Ph > 2.0 indicates oxidizing environment [17, 18].

The crude oil samples have the same distribution characteristics of n-alkane in this study (Figure 2). The carbon number distribution is C_{11}~C_{38}, the parity advantage is not obvious, the maximum carbon number is C_{17}~C_{21}, and $\sum C_{21}^{-} / \sum C_{21}^{+}$ ranges from 0.77 to 2.47 (Table 2), indicating that the crude oil is composed by hydrobiont and terrigenous plants and the aquatic bacteria play an important role. In addition, the values of Pr/nC_{17} and Ph/nC_{18} distribute in a narrow range, suggesting crude oil comes from a similar biological source [2, 12, 19] (Figure 3).

Table 2: Comparative data of n-alkane and isoprenoid alkanes of samples in Southwestern Yishan Slope.

	Sample number	Reservoir	C_{range}	OEP	$\sum C_{21-}/\sum C_{22+}$	Pr/Ph	Pr/nC_{17}	Ph/nC_{18}
Crude oil	S1	Chang 1	12~38	1.09	1.71	1.47	0.97	0.65
	S2	Chang 2	11~37	1.04	1.33	1.01	0.62	0.63
	S3	Chang 2	11~37	1.01	0.84	1.34	0.79	0.51
	S4	Chang 2	11~37	1.05	1.22	1.39	0.56	0.38
	S5	Chang 3	12~36	1.05	0.98	0.91	0.53	0.49
	S6	Chang 3	12~36	1.08	1.25	0.99	0.37	0.36
	S7	Chang 4 + 5	9~36	1.05	2.47	1.31	0.85	0.52
	S8	Chang 4 + 5	12~38	1.04	1.06	1.20	0.22	0.19
	S9	Chang 6	12~36	1.01	2.39	1.14	0.41	0.36
	S10	Chang 6	11~37	1.06	1.01	0.96	0.78	0.75
	S11	Chang 7	11~37	1.05	1.03	0.97	1.06	0.99
	S12	Chang 7	11~37	1.05	1.35	0.98	0.73	0.72
	S13	Chang 8	11~38	1.05	0.93	1.02	0.66	0.65
	S14	Chang 8	11~34	1.03	1.49	1.07	0.78	0.71
	S15	Chang 8	11~38	1.01	0.77	1.17	0.61	0.51
	S16	Chang 8	11~37	1.03	0.78	1.17	0.97	0.81
	S17	Chang 9	12~38	1.02	0.99	1.12	0.43	0.32
	S18	Chang 9	12~38	1.01	1.10	1.01	0.37	0.31
	S19	Chang 10	12~38	1.08	1.20	1.27	0.25	0.18
	S20	Chang 10	12~38	1.01	0.97	1.38	0.24	0.16
Source rock	R1	Yan 6	12~36	1.07	1.68	2.14	0.46	0.22
	R2	Yan 7	12~36	1.00	4.45	1.89	0.55	0.16
	R3	Yan 9	12~36	1.20	1.87	2.90	0.76	0.25
	R4	Chang 4 + 5	12~36	1.07	1.05	2.05	0.54	0.12
	R5	Chang 6	12~36	1.05	0.96	2.11	0.87	0.25
	R6	Chang 8	12~38	1.02	1.21	2.35	0.55	0.19
	R7	Chang 9	12~38	1.02	0.98	2.70	0.81	0.25
	R8	Chang 7	12~37	1.02	1.44	0.91	0.86	0.92
	R9	Chang 7	11~37	1.03	0.97	1.23	0.76	0.55
	R10	Chang 7	12~35	1.11	2.12	1.30	0.49	0.39
	R11	Chang 7	12~33	1.00	2.13	1.44	0.39	0.28
	R12	Chang 7	12~37	0.99	1.11	1.46	0.55	0.36
	R13	Chang 7	13~35	1.02	1.08	1.47	0.68	0.51
	R14	Chang 7	14~35	1.01	0.58	1.03	0.75	0.73
	R15	Chang 7	12~36	1.03	1.29	1.10	0.55	0.42
	R16	Chang 7	12~38	0.99	1.46	1.07	0.20	0.18
	R17	Chang 7	12~38	1.02	0.98	1.27	0.40	0.27

There is no parity advantage in the n-alkanes of crude oil and the value of OEP ranges from 1.01 to 1.09, closed to 1.0, indicating that the crude oil is mature. The Pr/Ph of the crude oil of Yanchang Formation and the source rocks of Chang 7 in study area ranges from 0.91 to 1.47 with relative concentrated distribution. Pristanes (Pr) and Phytane are not dominated, reflecting weak reducing-weak oxidizing sedimentary environment. The Pr/Ph of other source rocks ranges from 1.89 to 2.90, which indicates oxidizing sedimentary environment.

The distribution of Pr/nC_{17} and Ph/nC_{18} of crude oil is usually used to study the types of parent materials, formation environment, and maturity [12, 14, 19–21]. As shown is Figure 4 the values of Pr/nC_{17} and Ph/nC_{18} distribute in a narrow range, showing the crude oil comes from similar parent materials and similar formation environments. It is also shown in Figure 4 that the data points of the crude oil of Yanchang Formation and the data points of the source rocks of Chang 7 fall in the same range of weak reducing-weak oxidizing environment, while the other source rocks are in a oxidizing terrestrial environment, indicating the crude oil is mainly derived from the source rocks of Chang 7, and the contribution of other source rocks (the general term for the source rocks of Yan'an Formation, Chang 4 + 5, Chang 6, Chang 8, and Chang 9, below is the same) is not significant.

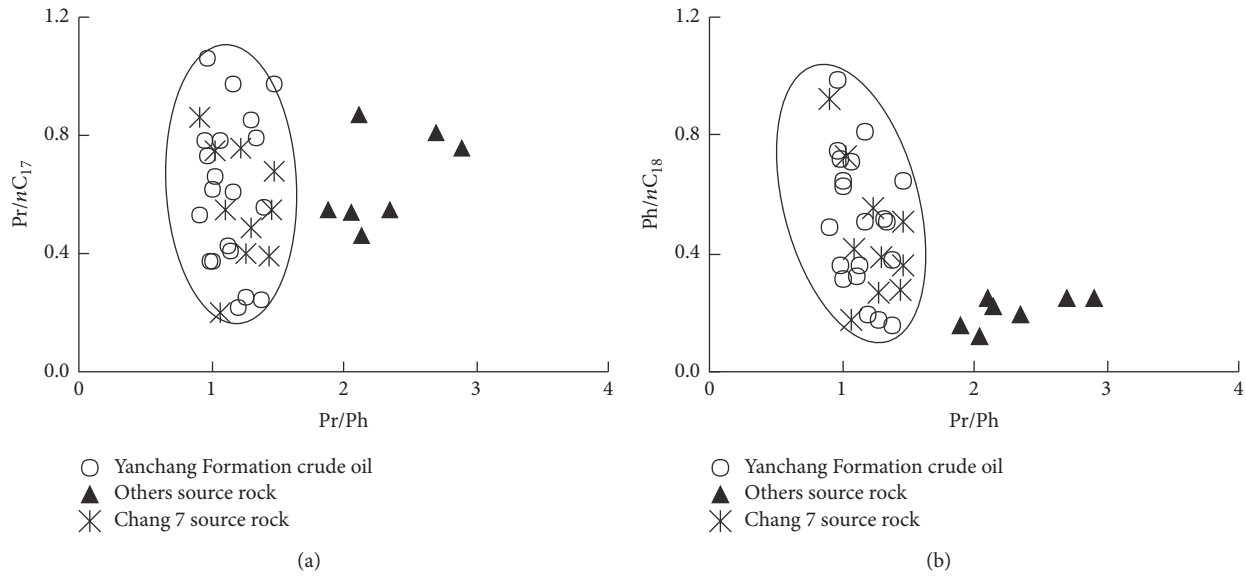

Figure 3: Cross plots of Pr/nC_{17} versus Pr/Ph ratios (a) and Ph/nC_{18} versus Pr/Ph ratios (b) of samples in Southwestern Yishan Slope.

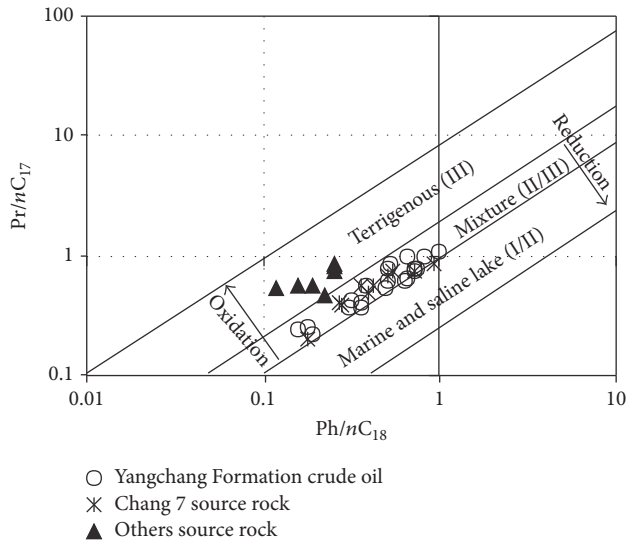

Figure 4: Cross plots of Pr/nC_{17} versus Ph/nC_{18} ratios of crude oil and source rocks in Southwestern Yishan Slope.

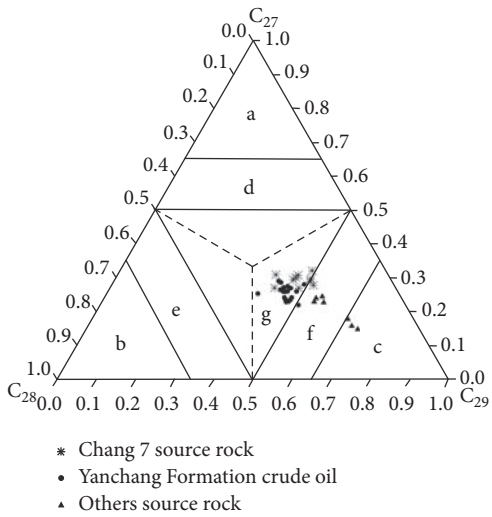

Figure 5: Distribution triangular chart of different carbon number regular Steranes of crude oil and source rock samples in Southwestern of Yishan Slope. (a-plankton; b-alga; c-terrestrial plant; d-dominated by phytoplankton; e-dominated by alga; f-dominated by terrestrial plant; g-mixed source).

3.2. Composition Characteristics of Steranes. The distribution of the Steranes in crude oil can reflect the sources of the parent materials of crude oil [22–25]. The values of ∑ regular Steranes/∑ Hopanes are usually used to represent the inputs of eucaryote (mainly alga and advanced plant) and procaryote (bacterium) in the parent materials of crude oil. The high ∑ regular Steranes/∑ Hopanes (≥1) value represents the marine organic characteristics of alga [23], while the low ∑ regular Steranes/∑ Hopanes value is the characteristics of terrigenous organic matter or the organic matter modified by microorganisms [26]. The content of diasteranes increases with the maturity of crude oil. Therefore, the value of ∑ diasteranes/∑ regular Steranes can be used to evaluate the maturity of crude oil [27].

The regular Steranes in the crude oil of Yanchang Formation have similar distribution to that of the source rock of Chang 7 and different from that of other source rocks in Southwestern Yishan Slope. In the crude oil of Yanchang Formation, the C_{29} Steranes in regular Steranes have the highest content (38.6~50%), but the contents of C_{27} Steranes (23~31%) and C_{28} Steranes (23~36%) are similar (Table 3). The three peaks showed a reversed "L" shape, indicating the parent materials of crude oil are from mixed source (Figure 5) and the contribution of terrestrial higher plant is great. In the source rocks of Chang 7, the C_{29} Steranes in regular Steranes have the highest content (40.4~51.4%) and

Table 3: Comparative data of steranes in crude oils and source rock samples in Southwestern Yishan Slope.

	Sample number	Reservoir	Regular Sterane abundance (%)			A	B	C	D	E	F
			C_{27}	C_{28}	C_{29}						
Crude oil	S1	Chang 1	23.1	29.4	47.5	0.19	0.38	0.13	0.51	0.55	0.54
	S2	Chang 2	24.2	28.1	47.7	0.25	0.18	0.16	0.51	0.59	0.51
	S3	Chang 2	26.4	29.7	43.9	0.25	0.22	0.14	0.52	0.55	0.52
	S4	Chang 2	27.1	28.6	44.3	0.26	0.19	0.14	0.49	0.53	0.45
	S5	Chang 3	26.1	28.2	45.7	0.26	0.11	0.12	0.53	0.59	0.69
	S6	Chang 3	25.9	28.9	45.2	0.24	0.07	0.11	0.52	0.61	0.70
	S7	Chang 4 + 5	31.1	31.2	37.7	0.74	0.29	0.11	0.52	0.53	0.69
	S8	Chang 4 + 5	28.1	28.0	43.9	0.25	0.75	0.14	0.54	0.51	0.68
	S9	Chang 6	25.3	36.0	38.7	0.29	0.19	0.14	0.54	0.59	0.67
	S10	Chang 6	23.6	28.7	47.7	0.25	0.23	0.15	0.52	0.59	0.55
	S11	Chang 7	22.1	27.4	50.5	0.16	0.18	0.13	0.50	0.56	0.52
	S12	Chang 7	25.9	29.3	44.8	0.26	0.24	0.14	0.55	0.58	0.56
	S13	Chang 8	23.0	30.1	46.9	0.28	0.16	0.20	0.51	0.62	0.54
	S14	Chang 8	26.5	29.7	43.8	0.34	0.21	0.16	0.55	0.61	0.55
	S15	Chang 8	23.7	29.9	46.4	0.19	0.14	0.21	0.53	0.58	0.52
	S16	Chang 8	24.2	29.9	45.9	0.19	0.17	0.20	0.53	0.50	0.47
	S17	Chang 9	28.0	23.0	49.0	0.64	0.1	0.11	0.55	0.55	0.73
	S18	Chang 9	27.0	27.0	46.0	0.8	0.07	0.08	0.53	0.63	0.62
	S19	Chang 10	30.0	30.0	40.0	0.64	0.21	0.11	0.53	0.54	0.69
	S20	Chang 10	28.0	28.0	44.0	0.28	0.18	0.14	0.57	0.53	0.77
Source rock	R1	Yan 6	18.0	17.0	65.0	0.12	1.82	0.14	0.45	0.43	0.60
	R2	Yan 7	15.0	16.0	69.0	0.05	0.20	0.13	0.45	0.43	0.59
	R3	Yan 9	16.0	17.0	67.0	0.09	0.15	0.16	0.44	0.35	0.57
	R4	Chang 4 + 5	24.0	22.0	54.0	0.13	0.56	0.15	0.55	0.52	0.58
	R5	Chang 6	21.0	19.0	60.0	0.13	0.61	0.12	0.53	0.51	0.56
	R6	Chang 8	23.0	23.0	54.0	0.63	0.06	0.11	0.51	0.51	0.72
	R7	Chang 9	23.0	19.0	58.0	0.68	0.24	0.14	0.47	0.47	0.73
	R8	Chang 7	30.8	28.7	40.5	0.37	0.37	0.16	0.56	0.57	0.61
	R9	Chang 7	27.7	20.8	51.5	0.12	0.34	0.16	0.55	0.54	0.59
	R10	Chang 7	29.4	25.1	45.5	0.17	0.20	0.16	0.53	0.53	0.46
	R11	Chang 7	30.7	23.2	46.1	0.22	0.22	0.16	0.54	0.54	0.58
	R12	Chang 7	26.9	24.9	48.2	0.18	0.26	0.16	0.55	0.56	0.60
	R13	Chang 7	30.0	24.1	45.9	0.28	0.48	0.21	0.54	0.52	0.58
	R14	Chang 7	29.6	20.6	49.8	0.29	0.52	0.15	0.48	0.54	0.61
	R15	Chang 7	29.0	21.0	50.0	0.53	0.39	0.10	0.47	0.61	0.56
	R16	Chang 7	27.0	31.0	42.0	0.31	0.02	0.15	0.48	0.51	0.71
	R17	Chang 7	32.0	19.0	49.0	0.89	0.17	0.06	0.51	0.45	0.78

A-$\sum$ regular Steranes/$\sum$ Hopanes; B-$\sum$ diasteranes/$\sum$ regular Steranes; C-$\sum$ 4-Methyl Steranes/$\sum$ regular Steranes; D-C_{29} Steranes 20S/(20S + 20R); E-C_{29} Steranes $\beta\beta/(\alpha\alpha + \beta\beta)$; F-$C_{29}$ diasteranes 20S/(20S + 20R).

C_{28} Steranes (26.9~30.8%) and C_{28} Steranes (19~31%) have similar content, while, in other source rocks, the content of C_{29} Steranes in regular Steranes has the highest content (52~69%) and C_{27} Steranes (15~23%) and C_{28} Steranes (16~23%) have similar content (Table 3). It can be concluded that the crude oil of the Yanchang Formation and the source rock of Chang 7 are comparable, while significantly different from other source rocks.

The $\sum$ regular Steranes/$\sum$ Hopanes of crude oil in the Yanchang Formation are low that range from 0.16 to 0.80, indicating that terrigenous higher plants make an important contribution to the parent materials and microbe degradation

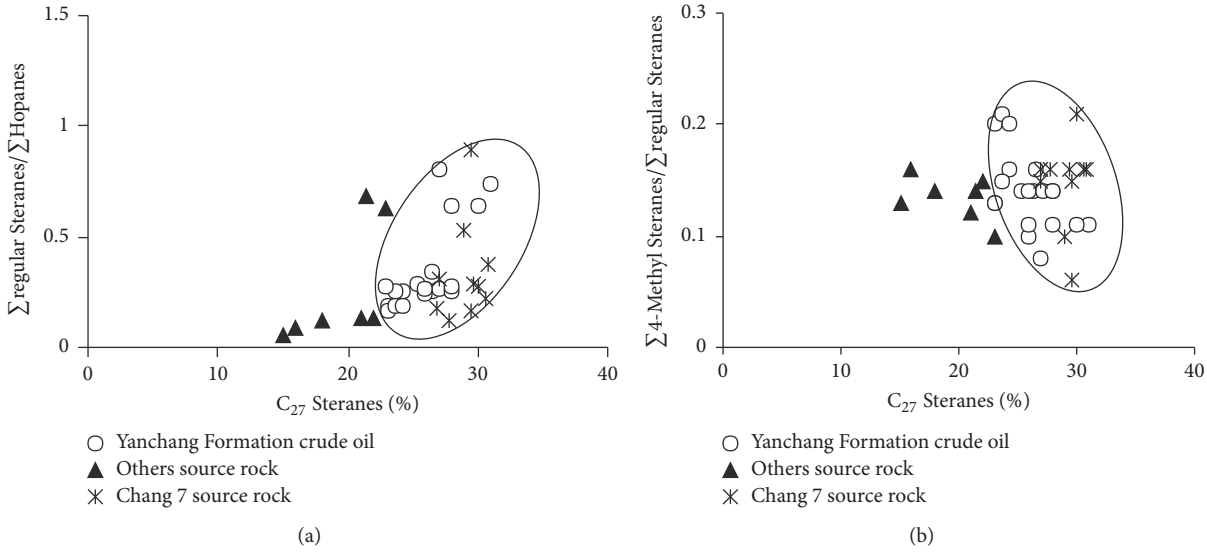

Figure 6: Cross plots of ∑ regular Steranes/∑ Hopanes versus C_{27} Steranes ratios (a) and ∑ 4-Methyl Steranes/∑ regular Steranes versus C_{27} Steranes ratios (b) of the crude oil and source rock samples in Southwestern of Yishan Slope.

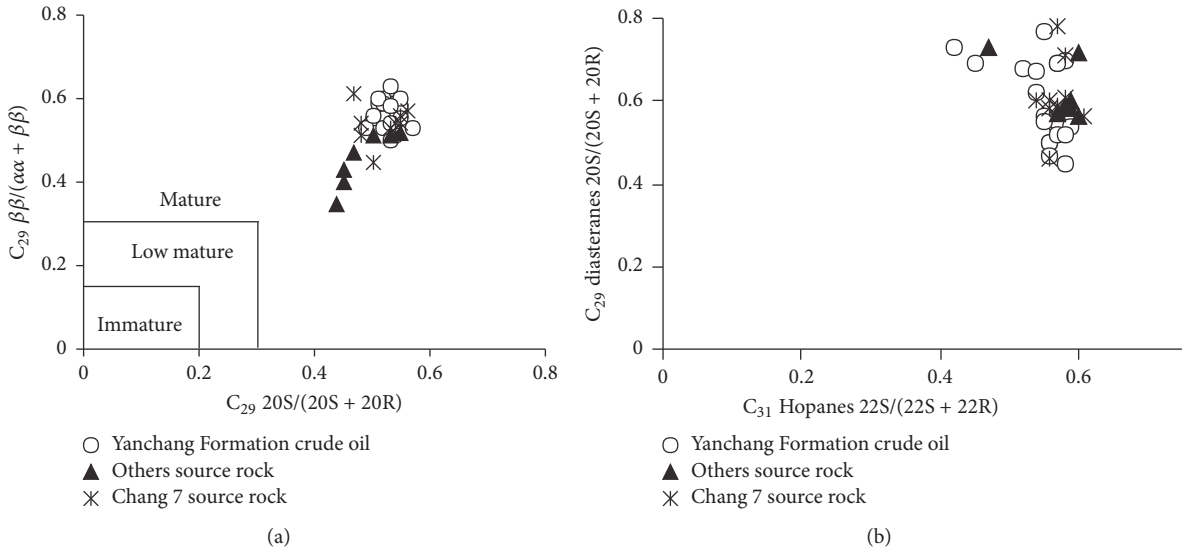

Figure 7: Cross plots of C_{29} Steranes $\beta\beta/(\alpha\alpha + \beta\beta)$ versus C_{29} Steranes 20S/(20S + 20R) (a) and C_{29} diasteranes 20S/(20S + 20R) versus C_{31} Hopanes 22S/(22S + 22R) (b) of the crude oil and source rock samples in Southwestern of Yishan Slope.

may occur weakly at the same time. 4-Methyl Steranes, which usually come from Dinoflagellata [28] and bacterium [24], are relatively abundant in the Yanchang Formation in Southwestern Yishan Slope. The value of ∑ 4-Methyl Steranes/∑ regular Steranes ranges from 0.08 to 0.21, indicating that Dinoflagellata and bacterium also contribute to the formation of crude oil in study area. The above-mentioned ratios are in concentrated distribution (Figure 6), suggesting similar sources of parent materials and the parent materials are mixed typed.

The value of C_{29} diasteranes 20S/(20S + 20R) in the Yanchang Formation crude oil is between 0.45 and 0.77 and ∑ diasteranes/ ∑ regular Steranes ranges from 0.07~0.75, reflecting the crude oil is mature.

Previous study [29] proposed that the values of C_{29} Steranes 20S/(20S + 20R) and $\beta\beta/(\alpha\alpha + \beta\beta)$ in mature crude oil are bigger than 0.4. The distribution ranges of C_{29} Steranes 20S/(20S + 20R) and $\beta\beta/(\alpha\alpha + \beta\beta)$ in crude oil are from 0.49 to 0.57 and from 0.50 to 0.63, respectively. They distribute in a relative narrow range, as shown in Figure 7(a), indicating

that the maturity of the crude oil of Yanchang Formation is similar and the crude oil is mature.

3.3. Characteristics of Terpanes Composition. Tricyclic Terpanes and tetracyclic Terpanes are abundant in crude oil, which can well reflect the nature of parent materials [30]. The $(C_{19} + C_{20})/C_{23}$ and C_{25}/C_{26} values of tricyclic Terpanes can be used to judge the parent materials of crude oil [21, 31]. In marine crude oil, the C_{25}/C_{26} value of tricyclic Terpanes is bigger than 1, while in terrestrial crude oil, it is smaller than 1 [32]. The β-dancane value can reflect of the oxidability of the formation environment of crude oil. The relative amount of gammacerane is positively correlated to the sedimentary paleosalinity [23, 24, 33, 34], which is an important index to characterize water salinity. The value of C_{31} Hopanes 22S/(22S + 22R) can reflect the maturity of crude oil [21, 31, 34, 35].

The $(C_{19} + C_{20})/C_{23}$ and C_{25}/C_{26} values of tricyclic Terpanes in the Yanchang Formation crude oil are concentrated and range from 0.44 to 1.05 and 0.30 to 0.53, respectively (Table 4, Figure 8(a)), manifesting the similar parent materials of crude oil of mixed type, in which terrestrial organic matter plays an important role. C_{24} tetracyclic Terpanes/(C_{24} tetracyclic Terpanes + C_{26} tricyclic Terpanes) range from 0.23 to 0.51, which also indicates that the parent materials of higher plant have great contribution on Yanchang Formation crude oil.

The low of β-dancane value in the crude oil suggests that the formation environment is weak reducing-weak oxidizing. The distribution ranges of gammacerane/$\alpha\beta$-C_{30} Hopanes and $\sum > C_{30}$ Hopanes relative amount are from 0.02 to 0.06 and from 19 to 28%, respectively, which are concentrated, as shown in Figure 8(b), indicating the crude oil of Yanchang Formation is formed in a similar low salinity environment.

The value of C_{31} Hopanes 22S/(22S + 22R) can reflect the maturity of crude oil [21, 31, 34, 35], which ranges from 0.52 to 0.61 (Table 4, Figure 7(b)) and reaches an equilibrium value of 0.57~0.64, indicating that the studied crude oil is mature. The same result can be got from the ratios of Ts/Tm, which are bigger than 0.5.

3.4. Oil Source Correlation Analysis. It can be concluded from the above-mentioned data that the crude oil of Yanchang Formation in Southwestern Yishan Slope is sourced from similar parent materials. In addition, the results of multiple tests and analyses suggest that these crude oils and the Chang 7 source rocks of the Yanchang Formation are very comparable as they have similar source materials, hydrocarbon generation environment, and maturity, while they are different from the other source rocks obviously in the important oil source correlation index (Pr/Ph) and the relative content of C_{29} Steranes.

The value of Pristanes/Phytanes (Pr/Ph) in n-alkanes and the relative content of C_{27}, C_{28}, and C_{29} in regular Steranes are important oil source correlation indexes, while the correlation diagram of Pr/nC_{17} versus Ph/nC_{18} can reflect the types of parent materials and formation environment directly and it also can be used as an index for oil source correlation. It can be found intuitively in Figures 4 and 9 that the crude oil of the Yanchang Formation and the source rocks of Chang 7 distribute in a relative narrow range, different from other source rocks, suggesting a genetic relationship in the studied area.

What is more, n-alkanes and isoprenoid hydrocarbon in the crude oil and Chang 7 source rocks are similarly distributed, whose carbon number distribution ranges broadly with one single peak; the terpenoid and steroid are similar obviously, the content of tetracycline is high, the homohopanes with high carbon number appears in pairs, the content of tricyclene is low, and the content of regular Steranes C_{29} is higher than C_{27} in steroid. It can be also found intuitively from the mass chromatogram that the distribution characteristics of the crude oil and the Chang 7 source rocks are similar, both with mixed source matrix, in which higher plants played an important role in forming weak reducing-weak oxidizing fresh water environment, and they have the geochemical characteristics of mature crude oil. All of these suggest that they are comparable.

It can be concluded from above-mentioned data that the crude oil of the Yanchang Formation and the source rocks of Chang 7 are comparable, which indicate that the crude oil is mainly derived from the source rocks of Chang 7 in the study area.

As shown in Table 1, the samples of crude oil are collected at the depth of 1614.2–2218.7 m; the samples of source rocks are collected at the depth of 1381.4–1970.6 m. The data of group component shows that, for crude oil samples, the content of saturated hydrocarbons is 43.75–76.95%, with an average of 63.37%; the content of aromatic hydrocarbon is 4.21–11.99%, with an average of 8.37%; the content of asphaltene + nonhydrocarbon is 15.40–44.26%, with an average of 28.26%; the value of saturated hydrocarbon/aromatic hydrocarbon is 3.65–17.27%, with an average of 8.47%.

Chang 7 source rock: the content of saturated hydrocarbons is 56.82–65.53%, with an average of 60.29%; the content of aromatic hydrocarbon is 5.37–11.92%, with an average of 8.52%; the content of asphaltene + nonhydrocarbon is 24.76–37.81%, with an average of 31.19%; the value of saturated hydrocarbon/aromatic hydrocarbon is 5.31–10.59%, with an average of 7.41%.

Other source rock: the content of saturated hydrocarbons is 15.88–53.67%, with an average of 35.62%; the content of aromatic hydrocarbon is 15.19–30.27%, with an average of 23.36%; the content of asphaltene + nonhydrocarbon is 31.13–63.54%, with an average of 41.01%; the value of saturated hydrocarbon/aromatic hydrocarbon is 0.77–3.53%, with an average of 1.68%.

The group components of the extract of Chang 7 source rock are significantly different from that of other source rocks but are similar to that of crude oil, so the samples of crude oil probably source from Chang 7 source rocks.

Based on the carbon isotopes of the monomeric compounds of the Mesozoic crude oil in the Ordos Basin and the results of oil source correlation, Zhang et al. [36, 37] considered that the crude oil of Yanchang Formation in the

Table 4: Comparative data of Terpanes in crude oil and source rock samples in Southwestern Yishan Slope.

	Sample number	Reservoir	A	B	C	D	E	F	G
Crude oil	S1	Chang 1	0.72	0.51	0.46	21.5	2.14	0.04	0.57
	S2	Chang 2	0.76	0.50	0.51	22.5	0.55	0.05	0.56
	S3	Chang 2	0.80	0.52	0.49	25.9	0.65	0.04	0.56
	S4	Chang 2	0.76	0.52	0.48	26.5	0.70	0.05	0.58
	S5	Chang 3	0.70	0.50	0.38	26.4	0.89	0.05	0.57
	S6	Chang 3	0.71	0.47	0.44	26.3	0.78	0.05	0.58
	S7	Chang 4 + 5	0.67	0.49	0.44	24.8	1.03	0.04	0.57
	S8	Chang 4 + 5	0.68	0.42	0.35	23.0	9.79	0.04	0.52
	S9	Chang 6	0.69	0.42	0.45	23.2	0.56	0.06	0.54
	S10	Chang 6	0.72	0.53	0.48	22.6	0.52	0.05	0.57
	S11	Chang 7	0.68	0.40	0.48	20.3	0.32	0.03	0.57
	S12	Chang 7	0.71	0.48	0.50	24.2	0.59	0.05	0.55
	S13	Chang 8	0.64	0.30	0.38	23.4	0.76	0.06	0.59
	S14	Chang 8	1.05	0.43	0.46	21.3	1.00	0.05	0.55
	S15	Chang 8	0.44	0.42	0.45	23.8	0.93	0.04	0.58
	S16	Chang 8	0.58	0.38	0.45	21.1	0.89	0.06	0.56
	S17	Chang 9	0.69	0.44	0.26	28.0	5.86	0.04	0.42
	S18	Chang 9	1.03	0.47	0.23	24.0	1.23	0.02	0.54
	S19	Chang 10	0.98	0.45	0.25	19.0	6.46	0.04	0.45
	S20	Chang 10	0.78	0.45	0.35	22.0	4.26	0.05	0.55
Source rock	R1	Yan 6	2.57	0.96	0.81	29.0	0.05	0.03	0.59
	R2	Yan 7	3.14	0.56	0.76	40.0	0.03	0.02	0.58
	R3	Yan 9	3.75	0.72	0.81	28.0	0.04	0.03	0.57
	R4	Chang 4 + 5	1.71	0.61	0.64	29.0	3.61	0.06	0.59
	R5	Chang 6	3.03	0.68	0.81	30.0	0.70	0.05	0.60
	R6	Chang 8	1.05	0.58	0.48	20.0	0.96	0.10	0.60
	R7	Chang 9	1.96	0.46	0.23	26.0	4.45	0.10	0.47
	R8	Chang 7	0.88	0.38	0.47	32.1	3.92	0.13	0.54
	R9	Chang 7	1.14	0.53	0.65	27.4	0.94	0.03	0.57
	R10	Chang 7	0.90	0.40	0.58	25.7	1.29	0.04	0.56
	R11	Chang 7	1.51	0.43	0.70	18.4	1.30	0.03	0.57
	R12	Chang 7	0.78	0.45	0.49	27.2	0.98	0.04	0.56
	R13	Chang 7	1.56	0.33	0.40	31.6	3.89	0.08	0.56
	R14	Chang 7	1.38	0.50	0.45	35.7	2.63	0.08	0.58
	R15	Chang 7	1.45	0.52	0.30	31.0	2.51	0.12	0.61
	R16	Chang 7	1.00	0.52	0.52	20.0	3.74	0.07	0.58
	R17	Chang 7	0.95	0.53	0.47	26.0	1.71	0.08	0.57

A-(C_{19} tricyclic Terpanes + C_{20} tricyclic Terpanes)/C_{23} tricyclic Terpanes; B-C_{25} tricyclic Terpanes/C_{26} tricyclic Terpanes; C-C_{24} tetracyclic Terpanes/(C_{24} tetracyclic Terpanes + C_{26} tricyclic Terpanes); D-$\sum > C_{30}$ Hopanes abundance (%); E-Ts/Tm; F-Gammacerane/$\alpha\beta$-C_{30} Hopanes; G-C_{31} Hopanes 22S/(22S + 22R).

Ordos Basin was sourced from Yanchang Formation lacustrine source rocks. The results of this paper are consistent with that obtained from isotope study.

4. Conclusions

In this paper, saturated hydrocarbon fractions were extracted from crude oil and source rocks using organic geochemical methods. And the characteristics of the biomarker compounds in saturated hydrocarbon fractions were analyzed. These parameters have strong stability and good correlation. By comparing the characteristics of the biomarker compounds of crude oil and source rock samples, the depositional environment, sources, and maturity of the parent materials of crude oil were clarified and the main source rock beds were determined.

(1) The parameters of biomarker compounds indicate that the crude oil of Yanchang Formation in Southwestern Yishan Slope is sourced from similar parent materials that are mixed type, and terrestrial higher

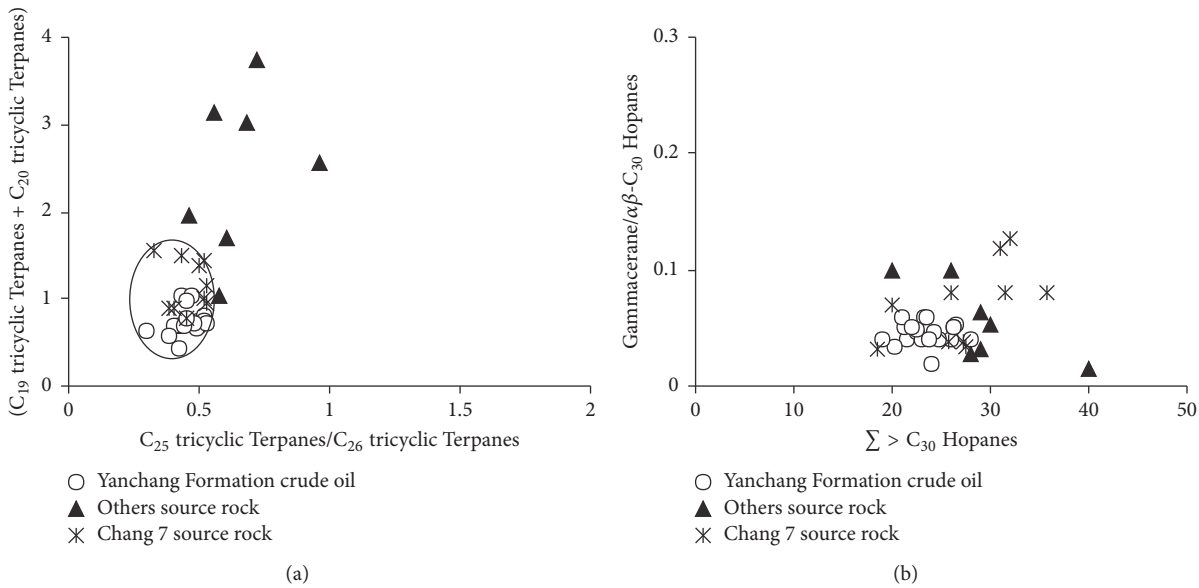

Figure 8: Cross plots of (C_{19} tricyclic Terpanes + C_{20} tricyclic Terpanes)/C_{23} tricyclic Terpanes versus C_{25} tricyclic Terpanes/C_{26} tricyclic Terpanes (a) and gammacerane/$\alpha\beta$-C_{30} Hopanes versus $\sum > C_{30}$ Hopanes ratios (b) of the study crude oil and source rock samples in Southwestern of Yishan Slope.

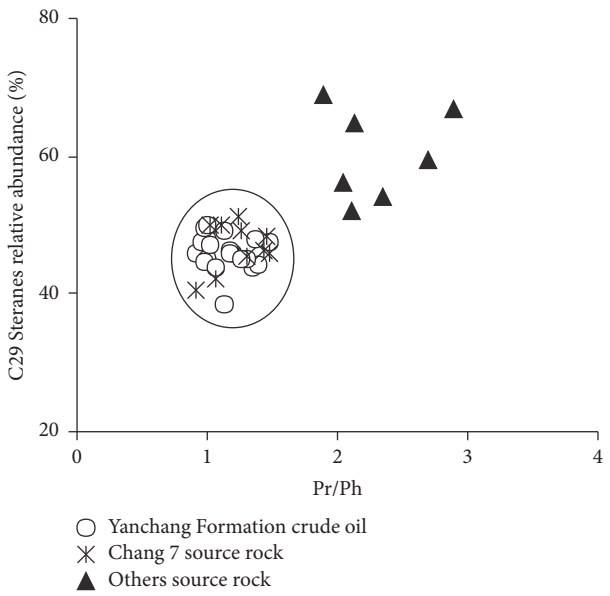

Figure 9: Cross plots of contents of C_{29} Steranes (%) versus Pr/Ph ratios of the crude oil and source rock samples in Southwestern of Yishan Slope.

plants play an important role. The crude oil is mature oil which is formed in weak reducing-weak oxidizing fresh or brackish water lake environment.

(2) Based on the study of the geochemical characteristics of the crude oil of Yanchang Formation, the source rocks of Chang 7, and other source rocks in Southwestern of Yishan Slope, it is discovered that the geochemical characteristics of the crude oil of Yanchang Formation are similar, indicating the same source of the crude oil. According to the analysis of oil source correlation, the crude oil of Yanchang Formation derives from the source rocks of Chang 7 subformation.

Conflicts of Interest

The authors declare that they have no conflicts of interest regarding the publication of this paper.

Acknowledgments

This study was supported by the Fundamental Research Funds for the Central Universities (2015QNB24) and a Project Funded by the Priority Academic Program Development of Jiangsu Higher Education Institutions.

References

[1] G. Eglinton and M. T. J. Murphy, *Organic Geochemistry: Methods and Results*, Springer-Verlag, Berlin, NY, USA, 1969.

[2] Y. Duan, B. X. Wu, H. Zhang, C. Y. Zheng, and C. Y. Wang, "Geochemistry and genesis of crude oils of the Xifeng oilfield in the Ordos basin," *Acta Geologica Sinica*, vol. 80, no. 2, pp. 302–310, 2006.

[3] Y. Duan, C. Y. Wang, C. Y. Zheng, B. X. Wu, and G. D. Zheng, "Geochemical study of crude oils from the Xifeng oilfield of the Ordos basin, China," *Journal of Asian Earth Sciences*, vol. 31, no. 4-6, pp. 341–356, 2008.

[4] Y. Duan, C. L. Ma, and Y. J. Yu, "Geochemical characteristics and genesis of crude oil from Dongzhi-Zhengning area of Ordos Basin," *Acta Sedimentologica Sin*, vol. 29, no. 5, pp. 1002–1009, 2011.

[5] X. L. Zhang, Y. Duan, J. X. He, B. X. Wu, and L. Xu, "Geochemical characteristics of crude oil in lower part of Yanchang formation and correlation of oil source in Huaqing area of Ordos Basin," *Natural Gas Geoscience*, vol. 22, no. 5, pp. 866–873, 2011.

[6] L. Xu, Y. Duan, L.-T. Xing et al., "Geochemical characteristics of crude oil from Linzhen area in the Ordos Basin, China," *Natural Gas Geoscience*, vol. 24, no. 2, pp. 406–413, 2013.

[7] S. Z. Tao, C. Wang, J. G. Du, L. Liu, and Z. Chen, "Geochemical application of tricyclic and tetracyclic terpanes biomarkers in crude oils of NW China," *Marine and Petroleum Geology*, vol. 67, no. 6, pp. 460–467, 2015.

[8] Z. Q. Meng, H. G. Ji, S. J. Qin, and C. L. Zhao, "Organic geochemical characteristics of source rocks in the Mizhi region of Ordos Basin," *Energy Exploration and Exploitation*, vol. 30, no. 3, pp. 373–388, 2012.

[9] G. D. Liu, W. W. Yang, Y. Feng, H. Y. Ma, and Y. G. Du, "Geochemical characteristics and genetic types of crude oil from Yanchang Formation in Longdong Area, Ordos Basin," *Earth Science Frontiers*, vol. 20, no. 2, pp. 108–115, 2013.

[10] N.-T. Deng, Z.-H. Zhang, F.-B. Wang et al., "Geochemical characteristics and oil-source correlation of crude oils in the Zhenjing Area, southern Ordos Basin," *Natural Gas Geoscience*, vol. 24, no. 3, pp. 604–611, 2013.

[11] L. Ji, C. He, M. Zhang, Y. Wu, and X. Li, "Bicyclic alkanes in source rocks of the Triassic Yanchang Formation in the Ordos Basin and their inconsistency in oil-source correlation," *Marine and Petroleum Geology*, vol. 72, pp. 359–373, 2016.

[12] Y. Duan, C. Zheng, Z. Wang et al., "Biomaker geochemistry of crude oils from the Qaidam Basin, NW China," *Journal of Petroleum Geology*, vol. 29, no. 2, pp. 175–188, 2006.

[13] K. E. Peters and J. M. Moldowan, *The Biomarker Guide: Interpreting Molecular Fossils in Petroleum and Ancient Sediments*, Prentice Hall, Englewood Cliffs, NJ, USA, 1993.

[14] K. E. Peters, T. H. Fraser, W. Amris, B. Rustanto, and E. Hermanto, "Geochemistry of crude oils from eastern indonesia," *AAPG Bulletin*, vol. 83, no. 12, pp. 1927–1942, 1999.

[15] Y. Duan, "Geochemical characteristics of crude oil in fluvial deposits from Maling oilfield of Ordos Basin, China," *Organic Geochemistry*, vol. 52, pp. 35–43, 2012.

[16] M. M. El Nady and A. Y. El-Naggar, "Petroleum geochemistry of crude oils and oil: source rock correlation of some wells in the North Western Desert, Egypt," *Arabian Journal of Geosciences*, vol. 9, no. 13, article 627, 2016.

[17] H. L. ten Haven, J. W. de Leeuw, J. Rullkötter, and J. S. S. Damsté, "Restricted utility of the pristane/phytane ratio as a palaeoenvironmental indicator," *Nature*, vol. 330, no. 6149, pp. 641–643, 1987.

[18] B. W. Mei and X. J. Liu, "The distribution of isoprenoid alkanes in china, s crude oil and it's relation with the geologic environment," *Oil Gas Geology*, vol. 2, no. 1, pp. 99–115, 1980.

[19] M. Li, R. Lin, Y. Liao, L. R. Snowdon, P. Wang, and P. Li, "Organic geochemistry of oils and condensates in the Kekeya Field, southwest depression of the Tarim Basin (China)," *Organic Geochemistry*, vol. 30, no. 1, pp. 15–37, 1999.

[20] J. Connan and A. M. Cassou, "Properties of gases and petroleum liquids derived from terrestrial kerogen at various maturation levels," *Geochimica et Cosmochimica Acta*, vol. 44, no. 1, pp. 1–23, 1980.

[21] A. D. Hanson, S. C. Zhang, J. M. Moldowan, D. G. Liang, and B. M. Zhang, "Molecular organic geochemistry of the Tarim basin, Northwest China," *AAPG Bulletin*, vol. 84, no. 8, pp. 1109–1128, 2000.

[22] W.-Y. Huang and W. G. Meinschein, "Sterols as ecological indicators," *Geochimica et Cosmochimica Acta*, vol. 43, no. 5, pp. 739–745, 1979.

[23] J. M. Moldowan, W. K. Seifert, and E. J. Gallegos, "Relationship between petroleum composition and depositional environment of petroleum source rocks," *AAPG Bulletin*, vol. 69, no. 8, pp. 1255–1268, 1985.

[24] R. P. Philp, P. Fan, C. A. Lewis, H. Zhu, and H. Wang, "Geochemical characteristics of oils from the Chaidamu, Shanganning and Jianghan Basins, China," *Journal of Southeast Asian Earth Sciences*, vol. 5, no. 1-4, pp. 351–358, 1991.

[25] Y. Duan and L. Ma, "Lipid geochemistry in a sediment core from Ruoergai Marsh deposit (Eastern Qinghai-Tibet plateau, China)," *Organic Geochemistry*, vol. 32, no. 12, pp. 1429–1442, 2001.

[26] B. P. Tissot and D. H. Welte, *Peteroleum Formation and Occurrence*, Springer-Verlag, Berlin, NY, USA, 1984.

[27] D. J. Hou and L. Y. Zhang, *Practical field guide of oil and gas geochemistry*, Petroleum Industry Press, Beijing, China, 2003.

[28] N. Robinson, G. Eglinton, S. C. Brassell, and P. A. Cranwell, "Dinoflagellate origin for sedimentary 4-methylsteroids and 5α(H) stanols," *Nature*, vol. 308, no. 5958, pp. 439–442, 1984.

[29] H. Difan, L. Jinchao, Z. Dajiang, H. Xiaoming, and Z. Zhuhong, "Maturation sequence of Tertiary crude oils in the Qaidam Basin and its significance in petroleum resource assessment," *Journal of Southeast Asian Earth Sciences*, vol. 5, no. 1-4, pp. 359–366, 1991.

[30] W. K. Seifert and J. Michael Moldowan, "Applications of steranes, terpanes and monoaromatics to the maturation, migration and source of crude oils," *Geochimica et Cosmochimica Acta*, vol. 42, no. 1, pp. 77–95, 1978.

[31] S. C. Zhang, A. D. Hanson, J. M. Moldowan et al., "Paleozoic oil-source rock correlations in the Tarim basin, NW China," *Organic Geochemistry*, vol. 31, no. 4, pp. 273–286, 2000.

[32] R. Burwood, P. Leplat, B. Mycke, and J. Paulet, "Rifted margin source rock deposition: a carbon isotope and biomarker study of a West African lower cretaceous 'Lacustrine' section," *Organic Geochemistry*, vol. 19, no. 1-3, pp. 41–52, 1992.

[33] Fu Jiamo, "Biomarker compounds of biological inputs in Maoming oil shale," *Geochimica*, vol. 2, pp. 99–114, 1985.

[34] Y. Duan, Z. P. Wang, H. Zhang, and B. X. Wu, "Geochemical characteristics of hydrocarbons in crude oils from the Qaidam basin," *Petroleum Geology Expeximent*, vol. 26, no. 4, pp. 359–364, 2004.

[35] M. Li, H. Yao, M. G. Fowler, and L. D. Stasiuk, "Geochemical constraints on models for secondary petroleum migration along the Upper Devonian Rimbey-Meadowbrook reef trend in central Alberta, Canada," *Organic Geochemistry*, vol. 29, no. 1-3, pp. 163–182, 1998.

[36] W. Z. Zhang, G. Pei, and S. D. Guan, "Study on carbon isotope of light hydrocarbon series molecules in Middle Paleozoic crude oil in Ordos Basin," *Chinese Science Bulletin*, vol. 37, no. 3, pp. 248–251, 1992.

[37] W. Z. Zhang, G. Pei, S. D. Guan, and K. F. Chen, "The carbon isotopic composition of the light hydrocarbon monomer and normail alkane series molecules form crude oil of some petroliferous basins in China," *Geological review*, vol. 39, no. 1, pp. 79–88, 1993.

Hindawi
International Journal of Analytical Chemistry
Volume 2017, Article ID 5840690, 9 pages
https://doi.org/10.1155/2017/5840690

Research Article

Particle Morphology Analysis of Biomass Material Based on Improved Image Processing Method

Zhaolin Lu,[1] Xiaojuan Hu,[2] and Yao Lu[1]

[1]*Advanced Analysis and Computation Center, China University of Mining and Technology, Xuzhou 221116, China*
[2]*School of Sciences, China University of Mining and Technology, Xuzhou 221116, China*

Correspondence should be addressed to Yao Lu; luyimao@163.com

Received 14 November 2016; Accepted 13 December 2016; Published 19 February 2017

Academic Editor: Ya-He Zhang

Particle morphology, including size and shape, is an important factor that significantly influences the physical and chemical properties of biomass material. Based on image processing technology, a method was developed to process sample images, measure particle dimensions, and analyse the particle size and shape distributions of knife-milled wheat straw, which had been preclassified into five nominal size groups using mechanical sieving approach. Considering the great variation of particle size from micrometer to millimeter, the powders greater than 250 μm were photographed by a flatbed scanner without zoom function, and the others were photographed using a scanning electron microscopy (SEM) with high-image resolution. Actual imaging tests confirmed the excellent effect of backscattered electron (BSE) imaging mode of SEM. Particle aggregation is an important factor that affects the recognition accuracy of the image processing method. In sample preparation, the singulated arrangement and ultrasonic dispersion methods were used to separate powders into particles that were larger and smaller than the nominal size of 250 μm. In addition, an image segmentation algorithm based on particle geometrical information was proposed to recognise the finer clustered powders. Experimental results demonstrated that the improved image processing method was suitable to analyse the particle size and shape distributions of ground biomass materials and solve the size inconsistencies in sieving analysis.

1. Introduction

With the depletion of fossil fuels and their corresponding undesirable effects on the environment, biomass utilization has received increased attention. Because of its renewability and abundance, biomass is considered to be one of the most promising resources, which can be converted into gaseous [1], liquid [2], and solid fuels [3] and other chemical raw materials or products [4–6].

Morphological characteristics of particles, including size distribution and shape factor, are important in these biomass applications [7–10]. Bridgeman et al. [11] studied the influence of particle size on the analytical and chemical properties of switchgrass and reed canary. Hendriks and Zeeman [12] found that a decreasing of biomass particle size involves higher hydrolysis yields of the lignocellulose. Gil et al. [13] also observed the underlying mechanism that govern the handling behavior for poplar and corn stover is partially influenced by the particle size and shape.

Size reduction, known as grinding process, is a critical procedure because it changes the particle size and shape of biomass. The surface area of ground particles increases the number of contact points for chemical reactions, which improves the energy conversion efficiency of biomass [14–18]. Mechanical sieving is the most standard method adopted by the American Society of Agricultural and Biological Engineers (ASABE) for particle size analysis of ground biomass. In practice, measured geometric mean length of biomass particles using sieve analysis is less than the actual size of the particles [19–21]. Other existing methods of PSD measurement use the principles of light scattering, acoustic spectroscopy and laser diffraction. Such methods often assume the particles to be spherical, which is not always the predominant case with ground biomass materials [22].

Image processing technology is considered as an alternative for mechanical sieving in PSD and shape identification analysis [23–26]. The two basic steps of image-based particle size and shape analysis are image acquisition and processing.

Devices for image acquisition include flatbed scanners [27] and digital cameras [28], which are limited by image resolution and depth of field, and are suitable only for photographing millimeter-sized or larger particles. By means of high magnification, scanning electron microscopy (SEM) has been widely applied in analysing micron-sized or smaller particles, such as wood dust from furniture manufacturing [29] and even atmospheric particles in industrial areas [30]. Owing to their built-in image analysis functions, most image processing algorithms reported in the literature use proprietary software, such as ImageJ [31]. To obtain special dimensional information of powders, some image analysis algorithms may require a flexible programming language environment such as Matlab (MathWorks, USA) with specialized image processing toolboxes [32].

Although particle morphology analysis based on image processing method has been the subject of many studies, the implementation of experiments and algorithms as important steps in the analysis procedure have received less attention. In this study, a series of improvements were conducted on sample preparation, image acquisition, and processing algorithms. The particulate sample was first divided into five groups by mechanical sieving approach to reduce wider size ranges. Considering the great variation of particle size from micrometer to millimeter, we utilized two acquisition units with different resolutions to photograph the particulate sample. Particle aggregation is an important factor that influences the recognition accuracy of the image processing method. In terms of sample preparation, the singulated arrangement and ultrasonic dispersion methods were used to disperse the powders. In addition, an image segmentation algorithm based on particle geometrical information was proposed to recognise the finer clustered powders.

2. Materials and Methods

2.1. Materials. Wheat straw is an herbaceous resource for the bioethanol production [33]. As a traditional crop with one of the highest yields, wheat straw obtained from the suburb of Xuzhou in China was chosen as the test sample in this study. Before grinding, wheat straw should be pretreated in size; the average length of the wheat straw materials was approximately 15 mm. Then, the samples fed into the laboratory-scale knife mill were placed in an oven at 103°C for 24 h before grinding, thereby reducing its wet basis moisture content from 27% to 5%, as measured by an infrared moisture meter.

2.2. Grinding and Sieving Stage. A commercially available knife mill (FW177, Laibu) operating at 28000 rpm was used to grind wheat straw based on the shearing action of the knife blades [34]. The corresponding grinding blades of the knife mill are shown in Figure 1.

Approximately 50 g of dried wheat straw samples, weighed by an electronic analytical balance (±0.001 mg accuracy, Sartorius), were ground using the knife mill. The ground materials were semiclassified using a mechanical sieving instrument (AS 200 Control, Retsch) with four sieves of mesh sizes 75, 250, 500, and 1000 μm. Commonly, sieving procedure is used to obtain the PSD, but for this study, is used to classify the particles that later will be photographed and analysed for the particle morphology analysis. After the shaking was completed, the stack was removed from the sieves and carefully weighed, and the mass of each sieve was recorded with its retained powders.

Figure 1: Blades of the knife mill.

Based on pretests, the grinding and corresponding sieving times were determined to be both 15 min, which were the times at which the mass of the test sieves did not change by more than 5% of the previous mass on the sieves [35]. Classification by sieving reduced the wide size range of ground particles, not only to precisely photograph the powders using an image acquisition device but also to understand the size range of particles generated by the knife mill. After grinding and sieving, the samples were sorted into five size fractions: >1000, 500–1000, 250–500, 75–250, and <75 μm.

2.3. Sample Preparation and Image Acquisition. Clear contrast between particles and background is essential to effectively recognise the particles. Igathinathane et al. [23] proposed that particles should be well spread in a singulated arrangement, where a thin layer of samples is laid in a manner that particles do not touch or overlap one another. However, when particles are considerably small, avoiding agglomeration caused by van der Waals force from a singulated arrangement is difficult. Thus, to address the wider size range and avoid particle agglomeration, an experimental method, including sample preparation and image acquisition was improved.

In this study, the singulated arrangement based on manual separation was used to spread larger particles, such as size ranges of >1000, 500–1000, and 250–500 μm. Then, the well-scattered samples were photographed by a flatbed scanner (Laser Jet M1213nf, HP) with a resolution of 600 dpi, which corresponded to a constant scale factor of 42.3 μm pixel^{-1}. Preliminary tests verified that the flatbed scanner without zoom function was unsuitable to photograph particles that were less than nominal size of 250 μm.

Ultrasonic dispersion method was used to scatter these particles, thereby weakening the particle agglomeration of size ranges of 75–250 and <75 μm. Approximately 5 mg of each size range was suspended in 10 ml of anhydrous ethanol.

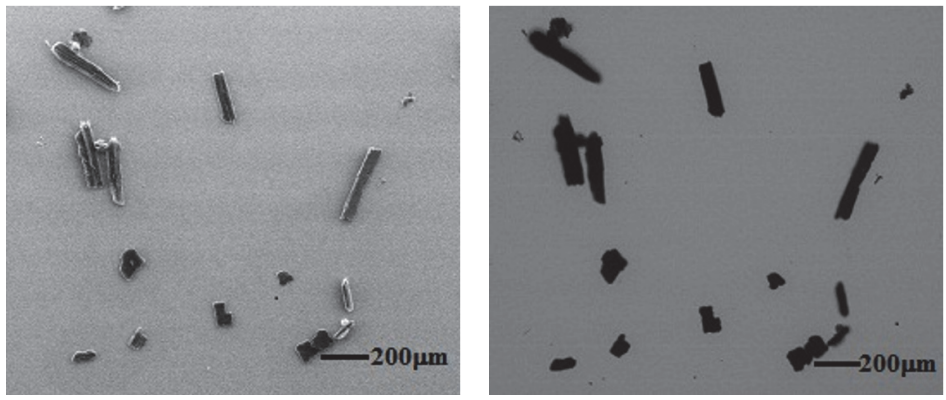

(a) (b)

Figure 2: Particle images acquired by SEM: (a) SE image; (b) BSE image.

Then, the suspension was stirred continuously for 10 min in an ultrasonic cleaner to avoid particle aggregation. About 0.5 ml of the aforementioned suspension was dropped on a mica substrate, which was flat enough to highlight the contrast between the particles and image background. After air drying, the samples along with substrate were placed in an SEM chamber (Quanta 250, FEI), which had a huge advantage over field of view and depth of field relative to an optical microscope. SEM has two imaging modes, namely, secondary electron (SE) and backscattered electron (BSE). Figure 2(a) shows that particles are inhomogeneous at grey level caused by Edge Effect which is due to the enhanced emission of electrons from edges within the specimen. These inhomogeneities of particles are unfavourable for segmenting particles from the background. The grey level of the BSE image was determined by the average atomic number of material. Biomass materials are classified as organic hydrocarbons with average atomic number smaller than that of mica substrate. Figure 2(b) shows the clear contrast between particles and background for the BSE image. In this test, the BSE imaging mode of SEM was used to acquire particle images, and the image magnification for size ranges of 75–250 and <75 μm was set to 200x and 300x, respectively; thus, the corresponding scale factors were 1.46 μm pixel^{-1} and 0.971 μm pixel^{-1}.

Based on the preceding analysis, the dispersive particle images of each size range were acquired by two imaging devices. For each size ranges, the minimum particle area to be taken into consideration was set to 4 pixels to ignore ultrafine particles. Figures 3(a)–3(c) show the larger particle images obtained by the flatbed scanner, and Figures 3(d)-3(e) show images photographed by SEM.

2.4. Image Processing and Dimension Measurement. Image processing, an essential preliminary step in most automated particle morphology analysis, is used to subdivide an image into constituent regions. The accuracy of this process determines the eventual accuracy of PSD. An image processing and dimension measurement method was proposed to recognise biomass particles of 75–250 μm in a BSE image following the steps shown in Figure 4.

Step 1. The noise from the original image was removed. For convenience, a Gaussian filter, a simple and quick denoising method, was selected to denoise the original image. Figures 4(a) and 4(b) show the original and denoised images, respectively.

Step 2. The denoised image was converted to binary image using a single global threshold value of the entire image. Otsu's method was used for binarisation, which was deemed suitable if all particles had obvious intensity difference from the background. Adopting mica as the sample substrate and BSE imaging mode emphasised the grey level difference and reduced the burden of threshold setting. The output of this procedure was a binary image shown in Figure 4(c).

Step 3. The holes of recognised particles were filled and the touching particles were separated. Holes were generated after binarisation for large particles because of their high grey level difference. The distance between the location of the hole and edge of the particles was used as basis to determine whether the holes needed to be filled or not. In addition, the touching particles were falsely recognised as one particle because of the agglomeration effect. Basic morphological operators, such as erosion, dilation, opening, and closing, cause changes in the size of particles in the binary images, which is not allowed for particle morphology analysis. The wedge pixel, which was positioned at the point of a contact wedge between two grains, was the key point for separating the touching particles. Further details for searching the wedge pixels can be found in the literature [36]. Moreover, the curvature information of particle outline was added to the search procedure to optimise wedge pixels. Then, the two wedge pixels were connected to complete the separation [37]. Figure 4(d) demonstrates the effectiveness of the program to separate the touching particles marked by different colours.

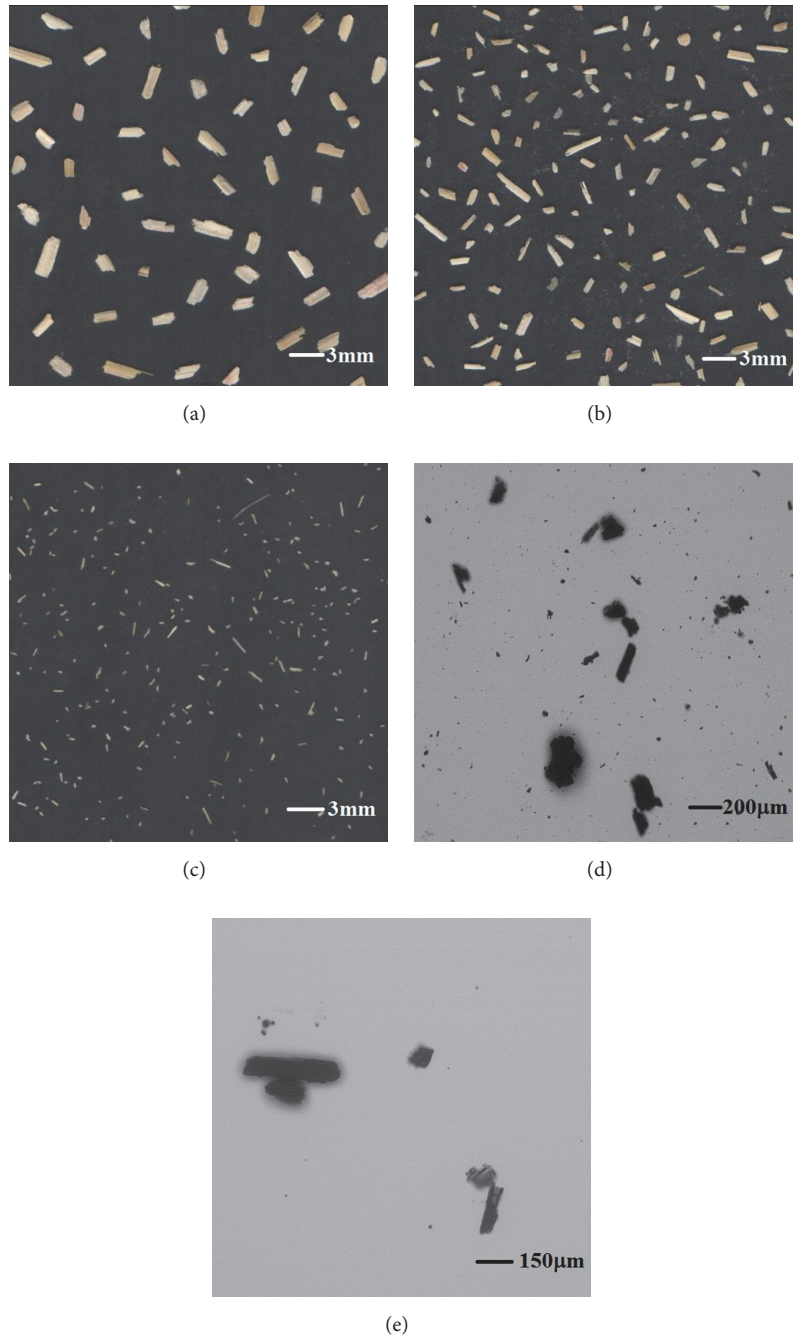

(a) (b) (c) (d) (e)

Figure 3: Sample images of ground wheat straw particles from five size ranges: (a) >1000 μm, (b) 500–1000 μm, (c) 250–500 μm, (d) 75–250 μm, and (e) <75 μm.

Step 4. The dimensions of particle size and shape were characterised. The maximum and minimum dimensions of the identified particle, termed as length and width, were the dominant and most significant dimensions for natural biomass particles. Once the particles were recognised, a method of dimension calculation analysed the geometry to measure the length and width. The measurement is depicted in Figure 5, where the width w is defined as the minimum distance between two parallel lines tangential to the projected outline of the particle, and length l is the distance between two tangents to the projected outline of the particle drawn perpendicularly to the tangent defining the width w. Particle shape had a significant effect on the probability that the particle would be classified in the correct range. In our study, wheat straw particle shape was described quantitatively by a parameter called aspect ratio (AR), which was expressed as

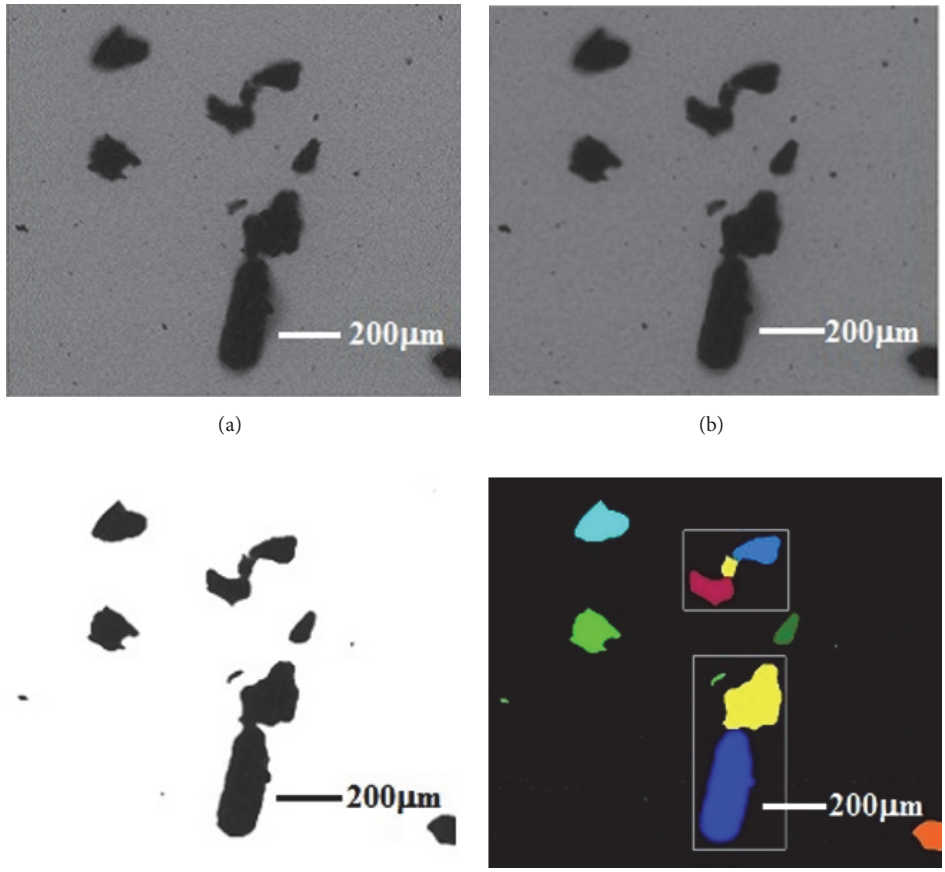

(a) (b)

(c) (d)

Figure 4: Processing results corresponding to each step.

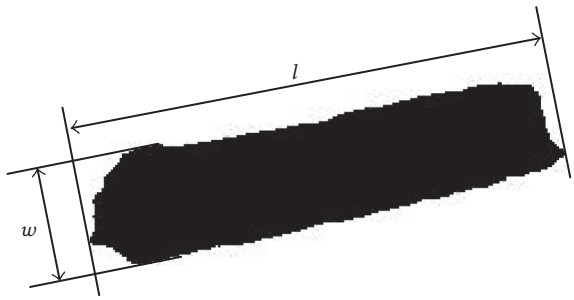

Figure 5: Measurement of length and width of wheat straw particle.

AR = l/w. The entire program, including image processing and dimension measurement, was developed based on Matlab R2012 software.

3. Results and Discussion

3.1. PSD Analysis from Mechanical Sieving. PSD analysis is considered as a standard procedure in evaluating the morphological features of particulate materials. In view of the wider size range of wheat straw particles ground by the knife mill, mechanical sieving was conducted to divide the ground particles into several groups. In general, PSD characteristics determined through sieving analysis are expressed as a plot of mass fraction of materials retained on sieves versus screen sizes.

In this test, the wheat straw sample ground by the knife mill was divided into five groups through mechanical sieving. The mass fractions of nominal size ranges containing >1000, 500–1000, 250–500, 75–250, and <75 μm were 4.18%, 13.30%, 18.77%, 37.91%, and 25.84%, respectively, where <250 μm accounted for 63.75% of the total mass. Clearly, the limited quantities of screens limit the PSD sieving analysis of the particulate sample. This analysis is a collection of hundreds of noticeable dimensioned particles with the available data from four screens, thereby restricting dimensional measurement accuracy.

In addition, any particles of width less than the sieve opening could pass through the sieves regardless of particle shape. This condition illustrates the width-based separation of sieving analysis. Guo et al. [28] reported that biomass particles ground by knife mill had a needle-like shape because of the anisotropy of the material. Length served as a dominant dimension of this type of biomass material with a size range that was not determined accurately by mechanical sieving analysis. Womac et al. [21] observed this length-based separation inconsistency in particle size analysis of knife-milled

Table 1: Average dimensional parameters of wheat straw powders in different size ranges.

Size ranges (μm)	Average length (μm) ± SD	Average width (μm) ± SD	Average AR ± SD
>1000	2817.95 ± 799.82	1214.96 ± 155.38	2.38 ± 1.89
500–1000	1479.89 ± 674.65	637.52 ± 133.62	2.25 ± 1.47
250–500	797.40 ± 807.23	367.01 ± 75.46	2.19 ± 1.32
75–250	280.83 ± 327.73	143.34 ± 75.15	2.12 ± 1.15
<75	65.14 ± 223.78	34.86 ± 39.14	1.91 ± 1.09

ground biomass material using ASABE design sieves. Thus, in this study, classification by sieving reduced the wide size range of ground particles, which is beneficial to photograph and analyse the particle morphology.

3.2. Particle Morphology Analysis Based on Image Processing. Preliminary investigation on the particle imaging method demonstrated that the biomass powders, which have a nominal size of <250 μm, were difficult to disperse by singulated arrangement. And these powders were too small to be easily photographed using the flatbed scanner with limited scanning resolution. Ultrasonic dispersion method and BSE imaging mode of SEM were combined to photograph the smaller particles. About 300 particles were identified randomly from pictures based on the above image processing technology to obtain detailed morphological information. After the particle dimensions were measured, the average lengths, widths, ARs, and corresponding standard deviations (SD) of ground powders in five size ranges, divided by mechanical sieving, were acquired. Table 1 shows the average dimensional parameters of wheat straw powders in different size ranges, where the average AR is not the ratio of average length to average width but the average value of the AR of 300 particles.

As shown in Table 1, the average widths of particles are in the ranges of screen sizes, but the average lengths almost exceed the screen sizes except for the largest sieve, which does not control the upper limit of the particles. Moreover, the larger screens resulted in greater range of width, which was demonstrated by descending SD parameters. Regarding SDs, the smaller values obtained for particle dimensions corresponded to a narrower distribution. Comparing the SDs of length and width of each size range also confirmed the separation mechanism of mechanical sieving based on width.

The PSDs of 300 particles were displayed as plots of lengths, widths, and ARs sorted in ascending order versus particle number, which are shown in Figure 6. Owing to the great disparity of particle sizes in different ranges, the curves of length and width distributions were displayed separately with nominal size of 250 μm as boundary. Figures 6(b) and 6(d) show the distribution curves of lengths and widths of wheat straw powders less than nominal 250 μm, respectively. Based on these semilog plots, various curves corresponding to different sizes overlap each other, thereby indicating the limited efficiency of the sieving method with the current number of screens in separating the particles of various sizes.

Biomass particles obtained by size reduction processing of the knife mill were irregular because of structural anisotropy. In this study, AR was used to describe particle shape. AR is equal to one when particles are circles and squares; otherwise it is greater than one when particles are more elongated. The average ARs and SDs in Table 1 and plots of AR distribution in Figure 6(e) show that the finer particles tend to be short just as the conclusions of literature [28].

A minimum sample size for testing was needed to represent the sample well. Igathinathane et al. [38] reported that even a few grams of sample could consist of thousands of particles. An electronic analytical balance was used to ensure the accuracy of sample weight. In addition, a large number of laboratory-scale experiments were conducted to ensure statistical significance and repeatability of PSD data.

4. Conclusions

Particle morphological characteristics greatly influence the physical properties of granular biomass materials. A computer vision-based image processing method can be considered as an alternative for sieve analysis [22]. However, because of the resolution limit of the image acquisition unit and agglomeration of fine particles, the ground biomass powders of wide size range were difficult to identify completely.

In this study, mechanical sieving was only used to divide the sample into five groups, thereby reducing the wide size range. The powders retained on sieves, with opening sizes greater than 250 μm, were photographed by a flatbed scanner without zoom function, and the others were photographed using SEM with high-image resolution. Actual imaging tests confirmed the excellent effect of BSE imaging mode of SEM.

To weaken the particle agglomeration, the singulated arrangement and ultrasonic dispersion methods were used to disperse the powders according to different size ranges. In a sense, mechanical sieving also dispersed the particles. Moreover, an image segmentation method based on geometrical information of particles, such as wedges and curvatures, was proposed to recognise the finer powders touching each other, which was the ultimate aim of this study. The distribution curves of particle size and shape obtained by experiments demonstrated that the improved image processing method can be applied to particle morphology analysis.

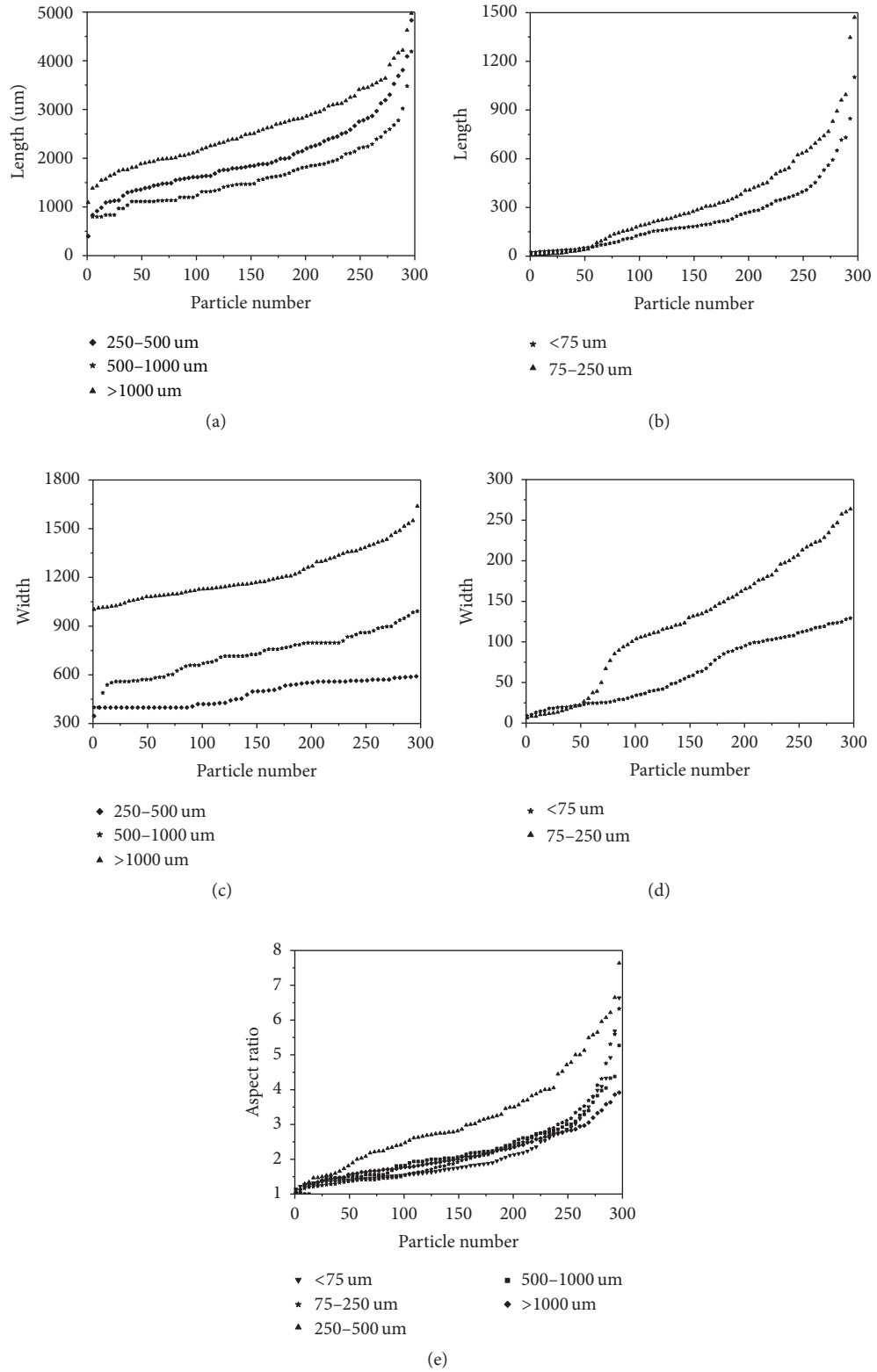

Figure 6: Particle size and shape distribution of ground wheat straw powders. (a) Distribution curves of lengths larger than nominal 250 μm, (b) distribution curves of lengths less than nominal 250 μm, (c) distribution curves of widths larger than nominal 250 μm, (d) distribution curves of widths less than nominal 250 μm, and (e) distribution curves of ARs.

Competing Interests

The authors declare that there is no conflict of interests regarding the publication of this paper.

Acknowledgments

This study was supported by the National Natural Science Foundation of China (nos. 51604217 and 21506250), Natural Science Foundation of Jiangsu Province of China (no. BK 20150182), and the Fundamental Research Funds for the Central Universities (no. 2013QNB25).

References

[1] J. J. Hernández, G. Aranda-Almansa, and A. Bula, "Gasification of biomass wastes in an entrained flow gasifier: effect of the particle size and the residence time," *Fuel Processing Technology*, vol. 91, no. 6, pp. 681–692, 2010.

[2] J. Lédé, F. Broust, F.-T. Ndiaye, and M. Ferrer, "Properties of bio-oils produced by biomass fast pyrolysis in a cyclone reactor," *Fuel*, vol. 86, no. 12-13, pp. 1800–1810, 2007.

[3] P. E. Mason, L. I. Darvell, J. M. Jones, and A. Williams, "Observations on the release of gas-phase potassium during the combustion of single particles of biomass," *Fuel*, vol. 182, pp. 110–117, 2016.

[4] L. Bai, Karnowo, S. Kudo, K. Norinaga, Y.-G. Wang, and J.-I. Hayashi, "Kinetics and mechanism of steam gasification of char from hydrothermally treated woody biomass," *Energy & Fuels*, vol. 28, no. 11, pp. 7133–7139, 2014.

[5] Y. Lu, X.-Y. Wei, Z. Wen et al., "Photocatalytic depolymerization of rice husk over TiO_2 with H_2O_2," *Fuel Processing Technology*, vol. 117, pp. 8–16, 2014.

[6] Y. Lu, X.-Y. Wei, Z.-M. Zong et al., "Organonitrogen compounds identified in degraded wheat straw by oxidation in a sodium hypochlorite aqueous solution," *Fuel*, vol. 109, pp. 61–67, 2013.

[7] S. P. S. Chundawat, B. Venkatesh, and B. E. Dale, "Effect of particle size based separation of milled corn stover on AFEX pretreatment and enzymatic digestibility," *Biotechnology and Bioengineering*, vol. 96, no. 2, pp. 219–231, 2007.

[8] L. Dong, Y. Zhao, C. Duan, Z. Luo, B. Zhang, and X. Yang, "Characteristics of bubble and fine coal separation using active pulsing air dense medium fluidized bed," *Powder Technology*, vol. 257, pp. 40–46, 2014.

[9] H. Lu, E. Ip, J. Scott, P. Foster, M. Vickers, and L. L. Baxter, "Effects of particle shape and size on devolatilization of biomass particle," *Fuel*, vol. 89, no. 5, pp. 1156–1168, 2010.

[10] D. R. Sudhakar and A. K. Kolar, "Experimental investigation of the effect of initial fuel particle shape, size and bed temperature on devolatilization of single wood particle in a hot fluidized bed," *Journal of Analytical and Applied Pyrolysis*, vol. 92, no. 1, pp. 239–249, 2011.

[11] T. G. Bridgeman, L. I. Darvell, J. M. Jones et al., "Influence of particle size on the analytical and chemical properties of two energy crops," *Fuel*, vol. 86, no. 1-2, pp. 60–72, 2007.

[12] A. T. W. M. Hendriks and G. Zeeman, "Pretreatments to enhance the digestibility of lignocellulosic biomass," *Bioresource Technology*, vol. 100, no. 1, pp. 10–18, 2009.

[13] M. Gil, D. Schott, I. Arauzo, and E. Teruel, "Handling behavior of two milled biomass: SRF poplar and corn stover," *Fuel Processing Technology*, vol. 112, pp. 76–85, 2013.

[14] P. McKendry, "Energy production from biomass (part 3): gasification technologies," *Bioresource Technology*, vol. 83, no. 1, pp. 55–63, 2002.

[15] V. S. P. Bitra, A. R. Womac, Y. T. Yang et al., "Knife mill operating factors effect on switchgrass particle size distributions," *Bioresource Technology*, vol. 100, no. 21, pp. 5176–5188, 2009.

[16] M. Gil and I. Arauzo, "Hammer mill operating and biomass physical conditions effects on particle size distribution of solid pulverized biofuels," *Fuel Processing Technology*, vol. 127, pp. 80–87, 2014.

[17] S. Paulrud, J. E. Mattsson, and C. Nilsson, "Particle and handling characteristics of wood fuel powder: effects of different mills," *Fuel Processing Technology*, vol. 76, no. 1, pp. 23–39, 2002.

[18] T. G. Bridgeman, J. M. Jones, A. Williams, and D. J. Waldron, "An investigation of the grindability of two torrefied energy crops," *Fuel*, vol. 89, no. 12, pp. 3911–3918, 2010.

[19] ASABE Standards, *Method of Determining and Expressing Particle Size of Chopped Forage Materials by Screening*, ASABE Standards, St. Joseph, Mich, USA, 2003.

[20] Y. Yang, A. R. Womac, and PI. Miu, *High-Specific Separation of Biomass Materials by Sieving*, vol. 1, American Society of Agricultural and Biological Engineers, St. Joseph, Mich, USA, 2006.

[21] A. R. Womac, C. Igathinathane, P. Bitra et al., "Biomass preprocessing size reduction with instrumented mills," in *Proceedings of the ASABE Annual International Meeting, Technical Papers*, ASABE, June 2007.

[22] C. Igathinathane, L. O. Pordesimo, E. P. Columbus, W. D. Batchelor, and S. Sokhansanj, "Sieveless particle size distribution analysis of particulate materials through computer vision," *Computers and Electronics in Agriculture*, vol. 66, no. 2, pp. 147–158, 2009.

[23] C. Igathinathane, L. O. Pordesimo, E. P. Columbus, W. D. Batchelor, and S. R. Methuku, "Shape identification and particles size distribution from basic shape parameters using ImageJ," *Computers and Electronics in Agriculture*, vol. 63, no. 2, pp. 168–182, 2008.

[24] B. P. Dubey, S. G. Bhagwat, S. P. Shouche, and J. K. Sainis, "Potential of artificial neural networks in varietal identification using morphometry of wheat grains," *Biosystems Engineering*, vol. 95, no. 1, pp. 61–67, 2006.

[25] Z. Zhang, J. Yang, L. Ding, and Y. Zhao, "An improved estimation of coal particle mass using image analysis," *Powder Technology*, vol. 229, pp. 178–184, 2012.

[26] T. Jeliński, C.-J. Du, D.-W. Sun, and J. Fornal, "Inspection of the distribution and amount of ingredients in pasteurized cheese by computer vision," *Journal of Food Engineering*, vol. 83, no. 1, pp. 3–9, 2007.

[27] N. S. Visen, J. Paliwal, and D. Jayas, "Image analysis of bulk grain samples using neural networks," *American Society of Agricultural and Biological Engineers*, vol. 1, 2003.

[28] Q. Guo, X. Chen, and H. Liu, "Experimental research on shape and size distribution of biomass particle," *Fuel*, vol. 94, pp. 551–555, 2012.

[29] M. E. Gómez Yepes and L. V. Cremades, "Characterization of wood dust from furniture by scanning electron microscopy and energy-dispersive X-ray analysis," *Industrial Health*, vol. 49, no. 4, pp. 492–500, 2011.

[30] J. M. Bernabé, M. I. Carretero, and E. Galán, "Mineralogy and origin of atmospheric particles in the industrial area of Huelva (SW Spain)," *Atmospheric Environment*, vol. 39, no. 36, pp. 6777–6789, 2005.

[31] M. Vaezi, V. Pandey, A. Kumar, and S. Bhattacharyya, "Lignocellulosic biomass particle shape and size distribution analysis using digital image processing for pipeline hydro-transportation," *Biosystems Engineering*, vol. 114, no. 2, pp. 97–112, 2013.

[32] M. Gil, E. Teruel, and I. Arauzo, "Analysis of standard sieving method for milled biomass through image processing. Effects of particle shape and size for poplar and corn stover," *Fuel*, vol. 116, pp. 328–340, 2014.

[33] S. Kim and B. E. Dale, "Global potential bioethanol production from wasted crops and crop residues," *Biomass and Bioenergy*, vol. 26, no. 4, pp. 361–375, 2004.

[34] Q. Guo, H. Liu, and X. Chen, "2 Dimensional finite stochastic breakup model of biomass particle breakup," *Bioresource Technology*, vol. 129, pp. 12–17, 2013.

[35] S. A. EL-Sayed and M. E. Mostafa, "Analysis of grain size statistic and particle size distribution of biomass powders," *Waste and Biomass Valorization*, vol. 5, no. 6, pp. 1005–1018, 2014.

[36] E. H. Van den Berg, A. G. C. A. Meesters, J. A. M. Kenter, and W. Schlager, "Automated separation of touching grains in digital images of thin sections," *Computers & Geosciences*, vol. 28, no. 2, pp. 179–190, 2002.

[37] Z. Lu, Y. He, B. Yu, and X. Hu, "Harmful effects of airborne dust diffused from ceramic tiles during home decoration," *Powder Technology*, vol. 267, pp. 86–94, 2014.

[38] C. Igathinathane, S. Melin, S. Sokhansanj et al., "Machine vision based particle size and size distribution determination of airborne dust particles of wood and bark pellets," *Powder Technology*, vol. 196, no. 2, pp. 202–212, 2009.

Hindawi
International Journal of Analytical Chemistry
Volume 2017, Article ID 4303596, 6 pages
https://doi.org/10.1155/2017/4303596

Research Article

Chemical Compositional Analysis of Catalytic Hydroconversion Products of Heishan Coal Liquefaction Residue

Xiaoming Yue, Yajun Wu, Shuangquan Zhang, Xiaoqin Yang, and Xianyong Wei

Key Laboratory of Coal Processing and Efficient Utilization (Ministry of Education) and School of Chemical Engineering and Technology, China University of Mining and Technology, Xuzhou 221116, China

Correspondence should be addressed to Xiaoming Yue; yuexiaoming_cumt@126.com

Received 6 December 2016; Revised 3 January 2017; Accepted 10 January 2017; Published 30 January 2017

Academic Editor: Xun Hu

Liquefaction residue of Heishan bituminous coal (HLR) was subject to two hydroconversion reactions under 5 MPa initial pressure of hydrogen at 300°C for 3 h, without catalyst and with acid supported catalyst (ASC), respectively. The reaction products were analyzed with gas chromatography/mass spectrometer (GC/MS). The results show that 222 organic compounds were detected totally in the products and they can be divided into alkanes, aromatic hydrocarbons (AHCs), phenols, ketones, ethers, and other species (OSs). The yield of hydroconversion over the ASC is much higher than that without catalyst. The most abundant products are aromatic hydrocarbons in the reaction products from both catalytic and noncatalytic reactions of HLR. The yield of aromatic hydrocarbons in the reaction product from hydroconversion with the ACS is considerably higher than that from hydroconversion without a catalyst.

1. Introduction

Direct coal liquefaction is a significant process for transforming coal to liquid fuel and chemicals, in which considerable coal liquefaction residue (CLR) is generated. The residue obtained by the process of direct liquefaction is about 30 wt% of raw coal [1]. It is important to find a way to utilize the CLR efficiently for improving the economy of coal utilization. Even after liquefaction, CLR still retains part of organic macromolecular structure such as aromatic hydrocarbons together with the unreacted coal, the minerals from coal, and the liquefaction catalyst [2–6]. But CLR is difficult to be used due to the fact that presence of an amount of polyaromatics and specific structures of CLR are not clear at present. Obtaining more information on the molecular structure of CLR as well as getting more soluble fraction from CLR is indispensable for utilization of CLR efficiently.

Catalyst plays a very important role for cutting off the chemical bonds in the macromolecule structure of coal and solid acid is a kind of the important and efficient catalysts in direct coal liquefaction [7–9]. Shui et al. [10] found that the acidic catalyst BF_3/SBA-15 they prepared has high hydroliquefaction of thermal dissolution soluble fractions. Other solid acids such as SO_4^{2-}/Fe_2O_3, SO_4^{2-}/SnO_2, and $SO_4^{2-}/Mo/Fe_2O_3$ were used in direct coal liquefaction [11–13]. However, few reports have paid attention to the use of solid acid catalyst in CLR hydroconversion.

In this study, a kind of acid supported catalyst (ASC) was prepared and ASC-catalyzed hydroconversion of a CLR from Heishan bituminous coal was investigated.

2. Experimental Methods

The liquefaction residue of Heishan bituminous coal (HLR) was obtained by direct liquefaction under 19 MPa H_2 at 455°C. The HLR was ground to <75 μm, dried in vacuum at 80°C, and stored with nitrogen. Table 1 lists the proximate and ultimate analyses of the HLR.

Solvent cyclohexane and petroleum ether (PE) were commercially purchased and then distillated using a rotary evaporator (BÜCHI Labortechnik AG, Flawil, Switzerland). Activated carbon (AC) and antimony pentachloride ($SbCl_5$) were commercially available. AC was ground to <75 μm, dried in vacuum at 80°C, and stored with nitrogen before use. The ASC was prepared with AC and $SbCl_5$ by impregnation method under microwave.

Table 1: Proximate and ultimate analyses (W%) of HLR.

Proximate analysis			Ultimate analysis (daf)				
M_{ad}	A_d	V_{daf}	C	H	N	O[a]	S
0.19	21.64	39.07	75.09	1.29	1.36	24.42	3.79

[a]By difference.

1 g HLR, 0.4 g ASC, and cyclohexane (30 mL) were put into a stainless autoclave (60 mL volume) with magnetic stirrer. After being purged with N_2 three times to remove air from the autoclave, the autoclave was pressurized with H_2 to 5 MPa, then heated to 300°C at a rate of 20°C/min, and kept for 3 h. After that, in an ice bath, the autoclave was cooled rapidly. The reaction mixture which was thoroughly removed from the autoclave using PE as solvent was filtrated by a membrane filter with pore size of 0.8 μm. The filter cake was thoroughly extracted with PE in a Soxhlet extractor and then dried in vacuum at 80°C for 12 h. The filtrate and PE extraction were combined and concentrated by a rotary evaporator to obtain concentrated reaction product. The form of the yield is expressed as

$$Y = \left(1 - \frac{m_1 - m_c}{m_0}\right) \times 100\%, \quad (1)$$

where m_1 refers to the mass of the dried filter cake (reaction residue); m_c is the mass of the catalyst in the reaction; m_0 is the mass of HLR in the reaction.

The organic compounds in the reaction product were identified with gas chromatography/mass spectrometer (GC/MS; Hewlett-Packard Company, Hewlett-Packard 6890/5973) and quantified with gas chromatography (GC; HP 6890). Fourier transform infrared (FTIR) was collected at room temperature on a Nicolet Magna IR-560 infrared spectrometer. N_2 adsorption-desorption isotherms were determined by an Autosorb-1-MP specific surface area and pore size analyzer at 77 K from Quantachrome Instruments Company to obtain pore volume, average pore diameter, and surface area of the AC and ASC.

As a comparison reaction, the procedure of noncatalytic hydroconversion (NCHC) is the same with the catalytic hydroconversion (CHC) but without any catalyst.

3. Results and Discussion

As Figure 1 shows, the absorbances at 2925 and 2857 cm^{-1} attributed to CH_3 group and >C-C< moiety [14] were observed in the AC, which had to be found in the ASC. The absorbances of -OH group at 3416 cm^{-1} and >C=C< moiety at 1620 cm^{-1} in the ASC are stronger than those in the AC [14]. The absorbance between 800 and 600 cm^{-1} attributed to C-Cl stretching vibration absorption [15]. The appearance of C-Cl bonds at 769 cm^{-1} in ASC indicates that the reaction of $SbCl_5$ with the AC was carried out during the process of ASC preparation [16, 17]. The pore volume, average pore diameter, and surface area of AC were 0.53 cm^3/g, 2.85 nm, and 743 m^2/g, respectively. However, the pore volume, average pore diameter, and surface area of ASC

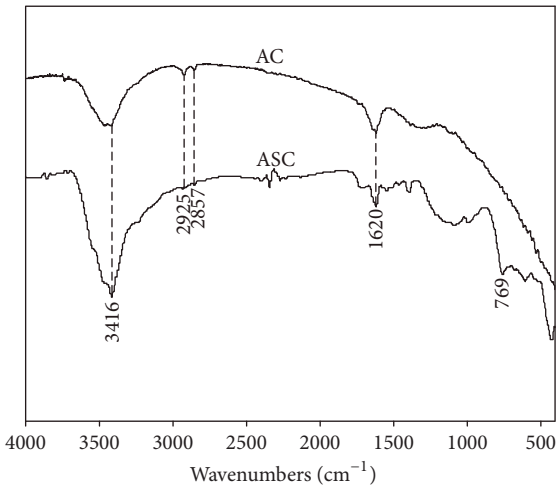

Figure 1: FTIR spectra of the AC and ASC.

were 0.26 cm^3/g, 2.66 nm, and 526.3 m^2/g, respectively. It indicates that the pore diameter of catalyst decreased after impregnation with $SbCl_5$; the active component loaded on the inner surface of the pore in AC was possibly the reason. Therefore, the pore volumes, average pore diameter, and surface areas were all decreased after impregnation.

The yields of NCHC and CHC of HLR are 35.49% and 57.11%, respectively. Compared with the NCHC, the yield of CHC is remarkably improved. These data show that the ASC plays a significant role to promote the decomposition of HLR.

The reaction products from NCHC and CHC of HLR are simplified as RPNC and RPC, respectively. Figures 2 and 3 exhibit the total ion chromatograms (TIC) of RPNC and RPC with GC/MS. Totally, 222 organic compounds were identified, and they can be divided into six groups: alkanes, aromatic hydrocarbons (AHCs), phenols, ketones, ethers, and other species (OSs), as listed in Tables 2 and 3 and Tables S.1–4 (see Supplementary Material available online at https://doi.org/10.1155/2017/4303596).

As shown in Figure 4, the yields of group components from RPNC increase in the order ethers < phenols < alkanes < OSs < ketones < AHCs, while the order of RPC is alkanes < ethers < ketones < phenols < OSs ≪ AHCs. The yield of RPNC (12.94 mg·g^{-1}, daf) is much lower than that of RPC (50.91 mg·g^{-1}, daf); extremely more organic compounds were determined in the RPC than those from RPNC.

As listed in Table 2, four alkanes (206.1 μg·g^{-1}, daf) were detected in the RPNC, including one cyclic hydrocarbon, two N-alkanes, and one branched alkane. Six alkanes (180.3 μg·g^{-1}, daf) were detected in the RPC, including five N-alkanes and one branched alkane, with carbon atoms number

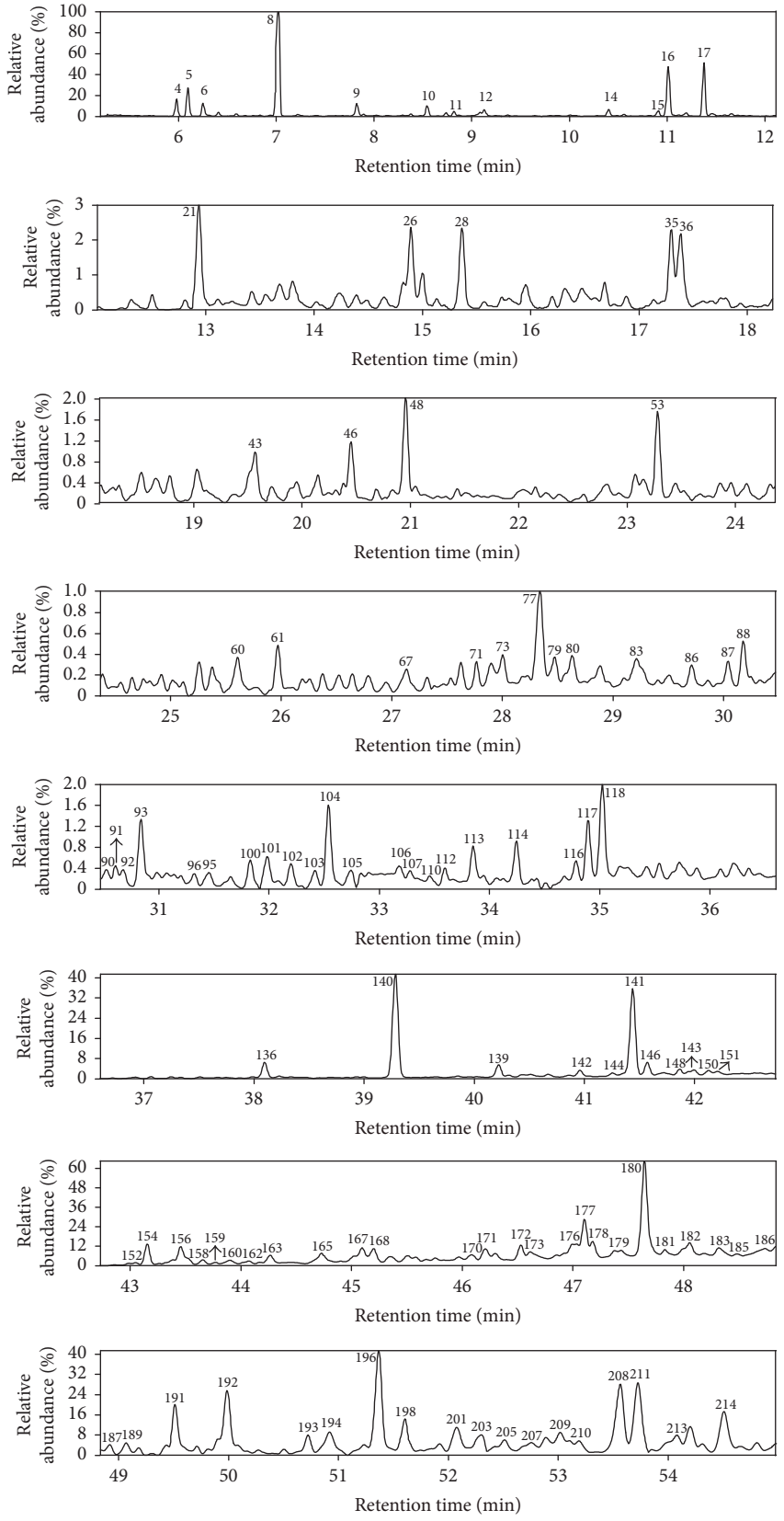

Figure 2: Total ion chromatogram of the reaction product from NCHC of HLR.

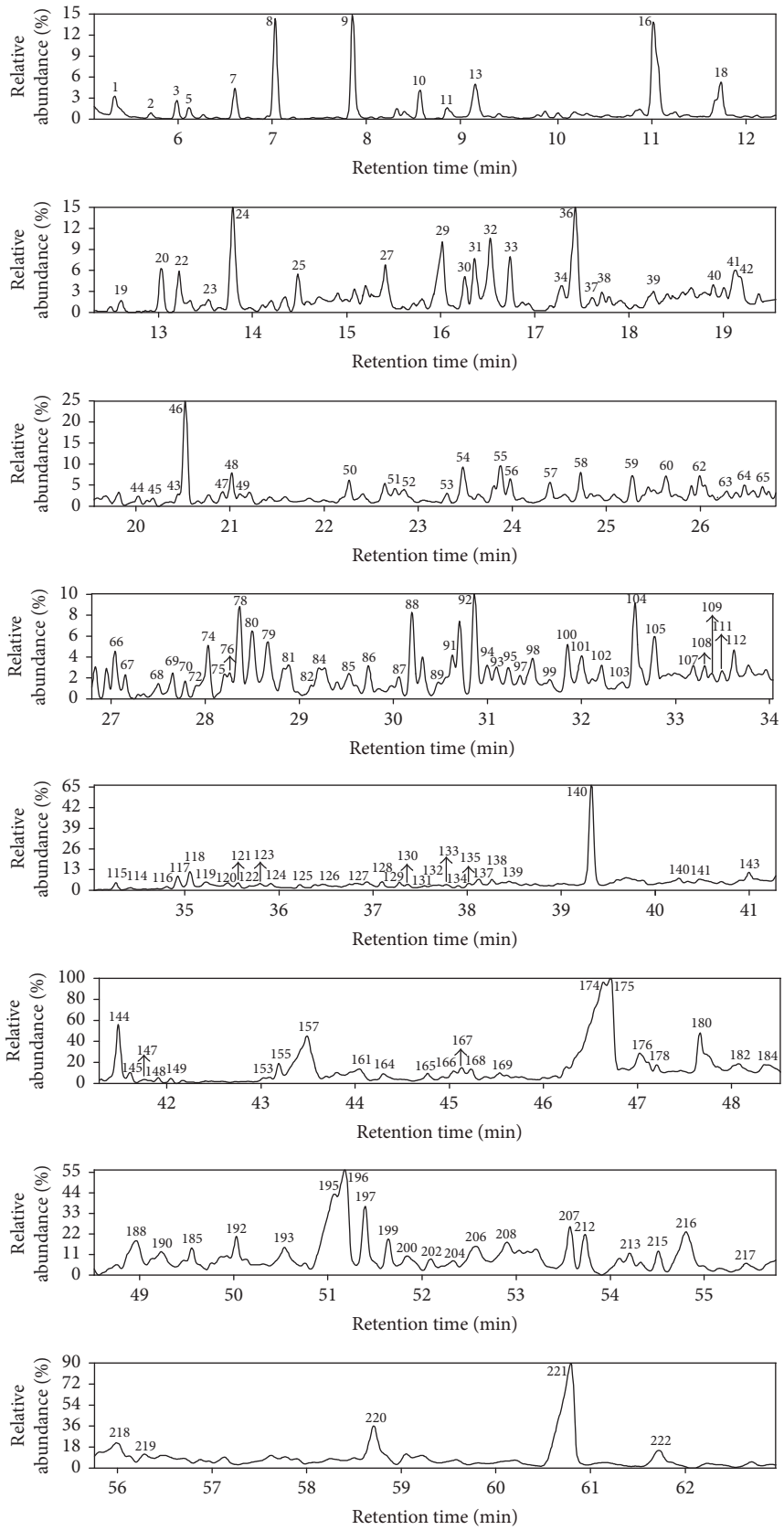

Figure 3: Total ion chromatogram of the reaction product from CHC of HLR.

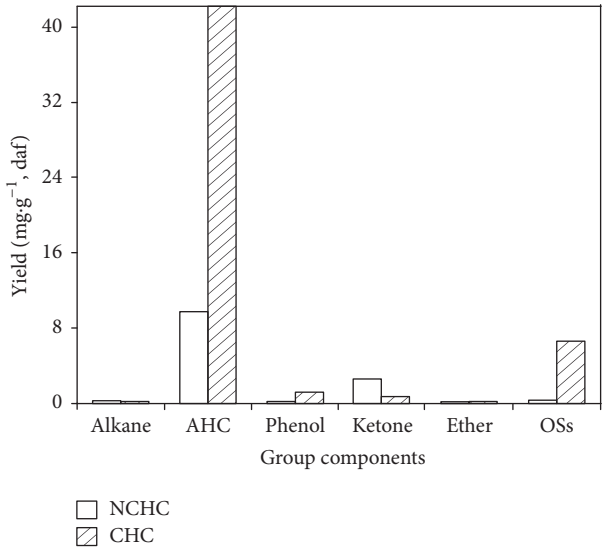

Figure 4: Distribution of group components in the reaction products from NCHC and CHC of HLR.

Table 2: Alkanes detected in the reaction product from NCHC and CHC of HLR.

Peak	Compounds	NCHC	CHC
4	Methylcyclohexane	√	
59	Pentadecane		√
70	Hexadecane		√
89	Heptadecane	√	√
106	Octadecane	√	√
107	8-Methylheptadecane	√	√
128	Eicosane		√

Table 3: Phenols detected in the reaction product from NCHC and CHC of HLR.

Peak	Compounds	NCHC	CHC
22	*o*-Cresol		√
24	*m*-Cresol		√
32	3-Ethylphenol		√
34	3,4-Dimethylphenol		√
40	2-Ethyl-6-methylphenol		√
47	2,3-Dihydro-1*H*-inden-5-ol		√
61	2,4,6-Triisopropylphenol	√	
118	(*E*)-4-Styrylphenol	√	√
119	(*E*)-4-Styrylphenol		√
167	Chrysen-6-ol	√	√

from 15 to 20. No olefin was detected. Most of the side chains in coal were removed during the coal liquefaction process; it is the possible and reasonable reason for the low yield of the alkanes.

In total, 171 AHCs were detected in the reaction products, including 81 and 130 AHCs appearing from RPNC and RPC, respectively, as shown in Table S.1 (supplementary data). The yields of AHCs are 9.7 and 42.1 mg·g^{-1} (daf) and the relative contents are 73.0% and 82.5% in the RPNC and RPC, respectively. 14 homologues of benzene, 7 homologues of fluorine, 17 homologues of naphthalene, 7 homologues of anthracene, 6 homologues of phenanthrene, and 30 condensed arenes with carbon atoms number greater than 4 were found in the RPNC. AHCs detected in the RPC include 33 homologues of benzene, 9 homologues of fluorine, 26 homologues of naphthalene, 10 homologues of anthracene, 12 homologues of phenanthrene, 4 homologues of indene, and 36 condensed arenes with carbon atoms number greater than 4. Among them, the yield of benzoperylene (peak 175) is the most and the relative content is 13.4% in the RPC of HLR. Secondly, the relative content of 2-methylbenzoperylene (peak 221) is 10.4%. The AHCs in the RPC (42.1 mg·g^{-1}, daf) are remarkably higher than those in the RPNC (9.7 mg·g^{-1}, daf). Our previous investigation showed that C_{ar}-C_{alk} bridge bond in di(1-naphthyl)methane can be especially ruptured over ASC to afford naphthalene and 1-methylnaphthalene under 5 MPa initial pressure of hydrogen at 300°C [18, 19]. H_2 was cleaved to H^- adhering on the surface of the catalyst with H^+ moving freely over the ASC with strong acidity. The addition of H^+ to the ipso-position of an aromatic ring in the macromolecule of HLR brings about cleavage of the C_{ar}-C_{alk} bridge bond, leading to the release of AHCs, which is the appropriate reason for the significantly higher yield of the RPNC. Furthermore, it can be speculated that a large number of AHCs are connected with the macromolecular skeleton of coal liquefaction residue by bridge bonds.

As exhibited in Table 3, 3 and 9 phenols were detected in the RPNC and RPC, respectively. The yields of phenols in the RPC (1193.2 μg·g^{-1}, daf) are dramatically higher than those in the RPNC (171.9 μg·g^{-1}, daf). There are many oxygen-containing functional groups in lignite and the C-O bond is a kind of the important bridge bonds linking aromatic hydrocarbons or alkanes [20]. The addition of H^+ to the ipso-position of the phenoxy in the HLR leads to cleavage of the C-O bond to receive the phenols; it should be the main reason for significantly higher yields of phenols in the RPC compared to those from RPNC [19]. The fracture of C-O bonds is facilitated more easily with the catalysis of the ASC.

4. Conclusions

Organic compounds of the reaction product from RPNC and RPC detected by GC/MS include alkanes, AHCs, phenols, ketones, ethers, and OSs. The yield of CHC is obviously improved compared with the NCHC and it shows that the ASC plays a significant role to promote the decomposition of HLR. Much more AHCs and phenols were released from RPC than those from RPNC. The hydroconversion of HLR under 300°C over the ASC not only provides an efficient approach for producing lots of value-added chemicals from the residue but also provides the information of macromolecular structures of the residue.

Competing Interests

The authors declare that they have no competing interests.

Acknowledgments

This work was subsidized by the National Natural Science Foundation of China (Grant no. 21506248), the Basic Research Program of Jiangsu Province (Grant no. BK20130171), Fundamental Research Fund for the Central Universities (China University of Mining & Technology) (Grant no. 2013QNA16), the Scientific Research Foundation of Key Laboratory of Coal-based CO_2 Capture and Geological Storage of Jiangsu Province (China University of Mining and Technology) (Grant no. 2015A03).

References

[1] M. Sugano, R. Ikemizu, and K. Mashimo, "Effects of the oxidation pretreatment with hydrogen peroxide on the hydrogenolysis reactivity of coal liquefaction residue," *Fuel Processing Technology*, vol. 77-78, supplement 1, pp. 67–73, 2002.

[2] J. Zhang, L. Jin, X. He, S. Liu, and H. Hu, "Catalytic methane decomposition over activated carbons prepared from direct coal liquefaction residue by KOH activation with addition of SiO_2 or SBA-15," *International Journal of Hydrogen Energy*, vol. 36, no. 15, pp. 8978–8984, 2011.

[3] N. Xiao, Y. Zhou, J. Qiu, and Z. Wang, "Preparation of carbon nanofibers/carbon foam monolithic composite from coal liquefaction residue," *Fuel*, vol. 89, no. 5, pp. 1169–1171, 2010.

[4] J. Zhang, L. Jin, S. Liu, Y. Xun, and H. Hu, "Mesoporous carbon prepared from direct coal liquefaction residue for methane decomposition," *Carbon*, vol. 50, no. 3, pp. 952–959, 2012.

[5] Y.-B. Wei, X.-Y. Wei, L.-C. Yu, P. Li, Z.-M. Zong, and W. Zhao, "The amorphous alloy-catalyzed hydroconversion of demineralized Shengli coal liquefaction residue under microwave irradiation," *Energy Sources, Part A: Recovery, Utilization, and Environmental Effects*, vol. 35, no. 24, pp. 2302–2309, 2013.

[6] J. Zhang, L. Jin, H. Hu, and Y. Xun, "Effect of composition in coal liquefaction residue on catalytic activity of the resultant carbon for methane decomposition," *Fuel*, vol. 96, pp. 462–468, 2012.

[7] Y.-B. Wei, Z.-M. Zong, R.-L. Xie et al., "Solid superacid-catalyzed hydroconversion of demineralized shengli coal liquefaction residue under microwave irradiation," *Energy Sources, Part A: Recovery, Utilization and Environmental Effects*, vol. 32, no. 6, pp. 551–558, 2010.

[8] A. A. Krichko, A. S. Maloletnev, O. A. Mazneva, and S. G. Gagarin, "Catalytic properties of high-silica zeolites in hydrotreatment of coal liquefaction products," *Fuel*, vol. 76, no. 7, pp. 683–685, 1997.

[9] A. M. Radwan, Z.-G. Zhang, P. Chambrion, T. Kyotani, and A. Tomita, "Hydrocracking of Orinoco tar over metal-free USY zeolite," *Fuel Processing Technology*, vol. 55, no. 3, pp. 277–284, 1998.

[10] H. Shui, L. Yang, T. Shui et al., "Hydro-liquefaction of thermal dissolution soluble fraction of Shenfu subbituminous coal and reusability of catalyst on the hydro-liquefaction," *Fuel*, vol. 115, pp. 227–231, 2014.

[11] V. R. Pradhan, D. E. Herrick, J. W. Tierney, and I. Wender, "Finely dispersed iron, iron-molybdenum, and sulfated iron oxides as catalysts for coprocessing reactions," *Energy and Fuels*, vol. 5, no. 5, pp. 712–720, 1991.

[12] B. Ren, M. Q. Fan, J. Wang, and X. Y. Jing, "Preparation and application of magnetic solid acid $SO_4^{2-}/ZrO_2/Fe_3O_4/WO_3$ for synthesis of fructone," *Solid State Sciences*, vol. 13, pp. 1594–1598, 2011.

[13] Z. C. Wang, H. F. Shui, Y. N. Zhu, and J. S. Gao, "Catalysis of View the MathML source solid acid for the liquefaction of coal," *Fuel*, vol. 88, no. 5, pp. 885–889, 2009.

[14] K. Nakanshi and P. H. Solomon, *Infrared Absorption Spectroscopy*, (X. M. Wang Trans.), Science Press, Beijing, China, 1984.

[15] L. J. Bellamy, *The infra-red spectra of complex molecules*, Springer Netherlands, 1975.

[16] J.-L. Zhu, X. Fan, X.-Y. Wei et al., "Molecular characterization of heteroatomic compounds in a high-temperature coal tar using three mass spectrometers," *Fuel Processing Technology*, vol. 138, pp. 65–73, 2015.

[17] S. Albert, K. Keppler, P. Lerch, M. Quack, and A. Wokaun, "Synchrotron-based highest resolution FTIR spectroscopy of chlorobenzene," *Journal of Molecular Spectroscopy*, vol. 315, pp. 92–101, 2015.

[18] X.-M. Yue, X.-Y. Wei, B. Sun et al., "A new solid acid for specifically cleaving the C_{ar}—C_{alk} bond in di(1-naphthyl)methane," *Applied Catalysis A: General*, vol. 425-426, pp. 79–84, 2012.

[19] X.-M. Yue, X.-Y. Wei, B. Sun, Y.-H. Wang, Z.-M. Zong, and Z.-W. Liu, "Solid superacid-catalyzed hydroconversion of an extraction residue from Lingwu bituminous coal," *International Journal of Mining Science and Technology*, vol. 22, no. 2, pp. 251–254, 2012.

[20] M. Wang, X. Fan, X.-Y. Wei et al., "Characterization of the oxidation products of Shengli lignite using mass spectrometers with 'hard', 'soft' and ambient ion sources," *Fuel*, vol. 183, pp. 115–122, 2016.